Experimental and Numerical Investigation of Polypropylene Foam Formation through Extrusion Process

Ali Mirzaee

A Thesis

In the Department

of

Mechanical, Industrial & Aerospace Engineering

Presented in Partial Fulfillment of the Requirements

For the Degree of

Master of Applied Science (Mechanical Engineering) at

Concordia University

Montreal, Quebec, Canada

April 2019

CONCORDIA UNIVERSITY
School of Graduate Studies

This is to certify that the thesis prepared

By: ALI MIRZAEE

Entitled: Experimental and Numerical Investigation of Polypropylene Foam Formation through Extrusion Process

and submitted in partial fulfillment of the requirements for the degree of

Master of Applied Science (Mechanical Engineering)

complies with the regulations of the University and meets the accepted standards with respect to originality and quality.

Signed by the final examining committee:

_____ Chair
Dr. CAROLE EL AYOUBI

_____ Examiner
DR. IDA KARIMFAZLI

_____ Examiner
DR. AHMED SOLIMAN

_____ Thesis Supervisor(s)
DR. MEHDI HOJJATI

_____

Approved by _____
DR. MAMOUN MEDRAJ Chair of Department or Graduate Program Director

_____
Dean,

Date _____

Abstract

Polymeric foams appear in diverse fields from automotive to medical applications due to their unique characteristics. The morphology of the polymer foams has a huge impact on their mechanical and physical properties such as strength and density. In this thesis, nucleation and growth of bubbles in foaming of Polypropylene through the extrusion process have been investigated both experimentally and numerically. Both cell nucleation and cell growth phenomenon should be controlled through the process in order to have a customized foam. Several models have been proposed for many years and theoretical and experimental investigations have been performed on both bubble nucleation and bubble growth phenomenon. In the nucleation step, a semi-experimental model has been adopted in our studies after reconciling between the accuracy and complexity of the models. This model uses the heterogeneous nucleation mechanism, proposed by classical nucleation theory, as the main mechanism of nucleation in the foaming process and modifies it by introducing energy reduction and frequency factors. For the growth stage, a two-dimensional model that accounts for the diffusion-driven growth of bubbles in the viscoelastic fluid (PP melt) has been chosen. The two-dimensional models have a higher accuracy in predicting the final bubble radius compared to the one-dimensional models (e.g. cell model) and is capable of predicting the exact shape of non-spherical bubbles in the polymer. Using a mini-extruder, the effect of processing parameters on the final foam morphology has been studied qualitatively. Then the governing equations for the diffusion-driven bubble growth have been solved by the finite element method. The sensitivity of the growth dynamic to the processing parameters has been studied by simulating the evolution of a single bubble enclosed inside an influence volume under the assumptions of the cell model. The interactions between the bubbles, which cannot be thoroughly considered in the cell model, have been simulated by the two-dimensional model and the predictions of the bubble shapes at different processing conditions have been performed. Finally, the ability of the cell model and the two-dimensional model in predicting the final foam density have been compared with the experimental data. The results show that the accuracy of the cell model decays as the cell density and the bubble-bubble interactions increases while the 2D model has the capability of predicting foam density and the average bubble size with acceptable accuracy in nearly all experimental conditions.

Acknowledgement

To My Family Who Always Supported Me

Table of Contents

Table of Figures:

Chapter 1: Introduction

1.1 Preamble:

Thermoplastic foam is a porous structure that is created by the expansion of the gaseous phase dissolved and spread throughout the polymer melt. Plastic foaming is a process on polymers that use blowing agents, nucleating agents, and other additives to generate a cellular structure in a polymer matrix. This internal structure creates unique properties in the foams such as lightweight, high strength to weight ratio, thermal and acoustic insulation and resistance to impact [1]. These characteristics make them suitable for a vast area of applications such as automotive, packaging, electronics, aerospace, building construction, bedding, medical, transportation and recreation [2]. Among all thermoplastics that can be used for foaming production, Polypropylene has outstanding characteristics. This material belongs to the semicrystalline polyolefin family and has a low cost, wide range of operating temperature and high resistance to chemicals and abrasion. In addition, it has a higher rigidity compared to other members of polyolefin family, higher strength than polyethylene and better impact resistance compared to polystyrene [3]. Due to these additional advantages, polypropylene has the biggest share in the thermoplastic foam markets [4]. This increasing interest in employing plastic foams (specifically PP) in daily life urged scientist to focus their researches on a more clear understanding of foaming process in order to optimize polymer foam properties for any individual application and produce a customized foam. In general, plastic foams are categorized in different ways, according to their nature as flexible and rigid, by considering their dimension as sheet and board, by weight as low density and high density, by the form of their structure as open cell and closed cell, and by the size of their cells as fine-celled, microcellular, or nanocellular foams. For decades, processes such as extrusion foaming, batch foaming, foam injection molding, bead foaming, and heat foaming were used to produce plastic foams. In all these methods, the base material where the foaming should happen is either a liquid or in a plastic state during the process. The porous structure in polymers may be produced chemically, physically or mechanically [5].

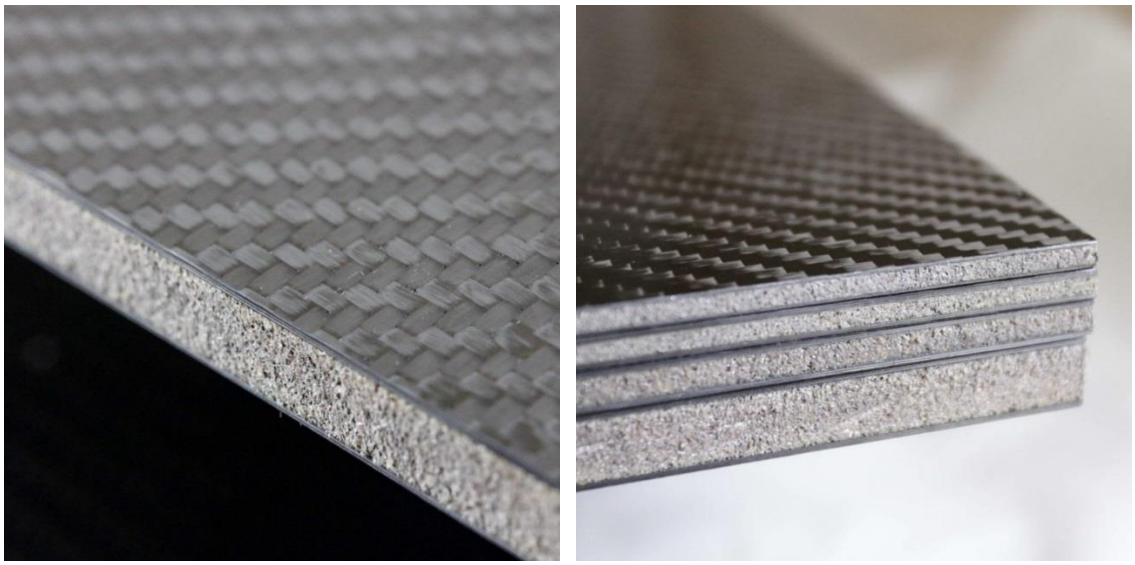

Figure 1.1 Carbon fiber sandwich panels with the foam core [6]

Comparing these methods, chemical foaming and physical foaming processes are more popular than the mechanical foaming approach. In chemical foaming processes, the cellular structure is produced by the gas that is generated through the decomposition of a chemical blowing agent (CBA). Some CBAs are decomposed in an exothermic reaction such as azodicarbonamide and *p*-toluenesulfonyl semicarbazide and others in an endothermic one such as citric acid and sodium bicarbonate. The most popular method for producing plastic foams is physical foaming process, which the gas is directly injected to the melted polymer from a gas tank. Foam production in this method can be divided into four steps: (I) dissolution of gas in a polymer matrix; (II) cell nucleation; (III) cell growth; and (IV) cell stabilization. The formation and expansion of cells from the dissolved gas are achieved by lowering the solubility of the polymer, either by reducing the pressure or increasing the temperature of the solution. The final foam morphology is the outcome of these steps which itself affects the properties of the foamed product [5]. In the batch foaming process, the polymer melt is saturated with blowing agents at high temperature and pressure in an autoclave and the cell nucleation initiates by rapid depressurization of the system to atmospheric pressure. The cell stabilization, which results in the final foam morphology, is achieved by cooling the polymer in a solvent or air [7]. In the extrusion foaming process, the materials are fed into the extruder through the hopper. The

polymer then is melted and mixed with the gas by the rotation of the screws inside the barrel. The gas is supplied either by chemical blowing agents which liberate gas upon decomposition at a certain temperature or by direct gas injection into the barrel from a gas tank. The mixture is pressurized up to the die section and then comes out of the extruder from high backpressure to the atmospheric pressure. Foam injection molding is similar to the conventional injection molding process except that an additional gas unit is integrated into the injection-molding machine. The rest of the process is very similar to the foam extrusion process [1].

1.2 Foam properties and Cellular structure

The properties of a polymeric foam including physical, mechanical and thermal properties are originated from its constituents namely the polymer matrix, gas phase, and the cellular structure. A polymeric foam is a type of composite structures that is formed when the gas phase is dispersed through the polymer matrix. Like other composites, the properties of the final material is determined by the properties of its components and the way they are distributed through the matrix. Due to the negligible weight of the gas phase, some of the properties of the foam volumetrically depend on the constituents such as density; however, some other properties still remain gravimetrically dependent on the participating components. The thermodynamic properties of the foam such as heat capacity and heat conductivity are the examples of the latter group. Since the share of each element can vary in the different composites, the properties of the foam would be affected by some components more than the others do. For example, when the expansion ratio is low and the gas content is limited, polymer dictates the properties of the foam and when the expansion ratio is high and the gas phase dominates; the contribution of the polymer is lower in the foam properties [8].

The following structural parameters have critical roles in determining the characteristics of the foamed polymer:

- Cell density
- Expansion ratio
- Cell size distribution
- Open-cell content
- Cell integrity

These structural parameters are governed by the foaming technology used for processing of the foam, and the foaming technology itself depends mainly on the type of the polymer. In other words, due to the difference in the physical properties of the polymers, different foaming technologies are also required to turn them into a cellular structure [8].

One of the examples of the effect of structural parameters on the characteristics of the foams is the heat insulation ability. At a given expansion ratio, cell size and the way they are dispersed have significant effects in the thermal flow through the foam. As is depicted in since the heat transfer by convection in the gas phase is negligible, the existence of bubbles restricts the heat transfer and detours the direction of the heat through the foam; thus a lower heat transfer capability and a higher insulation ability will be obtained. As a result, the insulation property of foams strongly depends on the cell sizes and cell densities [8].

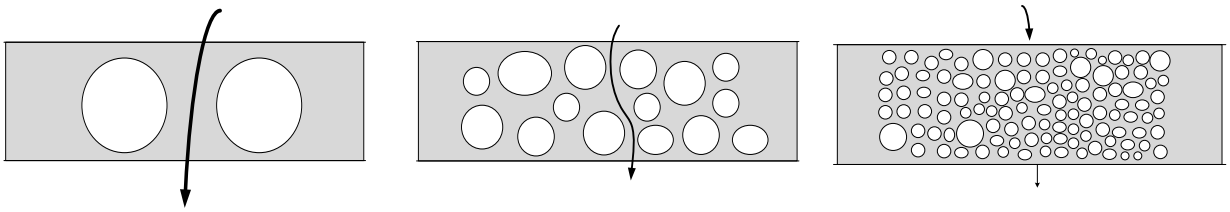

Figure 1.2 The effect of cell size and cell distribution on the heat insulation property of the foam [8]

As another example, the energy absorption ability of highly expanded foams is determined by their gaseous phase. The energy absorption capability is greatly enhanced when many grown cells are thoroughly dispersed in the polymer rather than being encapsulated inside a thin film of the polymer. The cell size also has a great impact on the disturbance distribution ability of the foam. Smaller cells provide a better energy absorption capability as in the case of microcellular foams with cell size in the order of 10 microns [5, 8]. In addition to the cell size, the number of cells and cell distribution, which are establishing the final property configuration of a given polymeric foam, the nature of the cells (open cell versus closed cell) similarly plays a vital role in determining the properties. When the cell wall is vulnerable to rupture, it cannot hold the gaseous phase together inside the cell, and as a result, interconnections between the cells are created. When the foam is subjected to an impact or undergoes a deformation, the gas compression mechanism, which is the underlying mechanism of energy absorption property, may no longer be useful. Thus, the compressive strength, the energy absorption ability, and other

mechanical properties of the foam would be weakened. Despite these drawbacks, open cells have enhanced capillaries that allow them to be used in the food industry due to superior fluid absorption features. In addition, they can be used in sound-deadening applications, where sound waves attenuate after some bounces [8].

1.3 Research Motivations and Thesis Objective

The popularity of the polypropylene foaming and its share in the foaming industry is a worldwide topic. Improving the quality of PP foams to turn them into high-performance materials requires a better understanding of the foaming process. Although thermoplastic foaming has been a topic of research for decades, more investigations are still needed to achieve to fully customized foams. Any improvement in this process results in a huge profit for the foaming industries. This industry is also very active in the region of Greater Montreal. "AS Composite Inc." [9] was one of the companies that were producing sandwich panel structures with the polypropylene foams as their core. Their requirements to improve the product properties such as better heat insulation and impact resistance as well as producing high cell density foams created a collaboration between the Concordia University and "AS composite Inc." for this purpose. As explained earlier, the cellular structure has a key role in determining the mechanical and physical properties of the foam; therefore, any advancement in the foam quality is a result of improving foam morphology. This can be achieved by either adopting practical recommendations and applying them through the extrusion process and using the trial and error method or, by performing numerical simulations of the whole process. The first method might be an easier one, but it is more expensive and time-consuming than the second method and will not yield the optimum possible properties. These drawbacks can be adjusted by taking advantage of both methods using both experimental and numerical approach simultaneously. Thanks to the lab scale extruder that had maximum control over the processing parameters and was available for this project, the results of the finite element analysis of the process could be compared and justified with the experimental data. The goal of this thesis was to gain a predictive ability over the bubble growth phenomenon through a two-dimensional simulation of the growth process using the finite element method. The predictions of the simulation were tested using a micro-extruder and compared with the experimental results. The comparisons showed that two-dimensional

methods have superior ability in predicting the bubble growth dynamics and bubble boundary deformation compare to the one-dimensional methods that were used extensively in the past.

Chapter 2: Literature Review

The unique properties of the plastic foams distinguished them from their unfoamed counterpart and allowed them to participate in almost every aspect of our daily lives. Producing useful foamed products requires a profound understanding of the underlying science and process technology as well as increasing the availability of raw materials. Foaming Industry has experienced many difficulties in producing high-quality foams during past decades, and still, many open challenges exist in this way. Foaming technology has been a topic of extensive research for a long time among both academia and the foam industry. These efforts have yielded novel solutions for the challenges and offered valuable insights for the advancement of foam applications into new fields. In addition, these studies have resulted in invaluable information about the fundamental science of the process and various phenomenon take place during plastic foaming. This chapter represents a summary of the previous studies in the literature that addressed the foaming mechanism and the underlying science behind it. It is divided into two main sections; the first one describes the cell nucleation process and the second section explains the cell growth. These two phenomena happen consecutively during the foaming process and have to be considered together.

2.1 Bubble Nucleation in Plastic Foaming:

"Cell Nucleation" is a term that refers to the formation of new bubbles inside the polymer matrix during the plastic foaming process. A polymer which is fully saturated with a blowing agent turns into a supersaturated state when the gas solubility in the polymer becomes lower. This can happen when the temperature increases [10-17] or the pressure decreases [18-21] from the saturated state; thus, the solubility of gas inside the polymer reduces [5].

This excess gas which is dissolved more than the solubility of the polymer creates an unstable condition for the polymer-gas solution. The solution has a tendency to restore to the previous lower energy level by exhausting the extra gas in the form of tiny bubbles and as a result, the nucleation process starts. The kinetic instability limit for the supersaturation conditions is predicted in the classical nucleation theory (CNT) [22-24] which is based on the

thermodynamics of the process. According to this theory, a bubble that has a radius larger than the radius of the critical bubble grows spontaneously while the one that has a smaller radius collapses. A bubble has a critical radius when it is at an unstable equilibrium where the energy of the system is at maximum. This maximum energy is called the free energy barrier for cell nucleation [5].

The state of the system such as temperature, pressure and gas concentration determines the length of the critical radius (R_{cr}) and nucleation refers to a time when a bubble grows beyond the size of the critical radius. The concept of R_{cr} was first proposed by Gibbs [25] which is the key concept in the CNT. This theory classifies cell nucleation into two types namely nucleation in the bulk of the liquid (homogenous) and nucleation on the surface of the solid particles that exist inside the liquid (heterogeneous). Various researchers have studied this theory and tried to examine the necessary conditions required to reach the maximum energy level using classical thermodynamics. They determined the free energy barrier for homogeneous nucleation [26-32] and that of heterogeneous nucleation [33-41] for different surfaces geometries. In addition, some researchers such as Volmer and Weber [42], Farkas [23], and Zeldovich [24] addressed the kinetic aspect of bubble nucleation in their works [43].

Extensive reviews on the CNT and its developed versions have been performed by Frenkel [44] and Cole [34] while Tucker and Ward [30] tried to verify the concept of critical radius through experimental studies. As mentioned above, the classical nucleation theory divides nucleation into two groups namely homogeneous nucleation and heterogeneous nucleation. In addition to this classification, other researchers [32,45-48] proposed a more important kind of nucleation that originates from the pre-existing gas cavities or microvoids which exist inside the supersaturated solution and serve as seeds in the cell formation. Considering these different opinions, Jones et al. [49] proposed a classification system in which the cell nucleation can happen in either of three ways i.e. classical homogeneous nucleation, classical heterogeneous nucleation, pseudo-classical nucleation which will be explained in the following sections [5].

2.1.1 Classical Homogeneous Nucleation

The cell nucleation in classical homogeneous type happens when a bubble forms inside the balk of the homogeneous polymer-gas solution and unlike two other methods, there are no pre-

existing gas cavities inside the solution before the supersaturation state. However, studies [50] [51] showed that the number of bubbles in the plastic foaming process is much higher than the prediction of classical homogenous nucleation. As a result, this type of nucleation cannot be the mechanism in which cells are formed in the plastic foaming [5].

2.1.2 Classical Heterogeneous Nucleation

Classical heterogenous nucleation proposes that the nucleation of bubbles in the supersaturation state happens on the surface of heterogeneous nucleating sites such as small solid particles which can be particles added to the material prior to the supersaturation state or impurities. In this type of nucleation, it is assumed that there are no gas cavities in the system either in the bulk of solution or on the surface of nucleating agents prior to the supersaturation state. Wilt [35] studied the solution of H_2O and CO_2 and showed that the predicted energy level for the supersaturation state in the classical heterogeneous nucleation is very high and therefore it is improbable for the bubbles to nucleate on the planar surface or even the conical or spherical shaped holes of the nucleating agents. However, this study indicates that despite the low chance of cell nucleation, it is theoretically possible for the bubbles to nucleate on the conical pits of the nucleating agents in the H_2O and CO_2 solution. In comparison to the plastic foams, the tension at the liquid-gas interface in the polymer-gas solution is even higher than the solution of H_2O and CO_2. Leung et al. [52, 53] showed that the classical heterogeneous nucleation can theoretically happen at a considerable rate during the plastic foaming of PS-CO_2 and the predictions were in qualitative agreement with the theoretical data. However, in all previous studies, the predictions of classical heterogeneous nucleation were, at best cases, in a qualitative agreement with the experimental data and a quantitative agreement was not achieved without using a correction factors such as pre-exponential factor [54] and energy reduction factor [54]. As a result, it seems that both types of classical nucleation theory (Homogeneous and heterogeneous) cannot explain the real mechanism underlying the cell nucleation in the plastic foaming [5].

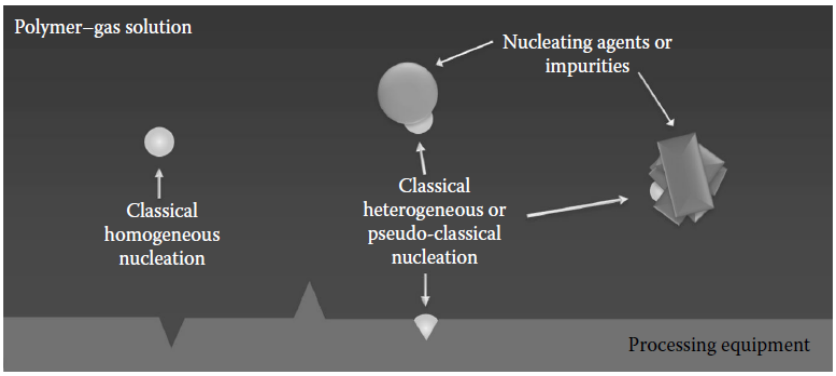

Figure 2.1 Different types of classical nucleation theory (Homogeneous and Heterogeneous) [43]

2.1.3 Pseudo Classical Nucleation

This theory proposes that nucleation occurs from metastable micro gas-pockets or microvoids in the solution (Homogeneous) as well as pre-existing gas that are entrapped in the cavities at the surface of the nucleating agents, processing equipment, or suspended impurities (Heterogeneous). During the continuous pressure drop, the degree of supersaturation increases. When the radius of microvoids and gas pockets are less than R_{cr}, there is still a finite amount of energy barrier for those voids to overcome the surrounding forces and start a nonstop expansion [51]. The remaining energy barrier will finally be overcome as the pressure drops further and sufficient amount of supersaturation accumulated.

Harvey et al. [45-48] introduced the concept of Harvey's nuclei and demonstrated that stable preexisting bubbles(Harvey's nuclei) which exist in the conical pits of nucleating sites. Lee [51] developed this concept and proposed that the existence of shear flow in the extrusion process would enhance the detachment of gas cavities from the surface of conical pits and thus increases the nucleation. On the other hand, Ward et al. [32] examined the concept of Harvey's nuclei and suggested a contact angle on the solid-liquid interface that is greater than 90 degrees is required for the existence of such nuclei, which is a rare condition. Despite this opposition, he mentioned the existence of tiny bubble nuclei when the gas concentration is more than the solubility of polymer (supersaturation condition) [32, 55, 5]. The presence of free volume in the polymer matrix has been reported by many studies [56]. Han and Han [57, 50] studied the nucleation of bubbles in the solution of polystyrene and toluene using the light scattering

method. They heated the solution under the high pressure, and upon releasing the pressure, bubbles were nucleated. Using the photomultipliers, they measured the light flux that was transmitted or scattered and with the aid of MIE scattering theory, they were able to determine the critical size of the bubbles. They observed and measured the distribution of bubble sizes and explained them by considering the effect of temperature, initial pressure and gas concentration. Later that year, they developed a theory for the nucleation of bubbles and determined a semi-empirical equation for the nucleation rate and compared the results with the data of their experiments. Ramesh et al. [58, 59] extended the model of Kweeder [60] , which was focusing on the microvoids resulted from the thermal history of the polymer, and used it in the microcellular foaming of polystyrene which was added with rubber particles. Their models focused on the small gas pockets (voids) trapped in the rugged surface of the rubber particles, which were used as the nucleation sites, and compared their results with the data of experimental setup. The size of rubber particles was less than 4μm with an average of 2 μm. They modeled the number of microvoids that can survive and overcome resisting forces such as surface tension and elastic forces to obtain cell density in the foam. The influence of processing parameters such as foaming temperature, saturation pressure, gas concertation, and rubber particles were studied. They related the size of rubber particles with the distribution of microvoids in the polymer composite materials and reported the significant influence of the parameters mentioned above on the cell nucleation. Their model showed a reasonable agreement with the experimental data; however, they did not apply their model to study the formation and growth of larger bubbles and only focused on the microcellular foams of polystyrene. Feng and Bertelo [61] studied plastic foaming with some particulate nucleating agents and a PFA that dissolved in a molten polymer. They derived a nucleation model based on the concept that heterogeneous nucleation originated from pre-existing microvoids on the solid particles and simulated the bubble nucleation and growth. They used the viscoelastic bubble growth model derived by Venerus et al. [62]. The calculation results of the number density of bubbles and bubble radius showed a good agreement with the experimental data obtained from the extrusion foaming experiment [5].

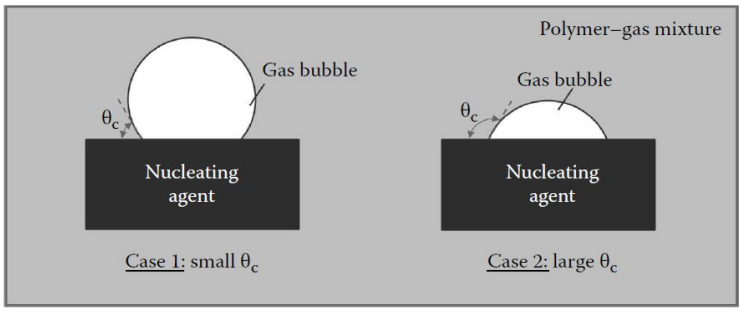

Figure 2.2 The illustration of the contact angle between a gas bubble and a nucleating agent [43]

2.2 Bubble Growth

Investigation about the theoretical and experimental aspects of bubble growth and collapse in many types of fluid (water, alcohols, and polymers) have been addressed by many researchers for more than 100 years [63]. Most of the models can be classified into three groups: (1) single bubble growth model (2) cell model (a swarm of bubbles growing without interaction between them) (3) two-Dimensional models (a swarm of bubbles growing near each other by considering their mutual interactions). These models can be applied to the processes that are based on the physical expansion of bubbles by environmentally friendly gasses such as nitrogen and carbon dioxide and do not apply to the processes that involve chemical cross-linking reaction. Models would become quite complex and completely different if chemical reactions are involved such as in the case of polyurethane foaming where isocyanate, polyols, water, and other catalysts chemically react with each other [64-70]. The principles of nucleation and foam growth can be applied to a wide variety of industrial applications, but due to the different processing conditions, the assumptions of nucleation and bubble growth models should be tailored to each process with their corresponding specifications. In addition, the complexity of the bubble growth dynamics and limitations in the computational capabilities forced researchers to adopt different assumptions in order to overcome those difficulties. These assumptions could vary in consideration of mass transfer, momentum transfer, heat transfer, rheological models, growth medium and blowing agent types. As a result, still, there is a lack of a comprehensive model that can be fitted well with all processes. However, due to the decades of experience and documented information on the bubble growth concept, experimental data, rheological models and numerical

simulation methods, there is a great source of information in the literature for the improvement of computational models in the foam expansion stage. In addition, due to the development of high-speed cameras and image processing techniques, it is possible to follow a bubble from the early moment at the nucleation stage to its final size at the stabilization step. These numerical simulations enable foam industries to develop their products at a much faster pace in order to produce more environmentally friendly foams at a lower cost. The historical development of the models mentioned above will be described in the next sections [43].

2.3 Single Bubble Growth Models

Between 1917 and 1984 [71-84] published models focused on the growth of a single bubble in an infinite sea of molten polymer with an unlimited amount of gas supply [43]. Rayleigh [71], Epstein and Plesset [72], and Scriven [73] were among the earliest researchers who used this model to study the bubble growth or collapse in different mediums. Among the earliest studies, Barlow and Langlois [74] analyzed the diffusion-induced bubble growth with mass and momentum transfer in a viscous liquid and used the assumption of a thin shell around a bubble where the dissolved gas concentration gradient exists in that shell and vanishes beyond that layer. This approximation was adopted extensively in the literature [72, 78, 77] that simplifies the problem especially in solving the mass transfer equation in a viscous liquid. Barlow and Langlois [74], as well as various researchers [72, 73, 78, 79, 85, 86], assumed the availability of the unlimited amount of gas for the bubble growth. The consequence of this assumption is that the concentration stays the same beyond the thin shell at any time during the process. Gent and Tompkins [76] developed an experimental setup to study the formation and growth of bubbles in the solutions of CO_2 and elastomers in the isothermal conditions and reported the bubble radius data in time. They used the Neo-Hookean model to describe the rheology of the elastomers and defined a threshold in the supersaturation state for the beginning of nucleation based on the shear modulus of the elastomer. Street et al. [87] extended the work of Barlow and Langlois [74] to formulate and numerically simulate the bubble growth process inside a sea of a liquid under non-isothermal conditions. Their theoretical model accounts for the heat, mass, and momentum transfer governing the growth of a vapor bubble in a solution consisting of a viscous liquid and a dissolved blowing agent. In their work, the viscous liquid was assumed to obey a

non-Newtonian fluid model (power law model). They identified the most important parameters controlling the rate of the growth as the diffusivity, the concentration of the blowing agent, the viscosity level of the melt, and the extent to which the liquid is shear thinning [5]. Han and Yoo [82] conducted experimental and theoretical studies to explain the oscillatory behavior of a gas bubble in a viscoelastic liquid in the foam molding process. They constructed a rectangular mold, filled it with the solution of gas and molten polymer and used a visual observation apparatus to record the growth of bubbles during the process. A chemical compound (Sodium bicarbonate) was used to generate carbon dioxide in this process. The rheological properties of the fluid were modeled by the Zaremba-DeWitt model and considered the effects of hydrodynamics and diffusion from the polymer to the gas bubble. The method of the finite difference was used in order to solve the governing equations by adopting a third order polynomial approximation for the gas concentration profile around the bubble. Their study showed that gas diffusivity has a significant influence on the occurrence of oscillatory behavior. Furthermore, they indicated that while the melt elasticity enhances the oscillatory behavior of bubble growth or collapse, the viscosity suppresses it. By considering convective and diffusive mass transport, surface tension, and inertia forces, Venerus et al. [62] developed a model that was capable of describing bubble growth and collapse in a non-linear viscoelastic fluid. They reported that the impact of considering a non-linear description for the polymer rheology on the bubble growth dynamic is minor compared to the fluid elasticity. They also evaluated the influence of several approximations, that were used in previous studies, on the evolution of bubbles and reported that the application of a thin boundary layer assumption is not vast [5].

The application of “Single Bubble Growth Model” was continued until the mid-80s with the adoption of different assumptions. Although these works gave valuable insights to the researchers, the applicability of this model for predicting the bubble morphology was limited in the experimental and industrial cases. In an industrial environment where the plastic foaming occurs, the dissolved gas concentration is finite in the polymer and therefore, a limited amount of gas available for the growth of each bubble. In addition, the growth includes the evolution of a swarm of bubbles in proximity to each other, which have mutual influences in many ways. Therefore, the practical applications of this model in the industry were limited. This led to the

development of a new model called “Cell Model” which will be explained in the next section [5].

2.4 Cell Model (1984–1998)

In 1984, Amon and Denson [88] proposed a new concept called “Cell Model.” In this model, each bubble is enclosed inside a thin layer of a polymer-gas solution and therefore a there is a finite amount of gas supply for the bubble to grow. In this model, the solution of melted polymer and gas is divided into spherical units with a constant mass inside which a single spherical bubble can evolve (Figure 2.3). Despite the Single Bubble Growth model which predicts a nonstop growth for a bubble, the Cell Model model has a more realistic assumption that leads to a finite diameter for the bubbles at the end of the growth process. The model of Amon and Denson was a fundamental improvement and caused more interest in this area of research, and several studies have emerged since then [43].

Amon and Denson [88], Arefmanesh and Advani [89], and Ramesh et al. [90] were among the first researchers who tested the validity of the cell model through experimental works. The first two groups used the injection molding process (structural foam molding setup), where the bubble growth occurs in a closed system, to obtain their experimental results in order to test the validity of the cell model, whereas the last group tested their model during the microcellular foaming process. Amon and Denson [88] studied the foaming of low-density polyethylene with a chemical blowing agent and measured the instantaneous density of the expanding foam in time and compared it to the prediction of their model. By assuming the behavior of the polymer melt as a Newtonian fluid and the gas in the cells like an ideal gas, they applied the cell model to simulate the bubble growth during plastic foaming. Unlike the single bubble growth model, their model yielded a finite radius for the growing bubble. Furthermore, they concluded that the effect of surface tension on the bubble growth dynamic is minor compare to the thermodynamic driving forces (e.g., the degree of supersaturation) and mass and momentum transfers. Later, they extended their work to a low-pressure structural foam molding process by considering the heat transfer and polymer flow effects [91]. The predicted bubble growth profiles were in good qualitative agreement with the experimental measurements of the bulk density of thermoplastic

foams. However, quantitative discrepancies existed between the two. These differences were believed to be related to the omission of melt elasticity and bubble coalescence in the model [43].

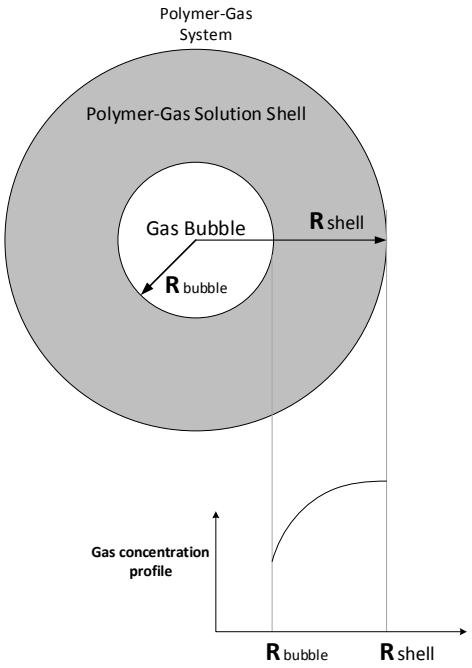

Figure 2.3 A schematic of the Cell Model [5]

Arefmanesh and Advani [89] used the cell model to predict the morphology of foam in a low-pressure structural foam molding process for a group of bubbles growing simultaneously in a Newtonian fluid (polycarbonate). They considered an isothermal condition for the system and an ideal gas behavior for the gas inside the bubble. They also assumed that the concentration of gas inside the polymer shell around each bubble varies with a polynomial profile. In their subsequent studies, they revised their assumptions and considered the viscoelastic behavior for the fluid that was explained by the Upper-Convected Maxwell model and considered the non-isothermal conditions in their studies. In addition, the influence of different parameters on the bubble evolution has been considered, and the results showed that a higher diffusivity coefficient

leads to a higher growth rate while higher viscosity acts as a retarding force against the bubble evolution; however, they reported that the effect of viscosity becomes negligible in the further stages of the growth. Moreover, they assumed that the gas loss in the system is negligible; however, this assumption may not hold in all cases such as foaming through the extrusion process when the extrudate is relatively thin. Despite this drawback, their work helped other researchers to have a better understanding of the foaming process [5].

In 1991, Ramesh et al. [90] proposed a modified viscoelastic cell model, which accounts for the effect of dissolved gas content and temperature on rheological and other physical properties. They developed an experimental technique using scanning electron microscopy and studied the foaming of polystyrene in the microcellular batch foaming process with N_2 and CO_2 as the blowing agent. In addition, the influence of parameters in the batch foaming process of polystyrene was investigated. They used Cell Model to numerically simulate the evolution of bubbles and adopted Power law and Upper-Convected Maxwell models to consider the non-Newtonian behavior of the polymer. They compared their results with the single bubble growth model and experimental data. They observed better compliance between the simulation results and the experimental data when Upper-Convected Maxwell model is used. However, they could only show that their simulations have a qualitative agreement with the trend of experimental results [5]. Later in 1996, Lee and Ramesh [92] modified the viscoelastic cell model to account for the non-isothermal foam growth and gas loss in the formation of foam sheets in the extrusion process. They used Polyethylene as the polymer and CFC-12 as the blowing agent and reported that the heat transfer becomes significant when the sheet thickness decreases to the millimeter range. They studied the effect of different parameters on the bubble growth and resulted that gas loss to the surrounding, dissolved gas content and transient cooling effects are the most crucial factors in their experiments that governed the bubble growth process. In general, the predicted equilibrium radius was in a reasonable agreement with the experimental data within the error bar. In addition, they suggested that the interaction between the bubbles should be considered in order to avoid the deviation from the growth data which were observed [43]. The effect of foam thickness on the foaming quality has been studied by Lee et al. [93]. They used a twin-screw extruder to extrude the solution of LDPE and HFCF-22 into a foam sheet with different thickness. They observed that higher sheet thickness and higher nucleation rate enhance foaming

efficiency. They also concluded that rheology, solubility, and gas loss are the main mechanisms that determine foaming efficiency of thin sheets. In addition, the effect of temperature and gas concentration on the polymer rheology was considered in their work. They showed that the modified model has better agreements with the experimental data; however; they observed that the agreement decreases at a high expansion ratio where the pronounced bubble-bubble interaction led to non-spherical bubbles [93]. Payvar [94] presented a mass transfer-controlled bubble growth model based on the integral method for rapid decompression of ethyl alcohol-CO_2 solution. He tested his model in a test chamber at 25°C where the pressurized ethyl alcohol-CO_2 solution was foamed by depressurization from 0.44- 1.21 MPa to the atmospheric pressure.

Since the bubble growth process follows the nucleation event and both of these processes are consuming and competing for the limited amount of gas dissolved in the polymer, it is essential to consider them together simultaneously to predict foam dynamics accurately. In light of this, Shafi et al. [95] and Joshi et al. [96] proposed an outstanding model, called the Influence Volume Approach (IVA), which describes cell nucleation and cell growth processes simultaneously and study the effects of various processing conditions on the final cell size distribution. By assuming an instant pressure drop, Shafi et al. [95] suggested that the nucleation rate is the highest at the beginning of the process because of the high initial dissolved gas content. As a nucleated bubble grows, both the bubble pressure and the gas concentration at the bubble surface decrease. Through the gas diffusion into the expanding bubbles, a concentration gradient is then generated in the polymer melt around the bubble with time. They derived a nucleation rate equation that included the effects of dissolved gas, small critical cluster size, elasticity, and non-ideal solutions. The volume of the polymer from the bubble surface to the radial position (S) where the dissolved gas concentration is equal to the nucleation threshold (Cs) is called the Influence Volume (V_L) in their work. This nucleation threshold is the concentration of dissolved gas at which the nucleation rate is 2% or less of the nucleation rate at the initial dissolved gas concentration. The volume of the melt outside the influence volume and the bubble is called the non-influenced volume. One of the assumptions of their model is that there is no bubble nucleation inside the Influence Volume. In order to simplify the numerical simulation, they adopted the integral method and approximated the gas concentration profile to be a polynomial function. As more and more bubbles are nucleated and each bubble grows with time, the V_L and

gas concertation inside it decreases with time. The IVA characterizes the interaction between cell nucleation and expansion behaviors by considering the gas depletion around the nucleated bubbles [95]. Various researchers [97, 52] extended the IVA or adopted a similar simulation scheme without using the IVA to conduct computer simulations of cell nucleation and cell growth. In 1998, Joshi et al. [96] extended Shafi's model [95] to the viscoelastic fluid. They described melt rheology using Larson viscoelastic model [98] and concluded that among influencing factors affecting both the nucleation process and bubble growth together, Gibbs number, which is a dimensionless number representing the energy barrier for the nucleation to happen, has the most substantial impact on the cellular structure and morphology of the foams. In 2001, Shimoda [97] extended cell model that was developed earlier by Shafi et al. [95] to the foam extrusion process. They studied the foaming of polypropylene - CO_2 mixture and conducted a series of computer simulations to study the simultaneous cell nucleation and growth in the extrusion process, which also was accounted for the effects of surface tension, diffusivity, and viscosity on plastic foaming. Their study assumed that the cell nucleation occurred heterogeneously on smooth planar surfaces. The computer simulation results of polypropylene foaming, with and without using the concept of IVA, were compared with the experimental data obtained by visual observations of the extrusion foaming. They suggested that polymers with lower surface tension and lower diffusivity are desired to produce foams with finer cells. Furthermore, they also reported that temperature is a critical parameter to control the gas diffusivity and viscosity in order to suppress cell growth and promote cell nucleation. Another beneficial study regarding bubble nucleation and growth in batch and continuous processes was published by Taki et al. [99, 100]. They quantitatively studied the effect of pressure release rate on bubble nucleation and growth in the batch foaming process with the help of an image processing technique. Homo-polypropylene was used in their experiments for the batch foaming process and high melt strength polypropylene for the continuous foaming process.

2.5 Two-dimensional models

Despite the single bubble growth model and cell model which were being investigated by a vast number of researchers and developed over the years, the two dimensional models of the bubble growth process is relatively new and scarce. The earliest simulations start at 2002 when Popinet and Zaleski [101] studied bubble collapse problem in cavitation phenomenon using front

tracking technique and finite volume formulations to solve Navier Stokes equations. Caboussat et al. [102, 103] used a 3D model for simulating liquid-gas flows with free surfaces. They used the volume-of-fluid (VoF) method to track the liquid domain and to calculate the pressure and velocity domain in the fluid. They considered an incompressible fluid and a compressible gas explained by ideal gas law equation. Beechem et al. [104] studied the two-dimensional growth of a non-spherical bubble in a Newtonian liquid of infinite extent assisted for a carbon foam fabrication process. Everitt et al. [105, 106] simulated the two-dimensional growth of a group of gas bubbles arranged in a hexagonal array in a polymeric melt and adopted the split Eulerian-Lagrangian method to solve the finite element formulations. Bruchon et al. [107] studied the two-dimensional expansion of small bubble clusters (mainly three and four bubbles) within a Newtonian fluid and solved Stokes equations to calculate the velocity and pressure contours. They used a level set method in combination with the mesh adaptation technique to track any deformation in the liquid-gas interface. Yue et al. [108] solved the diffusion driven bubble growth in polymer foaming with the moving mesh method that tracks the expanding and deforming bubbles surfaces. They obtained mesh velocity by reconciling between Eulerian and Lagrangian description of a moving boundary and solving the Laplace equation to do that. They studied the growth of a hexagonal array of cells and considered the effect of polymer viscoelasticity in the growth dynamic by choosing the Oldroyd-B model for describing the rheology of the polymer.

2.6 Summary of the literature Survey

In summary, there has been a substantial experimental and numerical effort for more than a century in proposing accurate models for both nucleation and growth processes. Despite the longtime efforts and interest in investigating bubble nucleation phenomenon in polymer foaming process, the consistency between the prediction of nucleation models and experimental results is still unsatisfactory. However, many studies [109, 97]showed that the cell nucleation during the polymeric foaming process is more likely to happen heterogeneously rather than in homogeneous type. As a result, they considered the heterogeneous nucleation mechanism as the main method for the bubble nucleation phenomenon in their simulation of plastic foaming processes [5].

In reality, cells are formed from pre-existing gas cavities during plastic foaming processes. These gas pockets can exist in any unknown additives as well as impurities, and the internal walls of the processing equipment, which contains many crevices. However, it is extremely difficult, if not impossible, to precisely determine the initial number of pre-existing cavities and their corresponding sizes. Therefore, a purely theoretical model that can predict the number of nucleated bubbles in the plastic foaming process having a quantitative agreement with the experimental data is not yet proposed [5]. Nucleation models that were proposed in the literature are semi-experimental, and they vary in the degree of reliance on the experimental data. Some of the researchers such as Leung [5] tried to reduce this reliance by estimating the number of nucleating agents that were added to the polymer and by modeling the surface of the nucleating agents as a series of conical pits and crevices. With this modified nucleation model, they could reach to a better estimation of the number of cells, however, since the nucleating agents vary in geometry and their surfaces are not identical, they used a probability density function to account for the randomness of the conical angles. In addition, they obtained the value of the contact angle (θ_c in Figure 2.2) by using the trial and error method and comparing with the experimental data. Therefore, although the reliance on the experimental data diminished but, it did not vanish. Moreover, the effect of gas cavities which are inside the polymer matrix still exists.

Another method is using correction factors such as pre-exponential factor and energy reduction factor [54] in the nucleation rate equation that will be explained in section 3.9. These factors should be chosen for a constant temperature profile and nucleating agent amounts and can be

used for various saturation pressure. Although these factors should be chosen again for different temperature profile and nucleating agent amount, it is much easier than the modified nucleation model proposed by Leung [5]. In this thesis, we adopted this model, and the formulations are presented in section 3.9.

The nature of the bubble growth dynamic is complicated and requires simultaneous consideration of mass conservation, momentum conservation, diffusion effect and viscoelastic nature of the polymer. Due to this complexity, the majority of the growth models that have been proposed so far have simplified the problem by assuming a uniform evolution of bubbles in all dimensions and solving the one-dimensional form of equations. The "single bubble growth model" and "cell model" are two well know models that use this simplification. They have been used by many researchers and developed over the years in different experimental environments. The cell model can predict the growth dynamic with enough precision before that the interaction of bubbles become important. However, if the mutual influence of bubbles become considerable, the cell model deviates from reality and overestimate the final bubble radius. Thanks to the increased computational capabilities of the computers, the two or three-dimensional forms of governing equations can be solved, and nonlinear behavior of the materials can be considered. Two-dimensional simulation of the foaming process has been addressed recently [101], and despite that the approach is relatively new, the results are promising. They can consider the nonuniform deformation of bubble boundaries and can consider the mutual interaction of cells. These interactions include the competition for the limited gas consumption and the retarding forces they exert to each other. In this thesis, two-dimensional forms of governing equations namely, mass conservation, Navier stocks equation, convection-diffusion equation, and Oldroyd-B equation, have been used to describe the bubble growth phenomenon. The complete forms of these equations are presented in section 4.2.1. The Finite element analysis based on Galerkin formula has been adopted to solve the coupled partial differential equations. Freefem++ software [110] have been used for this purpose, and the weak form of equations entered to this software for further analysis. The Eulerian approach has been used for moving mesh vertices, and mesh adaptation technique based on the velocity field in the domain was used whenever it was required.

Chapter 3: Experimental Analysis

3.1 Introduction

In order to address the practical aspect of this study, a series of experiments have been performed on the foaming of polypropylene in the extrusion process. The practical aspects of these experiments gave us valuable insights that were complementary to the results of numerical simulation. In this chapter, several aspects of experimental studies are discussed including the choice of the materials, material characterization, sample preparation, equipment capabilities, etc. This information helped us to have a more realistic vision of the extrusion process.

3.2 Differential Scanning Calorimetry (DSC) Test

In order to find the thermal characteristics of our polypropylene, Differential Scanning Calorimetry (DSC) test has been performed. DSC is a method for finding thermal properties of polymers or polymer composite materials. During DSC tests, the sample is heated with a specific temperature profile (linear ramp or step), and the amount of the energy that has been absorbed or released by the sample is recorded. This test can be used to measure important properties of the polymer such as glass transition temperature, melting temperature, heat capacity, the energy required to melt a polymer, degree of cure, the rate of cure, progress of a chemical reaction, and thermal history of a sample. DSC curves, which shows heat flow with respect to the temperature, have some important features that can be analyzed to derive the above properties. First, Negative value in the heat flow curves means energy is entered to the material sample, and a positive value means heat comes out of the sample. Figure 3.1 shows three different curves which correspond to three different heating and cooling cycles. The black line (darkest line) shows the first heating cycle of the polymer I which the temperature of the polymer increase from $-40℃$ to $250℃$. After the first heating cycle, the material cools down from $250℃$ to $-40℃$ and the grey curve at the positive side of Y-axis (heat flow) represents that cycle. The polymer again undergoes the second heating cycle and the second grey line in the negative side of Y-axis illustrates that. When the values of the heat flow is negative (heating cycles), the curve is placed in the negative side of the diagram, and when the heat flow is positive, it corresponds to the cooling cycle of the polymer. In order to obtain the glass transition temperature (T_g) and melting point (T_m) of the material, the first heating cycle of the polymer has to be considered. This curve has different

slopes at different temperatures. The slope at any point on the diagram indicates the amount of the energy required to increase the temperature of the material for an additional 1℃ and often refers to the heat capacity of the material. Figure 3.2 shows a magnified part of Figure 3.1 between 110℃ and 180℃. In Figure 3.1, there is a sharp change in the slope of the diagram at 124.63℃. As explained, a change in the slope of the diagram shows a shift in the heat capacity of the sample, and therefore a dramatic change in the microstructure of the materials. Above this temperature, the sample is a soft material and below this temperature is a glassy one. The temperature at this point of the diagram is called the glass transition temperature (T_g) of the material, and the midpoint temperature is selected here as the T_g. By increasing the temperature of the material, a negative peak appears at 164℃ in Figure 3.1which corresponds to the melting phenomenon. The area between the curve and the zero heat flow line up to this point indicates the amount of the energy that is required to break the bonds between the molecules of the polymer for the melting to happen.

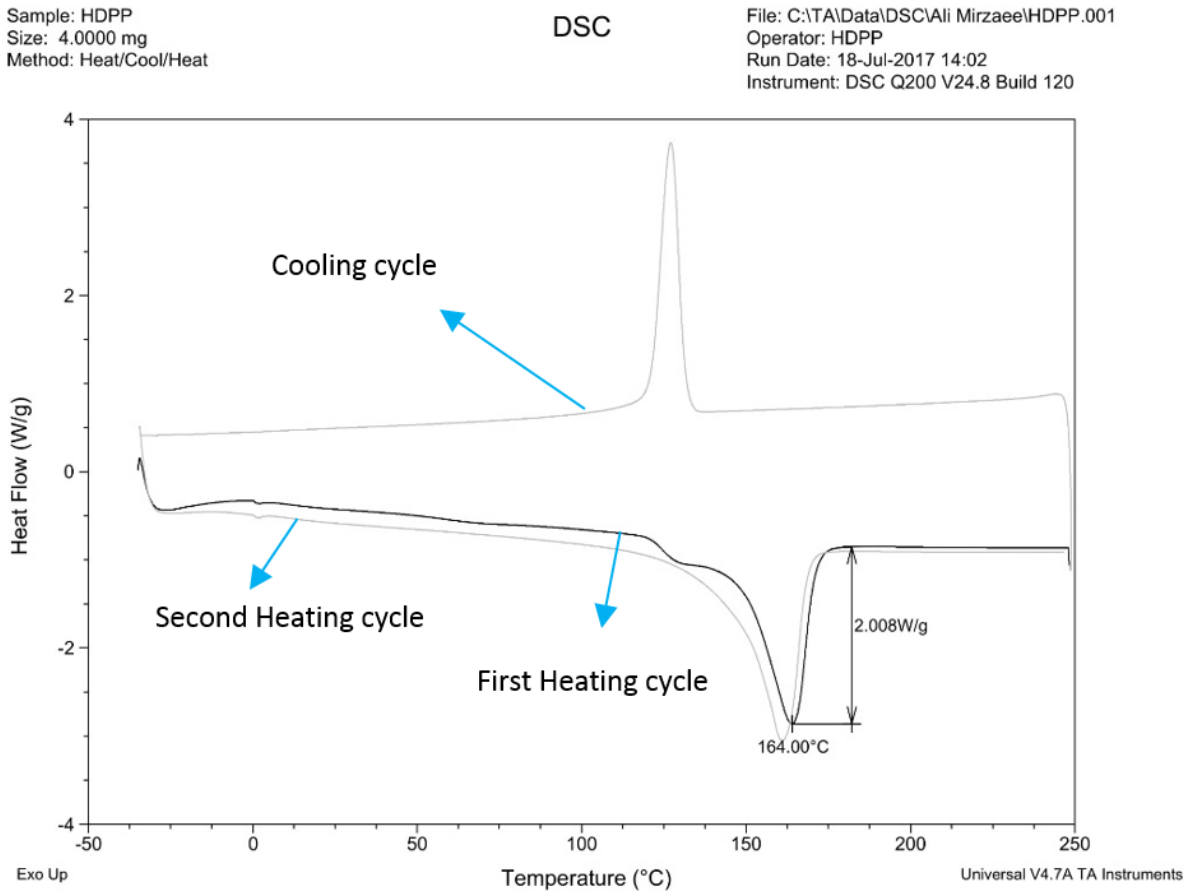

Figure 3.1- The results of the DSC test on the "Daploy™ WB140 HMS" Polypropylene

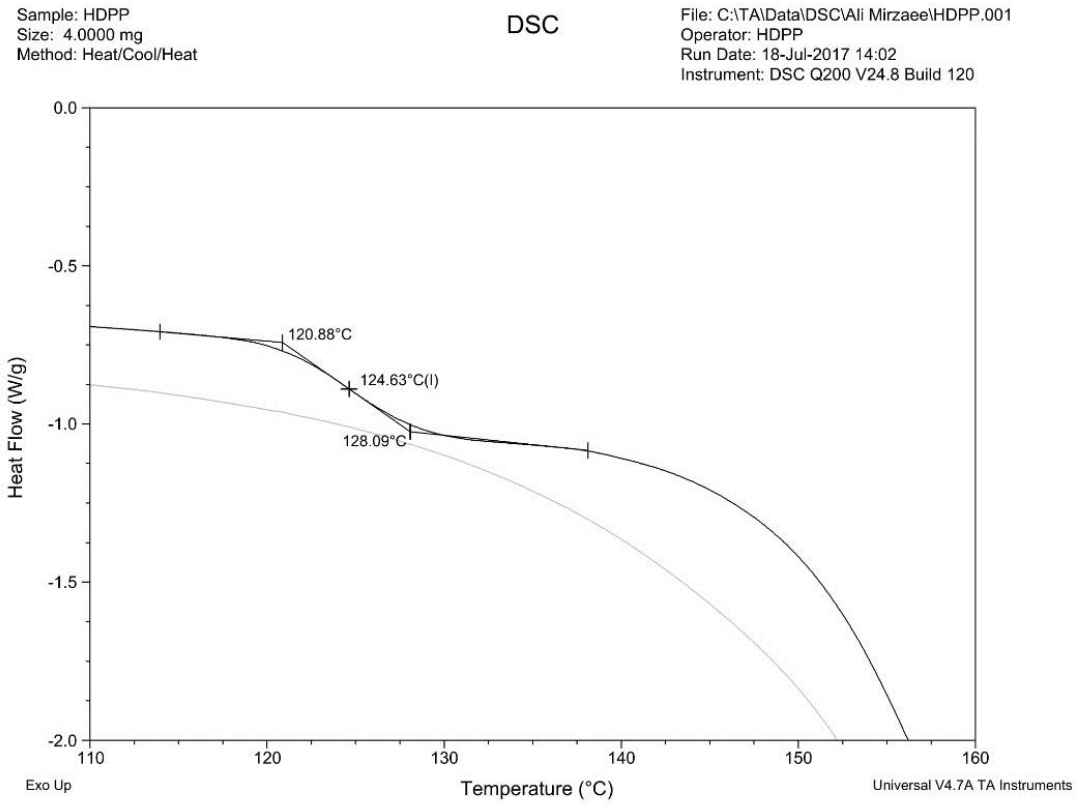

Figure 3.2- The changes in the slope of the diagram around the Glass Transition Temperature (Tg) at the hating cycle

3.3 Types of Chemical Blowing Agent

According to the explanations given in the previous chapter, chemical blowing agents (CBA) are materials in the form of powders or pellets that generate gas upon decomposition at high temperature. Depending on the heat flow during their decomposition, they can be classified into Exothermic CBAs or Endothermic CBAs. Endothermic CBAs are the ones that absorb energy from the environment during their decomposition and generate environmentally neutral gases such as CO_2 and water vapor. Examples of endothermic CBAs are sodium bicarbonate and citric acid [111]. One of the advantages of endothermic CBA is that if the heat source is removed, gas production comes to a standstill and resume state if further heat is provided, therefore, they are more controllable than Exothermic ones [112]. One the other hand exothermic CBAs release energy and liberate gases such as N_2, CO_2, and ammonia at the decomposition temperature. A

well-known example of Exothermic CBAs is Azodicarbonamide that generates N_2. Once decomposition starts among exothermic CBAs, it continues independent of the heat source, because the heat generated by one reaction triggers the decomposition of the others. Therefore, they are less controllable than exothermic ones; however, they can yield more gas content in a limited range of temperature and fewer amount of material which can be a huge advantage in an industrial case. In a large scale, any saving in the raw materials can results in a significant amount of revenue since they are usually more expensive than their physical blowing agents counterparts. Producing foam using CBA have some advantages over PBA such as it is not necessary to modify the equipment because the material can be used alongside the base material through the hopper and it is easier to achieve a more uniform distribution of gas in the polymer matrix.

There are some important points which require more attention when choosing a CBA for the extrusion foaming process. First, the decomposition percentage of the CBAs is a function of temperature; thus; they decompose more as the temperature goes up. In other words, the amount of gas they liberate depends on the temperature so they should be heated to a high enough temperature to generate a sufficient amount of gas in the extruder. On the other hand, each polymer has its range of operating temperature in the extrusion process, which beyond that may be degraded. Therefore, the selected CBA for a specific polymer should generate enough gas before reaching to the upper limit of that window and should not liberate more than the required gas at the lower limit of the window considering that the polymer has a high viscosity and is not suitable for mixing at that temperature. Furthermore, a great CBA should have a fast rate and enough decomposition in the range of operating temperatures since the liberated gas needs to have enough time to be mixed and solved evenly in the melted polymer.

Another critical issue is the size of CBA particles. They can vary in shape and size from powder forms of few micrometers to the pellet shapes or cubes of the size of 3mm in edges. The size of CBA has a significant impact on the final cell size and cell density. Many parameters can affect the size of CBA particles, but the most important parameters are the size of the extruder and the final cell sizes. A powdered CBA can better distribute inside the melt; therefore, gas molecules generated by them has a more interface area with the melted polymer and can be solved faster in the polymer to produce a uniform mixture. If a huge amount of gas is accumulated at a certain

point inside the polymer, they may create undissolved gas pockets inside the melt and severely undermine the uniformity of the resulting foam structure. Thus, small sized CBAs have important advantages for producing a uniform cell morphology and high-quality foams. However, in industrial case extruders, larger CBA also can be used due to the large scale of equipment and longer processing time. In addition, CBAs particles should not stick together or to the interior wall of the extruder at high temperatures. Agglomeration of particles severely undermines final foam quality due to the insufficient gas generation and non-uniform distribution of cells.

For the cases of our experiments, we tried different types of chemical blowing agents both endothermic and exothermic ones. In order to obtain the decomposition percentage of the CBAs as a function of the temperature, the Thermal Gravimetric Analysis test has been performed. Figure 3.3 to Figure 3.6 show the results of Thermal Gravimetric Analysis test (TGA tests) for two types of endothermic CBA and two types of exothermic ones. During the TGA test, a small sample of the chemical blowing agent, which was initially weighted, is heated up to be decomposed and generate the gas. The weight of the material is measured at each time during the test and the results will be calculated as the weight percentage at different temperatures. The endothermic CBAs were Foamazol 70 and Foamazol 90 from "BERGEN International Co. [113]" and exothermic ones were XOP-300 from "BERGEN International Co. [113]" and Azodicarbonamide from "Polychem Dispersions Inc. [114]". Among Endothermic CBAs, Foamazol 90 have a better decomposition ration (up to 32.5% until 215℃) compare to the Foamazol 70. In addition, Foamazol 70 agglomerated in the melt and stuck to the screws, which make it not a suitable choice for our lab-scale extruder. Exothermic ones have a better decomposition ratio compare to the endothermic ones. XOP-300 decompose up to 35% until 220℃ which is one of the maximum temperatures we can use. On the other hand, Azodicarbonamide have a high decomposition speed around 250℃. It can be decomposed up to 60 % in less than 2℃ which make it very much interesting for foaming application but the size of AZ pellets are relatively large compared to the size of our extruder. In addition, it is decomposed at a temperature higher than the range of interest. In conclusion, considering the pros and cons of all tested CBAs, Foamazol 90 and XOP-300 have been used mostly in our experiments and some rare cases Azodicarbonamide.

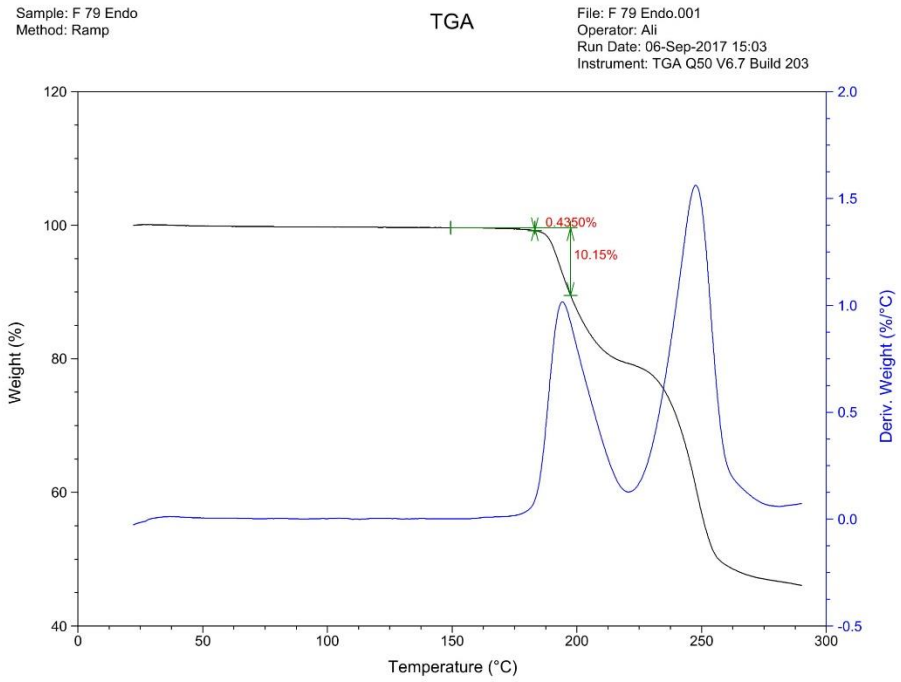

Figure 3.3 The result of the TGA test for Foamazol 70 (Endothermic)

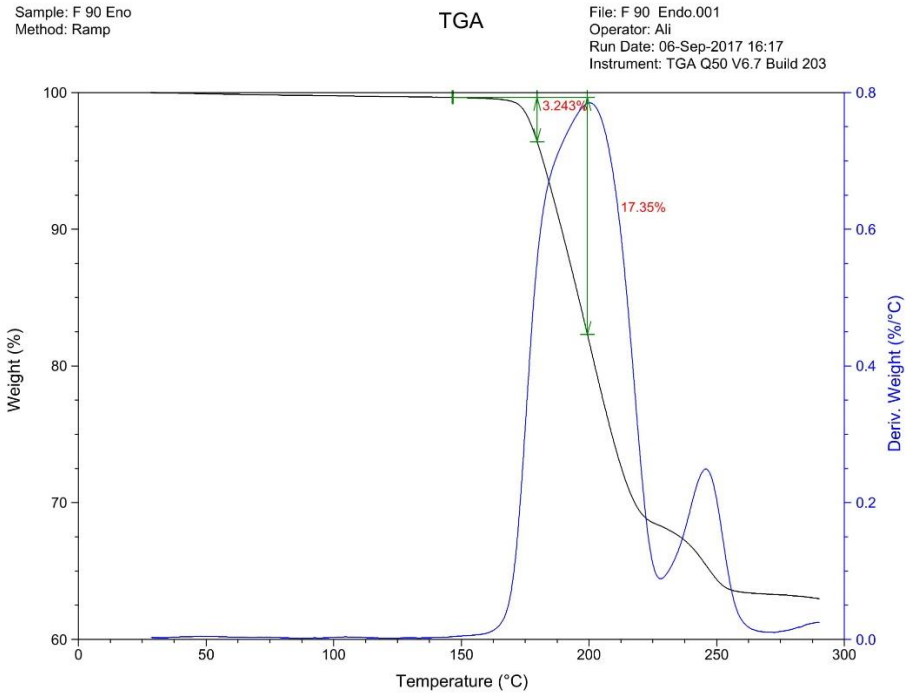

Figure 3.4 The results of the TGA test for Foamazol 90 (Endothermic)

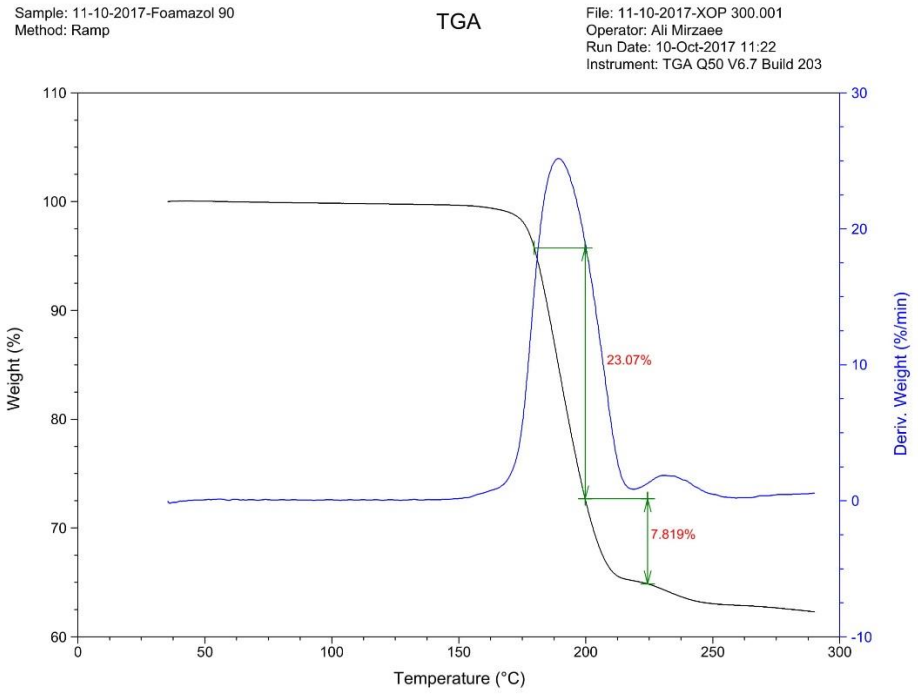

Figure 3.5 The results of the TGA test for XOP-300 (Exothermic)

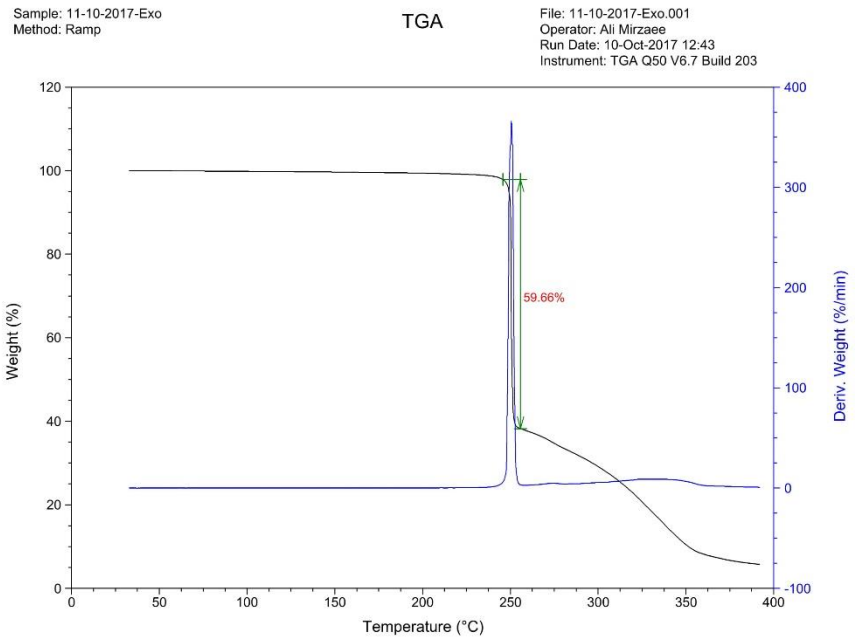

Figure 3.6 The results of the TGA test for Azodicarbonamide (Exothermic)

3.4 Equipment

"Thermo Scientific Process 11" [115] is a twin-screw extruder that was used for producing polypropylene foams in our experiments. This machine is a lab-scale extruder, which is ideal for producing small batches of foam. This device can be controlled precisely during the extrusion of high-viscous melts and therefore is ideal for scientific researches in the polymer foaming field. As shown in Figure 3.7, this device is composed of several units including a barrel in which the main extrusion process happens there, and a feeding device (Figure 3.8), a water bath (Figure 3.8), a Pressure sensor (Figure 3.9), a cooling system and a vacuum system (Figure 3.9). In addition, the specific characteristics of our micro extruder are summarized in Table 1.

Figure 3.7 Thermo Scientific Process 11 twin-screw extruder

Figure 3.8 Different parts of twin-screw extruder: The hopper and the barrel (Left) and the Water bath (Right)

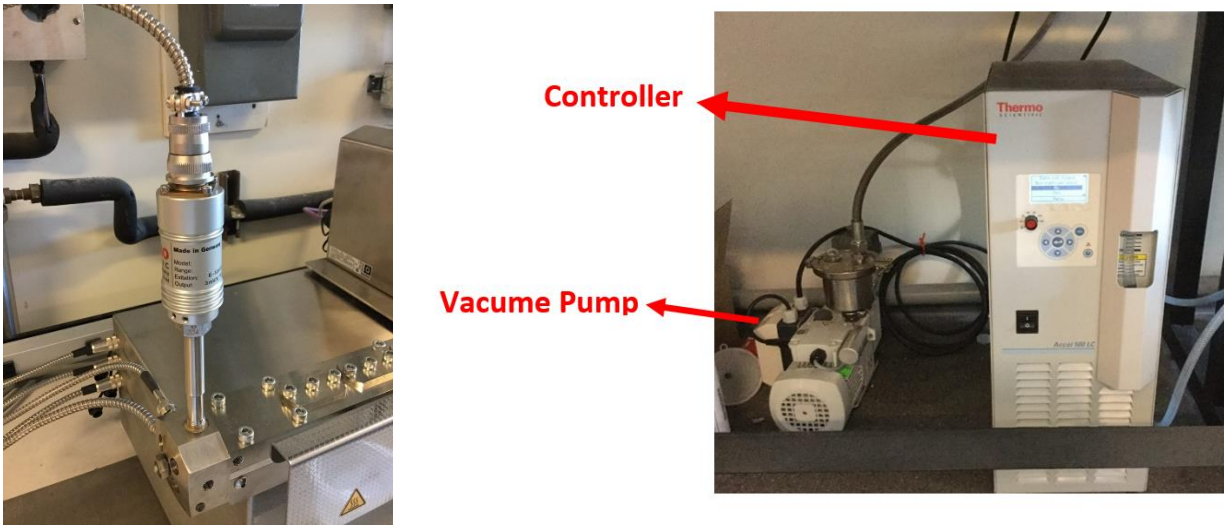

Figure 3.9 Different parts of twin-screw extruder: The pressure sensor (Left) and controller (Right)

Table 1 Characteristics of the "Thermo-Scientific Process 11" twin screw extruder

Quantity Name	Value
Barrel Diameter	11 mm
Barrel Length	440 mm
Barrel Segments	8
Independent heating zone	7 internal + 1 external for die
Heating capacity	1750 W
Temperature range	< 350℃
Maximum pressure	100 bar (1450 psi)
Screw speed range	10-1000 rpm
Max screw torque	12 N.m

3.4.1 Typical screw sections at the barrel

Based on the position in the barrel, an extruder screw can vary in geometry along the barrel. A typical screw has three different zones (Figure 3.10).

Feed Zone: The materials are fed to the barrel through this zone. This section is responsible for heating the materials and conveying them to the next sections. The design of the screws in this section should be performed to result in a smooth and constant flow of the materials to the next zones to avoid starvation and overflow conditions. At this zone, the materials turn to a softer state such that the extruder can push them forward [116].

Compression Zone: At this zone, the depth of the screws gradually decreases to reduce the amount of free spaces inside the barrel and to compact the material. At this point, those air pockets, which are not solved in the polymer yet, would be entirely mixed with the melted

polymer. In addition, the heat transfer from the barrel to the material increases at this zone since the contact area between the materials and barrel increases due to the compaction [116].

Metering Zone: The screw depth is reduced at this zone but remains constant throughout the zone. The polymer melt will be homogenized at this section and fed as a uniform polymer-gas solution to the die [116].

3.4.2 Temperature Profile inside the barrel

Our twin-screw extruder has eight heating zones, which can be controlled independently. The selection of a temperature profile for the extruder depends on several parameters such as equipment capabilities (extruder type, heating power, cooling system, maximum available torque, extruder size), polymer properties (glass transition temperature, melting temperature, degrading temperature, viscosity as a function of temperature), characteristics of the chemical foaming agent (decomposition data at each temperature), desired foam morphology (cell density, cell size, cell distribution). A complete understanding of the above parameters is necessary for selecting the temperature profile of the barrel. The first section of the barrel is the feeding section where the materials (polymer, CBAs, additives) are fed to the extruder and gain heat in the first heating zone. In order to prevent early decomposition of CBA particles and gas loss from the hopper, the temperature in the first heating zone should be lower than the decomposition temperature of the chemical foaming agents, adopted for the experiment. On the other hand, the temperature of the first zone should be above the melting point of the material to some degrees in order to prevent agglomeration of polymer pellets. The polymer pellets are fed as a solid material to the extruder, and if their temperature does not rise fast enough to turn them into the melted state, the screws cannot push particles forward to the next heating zone since screw torque cannot exceed a certain limit. By increasing the temperature of the polymer above the melting point, polymers can smoothly flow to the next stage and agglomeration, and over-torque situations will be prevented. At the next stages, the temperature should be increased gradually to a maximum in order to trigger the decomposition of CBA particles in the melt. By decomposition, CBA particles liberate gas that can be solved inside the melted polymer at high pressure. Another important effect of increasing temperature is decreasing the melt viscosity, which then itself facilitates the mixing process of the components inside the barrel. As a result, CBA particles, gas molecules and additives can disperse thoroughly in the polymer melt so that

a uniform mixture can obtain. The choice of maximum temperature depends on the required amount of gas in the foam. At higher temperatures, more gas will be generated, but if the generated amount exceeds the maximum solubility at the pressure and the temperature of the die, undissolved gas pockets will appear that will result to a non-uniform bubble structure and then severely deteriorates the mechanical properties of the final foam.

After that the maximum temperature and pressure have been reached, the temperature at the next heating zones can be selected equal or to some degrees lower than the maximum temperature. The reason is that after the maximum amount of gas has been liberated, it requires some time to be solved in the melt and to disperse evenly in the polymer. Moreover, lowering the temperature increases the solubility of the melt which results in the faster solution of the gas and possible gas pockets. In addition, higher viscosity at lower temperatures increases the pressure build up in the last final stages up to the die section. Therefore, lowering the temperature in the final stages is always favorable if feasible. A temperature profile has been illustrated in Figure 3.11 for the polypropylene with the melting point of 169ºC and XOP 300 as the CBA that aimed to be decomposed to 32.5 % at the 210ºC.

3.4.3 Pressure Profile inside the Barrel

A pressure profile sample is depicted in Figure 3.12. The filling point is a point where the melt inside the barrel fills the entire cross section of the extruder and after this point; the pressure starts to build up. If the decomposition of CBA and gas generation happen before the filling point, the resulting gas can be escaped partially or entirely through the hopper of the feeding zone. Any decomposition of CBA has to happen after the filling point and initiation of the pressure buildup. A typical industrial barrel for foam production has three zones (Feeding, Compression, and Metering/Mixing). A good result can also be achieved by having degassing screws or some other optional screws that can increase the efficiency of the process and eliminate the possible faults according to the requirements of each case. Valuable information about designing extruder screws is reported vastly in the literature [117, 118]

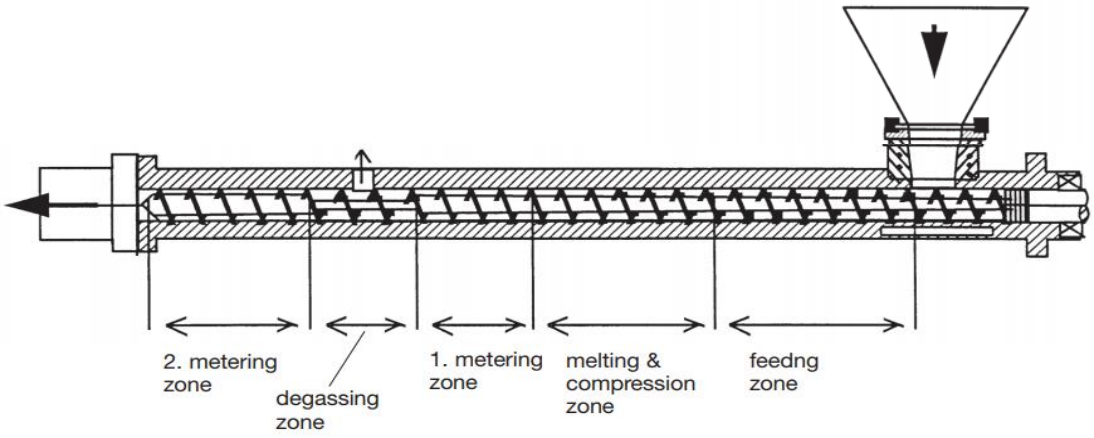

Figure 3.10 Typical screw sections at the barrel [119]

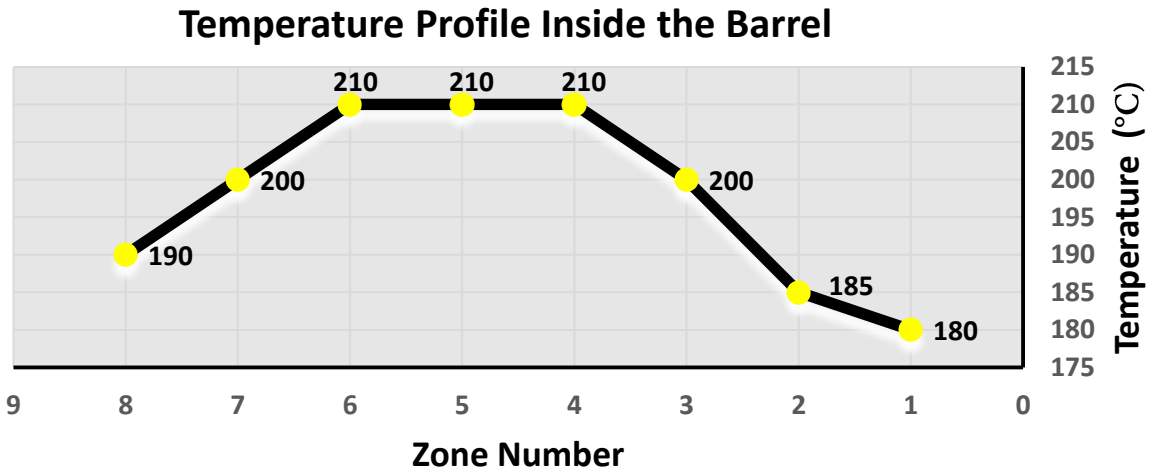

Figure 3.11 A typical temperature profile inside the barrel

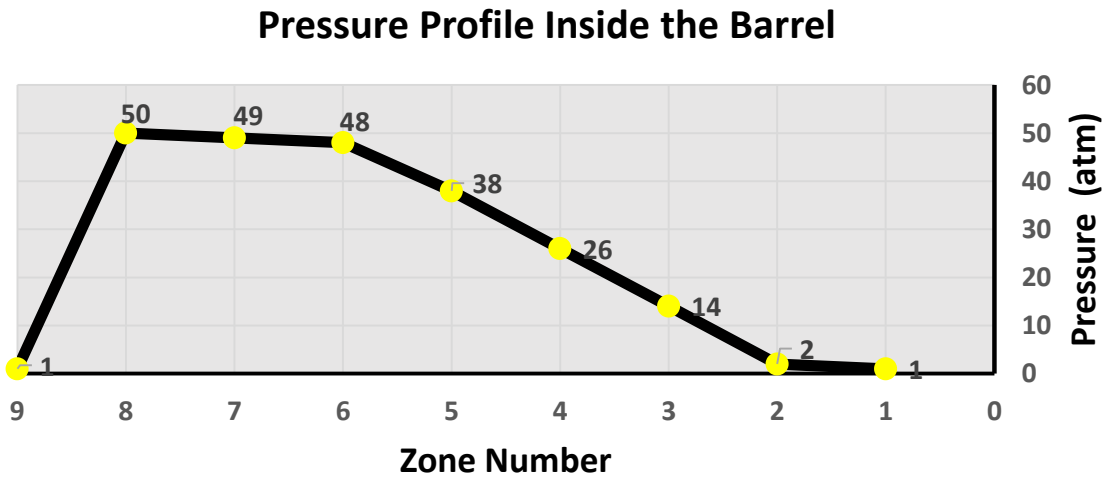

Figure 3.12 A typical pressure profile inside the barrel

3.5 Solubility

The formation of polymer/gas solution is a critical factor in foaming industry. Nucleation occurs when the dissolved gas in the polymer at high pressure and temperature is subjected to the thermodynamic instability. This thermodynamic instability can happen by either lowering the pressure or increasing the temperature so that the polymer becomes supersaturated and the excess amount of the gas appears in the form of bubbles in the polymer matrix. Therefore, a thorough understanding of the solubility of the blowing agent introduced into the polymer is a crucial factor in the foaming process. Understanding the maximum amount of the gas that can be solved in a polymer melt have a huge impact not only in the nucleation phenomenon but also in the subsequent steps such as cell growth and cell stabilization which are defined as the kinetic part of foaming process. There is substantial interest among researchers in measuring the solubility of blowing agents in the polymers, and they used several theoretical and experimental methods to do that. Sato et al. [120, 121] have investigated the solubility of N_2 and CO_2 in the PP and PS through pressure decay approach. This method involves measurement of any changes of the pressure inside a chamber that is filled with the gas and is in direct contact with the polymer melt. During time polymer tries to absorb the gas and causes some changes in the chamber pressure. This method is cost-effective and straightforward, but it is time-consuming and requires a pressure sensor with high precision and tolerance at elevated temperatures (melt temperature). Also, it is only applicable for gases whose equation of states are known. Wong et al. [122] used another method called the gravimetric technique by employing an electrobalance to measure the solubility of CO_2 in PS and PVC. In this technique, a balance is established between the sample and a reference by an electrobalance system at the beginning. The sorption of the gas by the melted polymer at a desired pressure increases the mass of the sample, and this extra mass requires different current to establish a new balance with the reference. This method is more accurate and requires less time for measurement. However, it is limited to work at low temperatures.

In order to solve the limitations associated with the operation range in gravimetric techniques, a new method called Magnetic Suspension Balance (MSB) is invented. In this method, a basket containing a sample material is connected to a rod which itself is connected to a permanent magnet. The whole system is enclosed inside a sorption chamber. An electromagnet placed outside of the chamber attract the permanent magnet and keep the rod-basket assembly in suspension. A microbalance measures a

weight that is proportional to the electromagnetic force which kept the rod-basket system in suspension. The gas which will be absorbed by the sample makes the rod-basket assembly heavier, and therefore more electromagnetic force is required to keep the assembly in suspension. The microbalance measures this force. Eventually, an equilibrium is reached when the weight of the sample stops increasing [123].

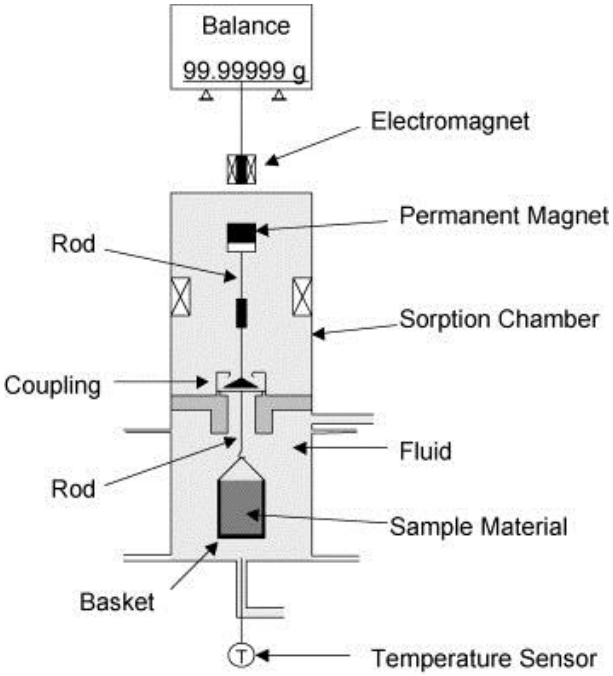

Figure 3.13 Magnetic Suspension Balance (MSB) method for measuring the solubility of a gas inside a polymer [124]

Sato et al. [120] also used the Magnetic Suspension Balance (MSB) method for finding the solubility of N_2 in PS and PP/PS mixture. Hasan et al. [125] used this method to measure the solubility of CO_2 in the linear and branched polypropylene. They observed that solubility increased linearly in both molten polymers by pressure increase up to 20 MPa, and decreased by increasing temperature.

Regardless of the method of solubility measurement, the buoyancy effect, which is a result of swelled polymer dissolved by the gas has to be considered. This effect causes all the solubility measurements by the mentioned methods to be less than their actual values. The measurements achieved by these methods is called apparent solubility and is less than the actual solubility. A proper equation of states is needed to account for the buoyancy effect. The Sanchez-Lacombe (SL) is a well-known equation

of states (EOS) to account for the buoyancy effect among researchers. Li et al. [126] measured the apparent solubility of N_2 and CO_2 in the polypropylene using MSB method. They used Sanchez-Lacombe (SL) equation of state to predict the swollen volume that accounts for the buoyancy effect. Their results are briefly mentioned here in Figure 3.14.

Solubility has important impacts on designing the extrusion process. Pressure profile and temperature profile have to be chosen such that no undissolved gas pocket appear inside the melt before exiting the die, therefore, it is required for the system pressure to be equal or higher than the solubility pressure of the amount of the gas presented in the molten polymer.

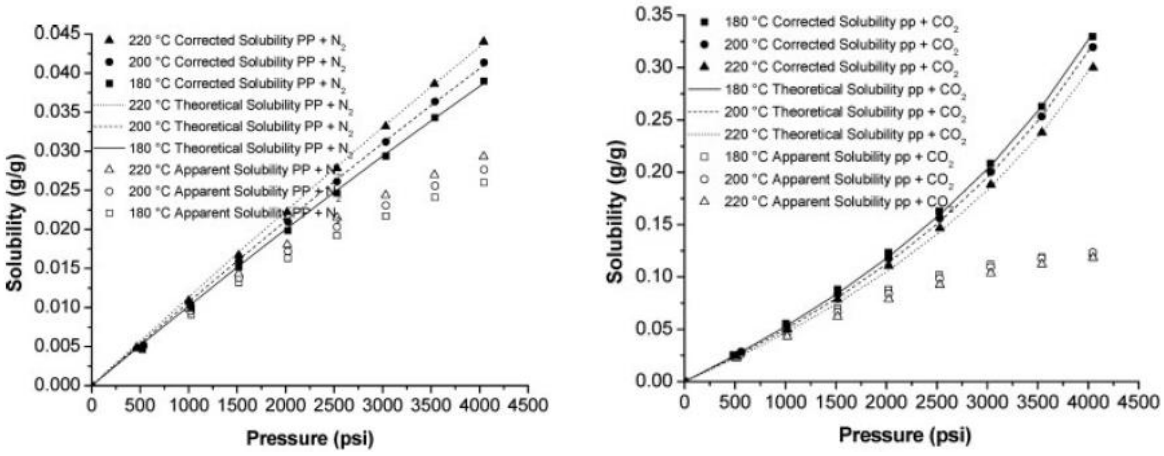

Figure 3.14 Solubility of CO_2 and N_2 in the polypropylene at different pressures and temperatures [126]

According to the the above figures, pressure changes have higher impacts on the solubility of CO_2 in polypropylene than that of N_2. In addition, CO_2 can be solved in a higher content in PP than N_2. The chemical blowing agent that was used in our experiments generate CO_2 upon decomposition; therefore, it is possible for us to use the results of Figure 3.14 in our calculations.

3.6 Diffusivity

The growth of bubbles in a polymer gas solution is a diffusion driven process, therefore understanding the effective parameter on the diffusivity is of great importance. Diffusivity of a gas in a polymer can be affected by the temperature, pressure and gas concentration inside the melt [111].

The dependency of diffusivity to the temperature can be approximated by the following formula [117]:

$$D = D_0 \exp\left(-\frac{\Delta E_D}{R_g T_{sys}}\right) \qquad \textit{Equation 3.1}$$

Where D_0 is the diffusivity coefficient constant, ΔE_D is the activation energy for diffusion, R_g is the universal gas constant, and T_{sys} is the system temperature (melt temperature). This relation shows that the diffusivity increase at a higher temperature. Because it is required to have advanced equipment to measure the diffusivity for the polypropylene, we used the data that was available in the literature for the PP at 180℃ by Park et al [127] .

3.7 Classical Nucleation Theory (CNT)

The Classical Nucleation Theory (CNT) is a theory to predict the onset of bubble nucleation based on thermodynamics. The history of the evolution of this theory has been explained extensively in chapter 2. In this section, the theory is explained briefly, and the formulas that are required for further calculations is presented completely. This theory was first proposed by Gibbs [128] and developed and revised by many researchers during the years [129]. CNT suggests that if the size of a bubble is larger than the size of the critical bubble (R_{cr}) can overcome the energy barrier for bubble nucleation and grows spontaneously and those that have a radius smaller than the radius of the critical bubble cannot survive. This theory is classified into two types namely classical homogeneous nucleation and classical heterogeneous nucleation. CNT can describe nucleation processes with enough precision when the process is under the extreme control that no pre-existing gas pockets exist inside the medium of interest [43], however, in some applications such as plastic foaming, it is reported by many researchers that CNT overestimates the energy barrier needed for bubble nucleation [129]. The actual cell nucleation rate is higher than the one predicted by CNT; therefore, researchers have proposed another class of nucleation by refining the assumptions of CNT. They proposed that the activation of pre-existing gas cavities inside the medium is the main reason for nucleation. This type of nucleation is called Pseudo-Classical Nucleation [5]. In summary, the nucleation phenomenon can be classified as below:

3.7.1 Classical Homogeneous Nucleation

This type of nucleation explains nucleation in the uniform bulk of liquid and assumes that there are no impurities or gas cavities prior to depressurization. This theory showed acceptable compliance with the experimental results only in the simple liquid-gas solution when extreme care is taken to remove any impurities from the liquid [43]. Tucker et at. [130] performed some experiments to test the validity of CNT in predicting the critical radius during the growth and collapse of two bubbles in water-oxygen solution. However, in other applications with more complexity such as plastic foaming, CNT oversimplifies the problem and will no longer able to predict the nucleation process accurately [5].

3.7.2 Classical Heterogeneous Nucleation

Classical Heterogeneous nucleation accounts for the nucleation at the solid/liquid or liquid/liquid interface. In this type, nucleating sites such as small solid particles dispersed inside the liquid are the only places where bubbles can appear and grow. Like the first type, it assumes that there are no gas cavities in the liquid or at the surface of nucleating sites. The energy barrier for nucleation is lower in this type compared to its homogeneous counterpart, and therefore, it is more likely for the bubbles to appear and grow on the surface of impurities or solid particles that were added to the liquid or had been existed initially in the polymer. The geometry of the nucleating sites affects the amount of energy required for heterogeneous nucleation. These geometries can vary from planar surfaces to the conical or spherical surfaces [5].

3.7.3 Pseudo-Classical Nucleation

Pseudo-Classical Nucleation explains the nucleation as the growth of pre-existing gas cavities which are trapped between the molecules of polymer or are stored in the pores and cracks of impurities or nucleating agent or wall of the equipment. When supersaturation occurs in the solution due to the depressurization, the value of R_{cr} starts to drop. When R_{cr} becomes smaller than the radius of gas pockets, they start to grow immediately. These microvoids can exist anywhere inside the bulk solution or at the surface of nucleating agents. Hence, Pseudo-Classical Nucleation accounts for both homogeneous and heterogeneous nucleation at the same time [43].

3.7.3.1 Free energy barrier for homogeneous nucleation

According to CNT, the energy required for a bubble to nucleate in a homogeneous liquid-gas solution is given by:

$$\Delta F_{hom} = -\left(P_{bub} - P_{sys}\right)V_g + \gamma_{lg} A_{lg} \qquad \textit{Equation 3.2}$$

Where P_{bub} is the pressure inside the bubble, P_{sys} is the pressure of the system surrounding that bubble, γ_{lg} is the surface tension of the gas-liquid interface, V_g is the bubble volume and A_{lg} is the bubble area. Equation 3.2 is composed of two components. The first term, $-\left(P_{bub} - P_{sys}\right)V_g$, is the work done by the expansion of the bubble to the volume V_g, and the second term is the work required for to create the liquid-gas interface. If we assume that the bubble is a perfect sphere, the volume and surface are of the bubble can be expressed in terms of its radius namely:

The result of plotting ΔF_{hom} versus R_{bub} is Figure 3.15. As can be seen in this plot, there is a maximum for ΔF_{hom} in this diagram which is the free energy barrier for homogeneous nucleation and R_{bub} corresponding to this maximum is the critical bubble radius (R_{cr}) for homogeneous nucleation. By

$$\Delta F_{hom} = -\left(P_{bub} - P_{sys}\right)\left(\frac{4}{3}\pi R_{bub}{}^{3}\right) + \gamma_{lg}\left(4\pi R_{bub}{}^{2}\right) \qquad \textit{Equation 3.3}$$

differentiating from Equation 3.3 with respect to R_{bub} and equating it to zero, R_{cr} can be obtained as below:

$$R_{cr} = \frac{2\gamma_{lg}}{P_{bub,cr} - P_{sys}} \qquad \textit{Equation 3.4}$$

Where $P_{bub,cr}$ is the pressure inside the bubble at the critical state. By substituting this expression into Equation 3.3, W_{hom} which is the energy barrier for homogeneous nucleation can be obtained as:

$$W_{\text{hom}} = \frac{16\pi\gamma_{\text{lg}}^{3}}{3\left(P_{bub,cr} - P_{sys}\right)^{2}} \qquad \textit{Equation 3.5}$$

The difference between bubble pressure at a critical state and system pressure $\left(P_{bub} - P_{sys}\right)$ is called the degree of saturation. Equation 3.3, 3.4, 3.5 indicating their dependency to the surface tension and degree of saturation. Among these, surface tension seems to have a higher influence on W_{hom} than the degree of supersaturation due to its higher power.

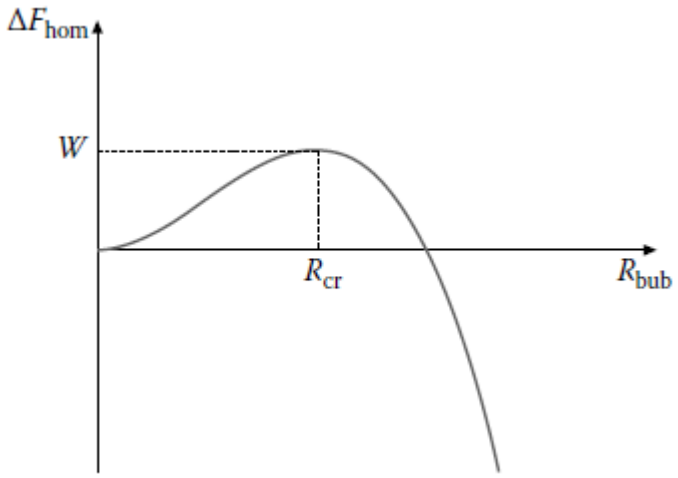

Figure 3.15 W_{hom} versus R_{bub} [5]

3.7.3.2 Free energy barrier for heterogeneous nucleation

The approach for finding R_{cr} and free energy barrier for heterogeneous nucleation (W_{het}) is the same as homogeneous one. The free energy changes for the formation of a bubble heterogeneously on the surface of the liquid/solid interface from a metastable state of liquid-gas solution can be obtained as:

$$\Delta F_{het} = -\left(P_{bub} - P_{sys}\right)V_g + \left(\gamma_{\text{sg}} - \gamma_{sl}\right)A_{s\text{g}} + \gamma_{\text{lg}}A_{\text{lg}} \qquad \textit{Equation 3.6}$$

Where γ_{sg}, γ_{sl} and γ_{lg} are the surface tensions between solid/gas, solid/liquid and liquid/gas respectively. A_{sg} and A_{lg} are the interface areas between solid/gas and liquid/gas phases respectively. Similar to the homogeneous case, $-(P_{bub} - P_{sys})V_g$ represents the work required for the expansion of gas inside the bubble, $(\gamma_{sg} - \gamma_{sl})A_{sg}$ is the work required to replace the solid-liquid interface with the solid-gas interface and $\gamma_{lg}A_{lg}$ is the work needed to form the bubble interface that is a liquid-gas interface. The same approach is needed to obtain R_{cr} for heterogeneous nucleation. The plot of ΔF_{het} versus R_{bub} yield a similar graph to Figure 3.15 but with a smaller maximum. If we derivate Equation 3.6 with respect to R and set it to zero, R_{cr} will be obtained as:

$$R_{cr} = \frac{2\gamma_{lg}}{P_{bub,cr} - P_{sys}} \qquad \textit{Equation 3.7}$$

Which is identical to the one obtained for homogeneous nucleation. Again, by substituting R_{cr} to Equation 3.6, the free energy barrier for heterogeneous nucleation will be obtained as:

$$W_{het} = \frac{16\pi\gamma_{lg}^3 F}{(P_{bub,cr} - P_{sys})^2} \qquad \textit{Equation 3.8}$$

Where F is the energy reduction factor and is a function of geometry of the interfaces. If bubble nucleates on a smooth planar surface similar to Figure 3.16, F will be obtained as [5].

$$F(\theta_c) = \frac{2 + 3\cos\theta_c - \cos^3\theta_c}{4} \qquad \textit{Equation 3.9}$$

Where θ_c is the contact angle between the solid and the liquid and is illustrated in Figure 3.16.

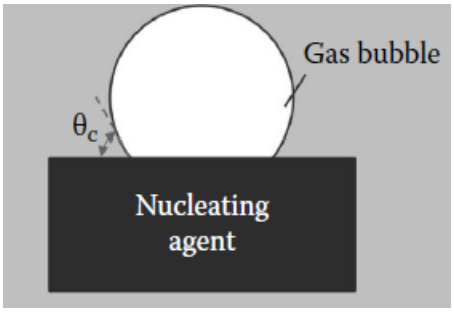

Figure 3.16 Illustration of the contact angle of a planar nucleating agent [43]

The contact angle is the material property and is related to the interfacial energy by Young's equation:

$$\gamma_{sg} = \gamma_{sl} + \gamma_{lg}\cos\theta_c \qquad \textit{Equation 3.10}$$

As mentioned earlier, F depends on the geometry in which bubble is nucleated on. Many of the nucleating agents such as talc particles have rugged surfaces in micro scale or smaller. These nonuniformities can be modeled as a series of conical cavities and F is obtained for them as [5]:

$$F(\theta_c,\beta) = \frac{1}{4}\left[2 - 2\sin(\theta_c - \beta) + \frac{\cos\theta_c \cos^2(\theta_c - \beta)}{\sin\beta}\right] \qquad \textit{Equation 3.11}$$

Where β is the semi-conical angle as depicted in Figure 3.17 .

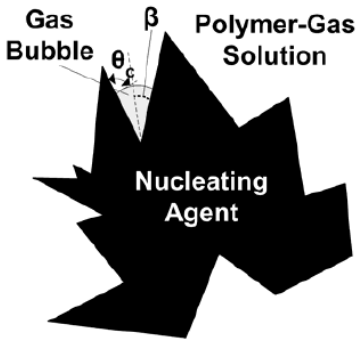

Figure 3.17 Illustration of contact angle and semi-conical angle on the surface of a nucleating agent [5]

3.8 Nucleation Rate

The concepts of R_{cr} , W_{hom} and W_{het} define conditions that is needed for a system of the liquid-gas solution to turn into a metastable state, however, it does not predict about the time when a system starts to create bubbles with the size of R_{cr} from a metastable state reached before. Thus, it is necessary to look at the kinetics of this process to predict the rate of bubble nucleation. By combining the thermodynamic models with kinetic theory, Blander and Katz [131] defined the rate of nucleation as the rate at which bubbles at the critical state gain gas molecules and grow. They defined homogeneous nucleation rate (J_{hom}) and heterogeneous nucleation rate (J_{het}) as [43]:

$$J_{\text{hom}} = N\sqrt{\frac{2\gamma_{\text{lg}}}{\pi m}}\exp\left(-\frac{16\pi\gamma_{\text{lg}}^{3}}{3k_{B}T_{sys}\left(P_{bub,cr}-P_{sys}\right)^{2}}\right) \qquad \textit{Equation 3.12}$$

$$J_{het} = N^{\frac{2}{3}}Q\sqrt{\frac{2\gamma_{\text{lg}}}{\pi mF}}\exp\left(-\frac{16\pi\gamma_{\text{lg}}^{3}F}{3k_{B}T_{sys}\left(P_{bub,cr}-P_{sys}\right)^{2}}\right) \qquad \textit{Equation 3.13}$$

Where N is the number of gas molecules per unit volume of polymer, m is the molecular mass of gas molecules, k_B is Boltzmann's constant, and Q is the ratio of the surface area of the heterogeneously nucleated bubble to that of a spherical bubble with the same radius of curvature. By integrating the nucleation rate with respect to time, the expression for cell density, $N_{unfoamed}$, can be obtained as follows [5]:

$$N_{unfoam}(\text{t}) = \int_{0}^{t}[J_{\text{hom}}(\text{t}') + \text{A}_{het}\,J_{het}(\text{t}')]\,dt' \qquad \textit{Equation 3.14}$$

Q is a geometry dependent parameter and the expression of Q for different parameters is available In the literature [132, 133, 134, 135, 136]. For conical cavities, Q is expressed as a function of θ_c and β as below [5]:

$$Q(\theta_c, \beta) = \frac{1 - \sin(\theta_c - \beta)}{2} \qquad \textit{Equation 3.15}$$

3.9 Adopted Nucleation Model

According to the explanations given in section 2.6, the nucleation model adopted in this thesis is based on a modified nucleation model proposed by Taki [54]. This model applies the pre-exponential factor (f_0) and energy reduction factor (F) to the nucleation rate equation in order to reach a consistency between the experimental data and model predictions. Considering the heterogeneous nucleation mechanism as the main mechanism in the plastic foaming process and applying the correction factors to Equation 3.13, it will be modified into the following equation.

$$J = f_0 \exp\left(-\frac{16\pi\gamma_{lg}^3 F}{3k_B T_{sys}\left(\frac{\bar{C}(t)}{K_H} - P_{sys}\right)^2} \right) \qquad \textit{Equation 3.16}$$

Both factors can be obtained by fitting the model results to the experimental data at a constant temperature and nucleating agent content. Once they have been set for a set of experimental data, they can be used again at other saturation pressure provided that the temperature and content of nucleating agent remain the same.

3.10 Experimental procedure

3.10.1 Materials

The Polypropylene used in our experiments was "Daploy^{TM} WB140HMS-PP [137]" a product of "Borealis AG Company. [138]" This polymer is a member of long-chain branched polypropylene family and has an average molecular weight of 394 Kg/mol. It has a glass transition temperature of 124.63℃ and a melting temperature of 164℃. It has a zero shear viscosity of 22500 Pa.s and a relaxation time of 78 seconds according to the material's data sheet.

In addition, three types of blowing agents have been used; two exothermic (XOP-300 from Bergen International [113] and Azodicarbonamide from "Polychem Dispersions Inc. [114]") and one endothermic (Foamazol 90 from "Bergen International" company [113]). According to their manufacturer, the products of Bergen International liberate CO_2 upon decomposition, and that of Azodicarbonamide releases N_2. The graph of their decomposition ratio relative to the temperature was reported in Figure 3.3 to 3.6. The physical properties of the high melt strength polypropylene explained above are summarized in Table 2.

3.10.2 Sample preparation and experimental procedure

At each experiment, 30 grams of Polypropylene has been weighted, and dry mixed with a proper amount of chemical blowing agents (that will be explained in the next sections) and other additives such as talc in the case it was needed and they were loaded to the extruder through the feeder. The speed of the feeder has to be regulated with the rotational speed of screws. Samples need time to be melted after entering the extruder. As explained in section 3.4.2, the temperature profile is chosen in a way that prevent any decomposition of CBA at the feeding zone. Therefore, samples are normally in their glassy state at first few centimeters of the screws, and too much feeding leads to the agglomeration and clogging of the mixture inside the extruder and results in over-torque of the screws, which itself, force the machine to stop working. On the other hand, too low feeding results in an unsteady flow of the melt and a non-uniform foam. The temperature profile for each zone was chosen in accordance with the gas concentration planned to be dissolved inside the polymer, final pressure, pressure drop rate and CBA type. The resulting foam comes out of the die, and they are cooled either in the air or in the water using a cold-water tank. It is important to mention that temperature and pressure profile were maintained at their set points for the entire duration of the test for each sample. Despite this consistency, it was observed that nucleation rate was lower than the maximum rate at the first moments of feeding. As the process goes on, it reaches to a steady state that was planned. Finally, Nucleation and foaming decrease at the end of the process. We captured our samples from the middle of the process where the nucleation rate of the extruded foams reached a steady state. Samples were cut for visual observation under the microscope with the range of magnification from 50 to 500 times magnification. A data acquisition system that was linked to the extruder recorded all the information related to the parameters including temperature of zones, the pressure of the die, screw speed, screw torque, and feeding rate.

Table 2 Properties of the WB140 high melt strength Polypropylene (WB140 HMS-PP)

Property	Value	Reference
Zero Shear Viscosity (Pa.s)	22500	[139]
Relaxation time (s)	78.0	[139]
Average Molecular Weight M_n (Kg mol^{-1})	312	[140]
Glass Transition Temperature	124.63℃	Current Study
Melting Point	164℃	Current Study
MFI (g/10 min)	2.1 (at 230 °C, 2.16 kg)	[139]
Specific gravity	0.9	[141]
Melt density (Kg m^{-3})	750 (at 200℃)	[141]

3.11 Effect of processing conditions on cell nucleation

Understanding the nature of the extrusion process and predicting the possible effects of changing operational parameters on the extruded foams are extremely important especially in foaming industry. These practical feelings are precious in the industry when considering that the numerical simulation is not always a convenient way of predicting probable results. In order to address that issue, a series of experiments were conducted following the procedure mentioned in section 3.10.2, and the consequence of changing die pressure, gas concentration and additives are studied qualitatively. The pressure at the die and the pressure drop rate could be controlled using the screw speed, die diameter and melt viscosity. The concentration of gas had been calculated according to the temperature profile, and the correct amount of nucleating agents were used in order to prevent any undissolved gas pockets inside the melt. Temperature profile could be selected through the digital screen of the extruder, and the temperature of each the heating zone could be controlled independently.

3.11.1 Effect of pressure and pressure drop rate on cell nucleation

In order to observe the effect of pressure and pressure drop rate on the cell nucleation, two different die pressure have been selected for the 2.5 wt% of CO_2 dissolved at 190° C. Figure 3.18 shows that when the system pressure and pressure drop rate are higher, the final cell density varies and increase from 740 cells/cm^3 to 1430 cells/cm^3. This is quietly in accordance with the expectations. According to Equation 3.5, 3.8, the energy barrier for bubble nucleation in both heterogeneous and homogenous nucleation type, namely W_{hom} and W_{het}, depends on the degree of saturation ($P_{bub} - P_{sys} = P_{melt} - P_{atm}$). When the bubble pressure drop is higher, the energy barrier for bubble nucleation gets lower and more bubbles can be formed. In addition, the distance between the beginning and the end of the die is same for all experiments therefore, when the pressure at the beginning of the die is higher, it means that it drops faster to the atmospheric pressure. Thus a higher pressure leads to a higher pressure drop rate which itself causes nucleation to happen faster after exiting the die. The same trends were reported in the literature about the effect of pressure and pressure drop rate on the bubble nucleation [142].

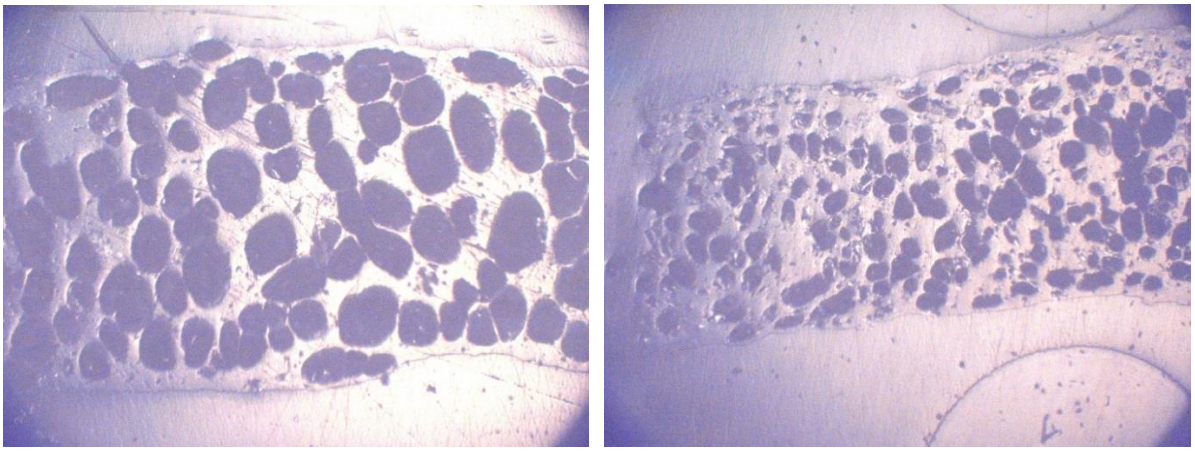

Figure 3.18 Effect of pressure and pressure drop rate on cell nucleation

3.11.2 Effect of blowing agent concentration on cell nucleation

In order to examine the effect of gas concentration on the bubble nucleation, the results of two experiments with 1.5 wt% and 3 wt% of dissolved gas have been compared together. As you can see in Figure 3.19, cell density increased by increasing the gas concentration. The maximum cell density increased from 230 cells/cm^3 to 770 cells/cm^3. In order to fully understand the reason behind this

change, we need to look at the thermodynamics of the solution namely liquid (melt)-gas solution. Interfacial energy and surface tension are two concepts that can explain cell density changes due to the concentration difference. According to Zeldovich [143], the relation between surface tension γ and chemical potential μ (which can be related to the concentration of the component) can be expressed as:

$$d\gamma = -\sum_{i=1,2} \Gamma_i \, d\mu_i \qquad \textit{Equation 3.17}$$

$$d\gamma = -\left(\Gamma_1 \, d\mu_1 + \Gamma_2 \, d\mu_2\right) \qquad \textit{Equation 3.18}$$

These relations show that if the i^{th} component in a solution is positively added to solvent and is absorbed on the surface density Γ_i, the tension at the surface of two medium will be decreased. In other word, upon increasing the gas concentration in the polymer, the chemical potential of the gas increases and causes the right hand side of the Equation 3.18 to be a bigger negative number which in turn decrease the surface tension. This means that lower energy is required to create a new surface. By decreasing the surface tension between the liquid phase and gas phase (γ_{lg}), all three parameters (R_{cr}, W_{hom} and W_{het}) in Equation 3.5, 3.7 and 3.83.13 decrease and therefore the energy barrier for bubble nucleation will be reduced. In addition, swelling effect will be more pronounced at higher gas concentration which itself increases the number of pre-existing gas cavities in the polymer. Conclusively, higher number of pre-existing gas cavities can act as nucleation spots and cell nucleation will be prompted.

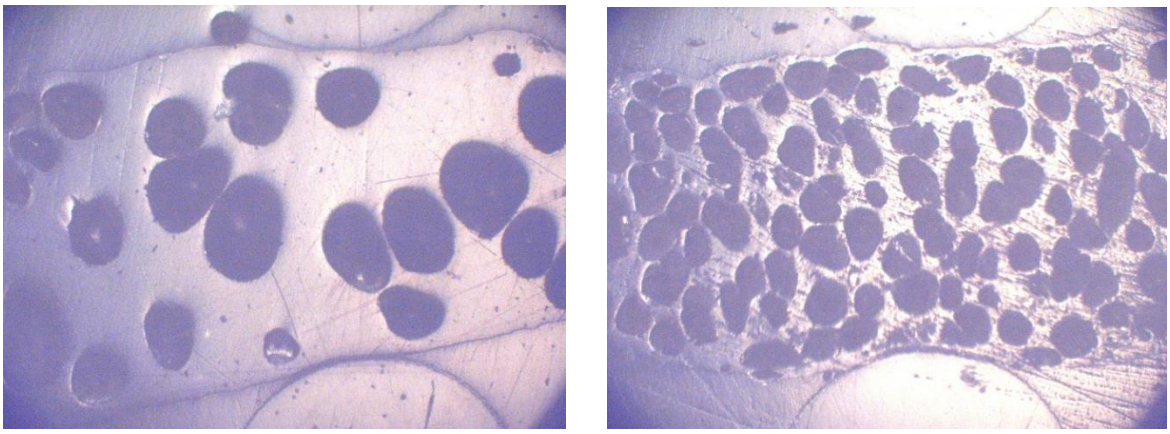

Figure 3.19 Effect of blowing agent concentration on cell nucleation

3.11.3 Effect of additive on the cell nucleation

Introducing additives to the foaming process has always been a good way among researchers and manufacturers to add desired characteristics or improve the existing ones such as increasing strength or heat insulation besides being lightweight. Additives can be either organic or inorganic. Talc, glass fibers and carbon fibers are among those inorganic additives that are very popular between both researchers and manufacturers. In this context, the effect of talc on cell nucleation have been studied in our experiments. Two samples have been prepared at 190°C pressurized to 40 atm and satured with 3.5 wt% CO_2 and 5wt% of talc were added to one of the samples in and the other one without any additive and the results are shown in Figure 3.20. It is clear that the presence of fillers could dramatically increase the cell nucleation phenomenon. The same result have been reported in the literature by many researchers [53]. According to the CNT, the presence of additives such as talc or glass fibers promote heterogeneous cell nucleation by providing more nucleating site and lowering the energy barrier required for cell nucleation. The rough surface of nucleating agents is a home for gas molecules which will be trapped there and remain in place until the final depressurization happens and supersaturation causes R_{cr} to reduce. When R_{cr} become less than the size of these gas cavities, they start to grow. On the other hand, the surface of nucleating agents increase heterogeneous nucleation which according to Equation 3.8 for W_{het}, requires less energy to happen compare to the homogeneous one.

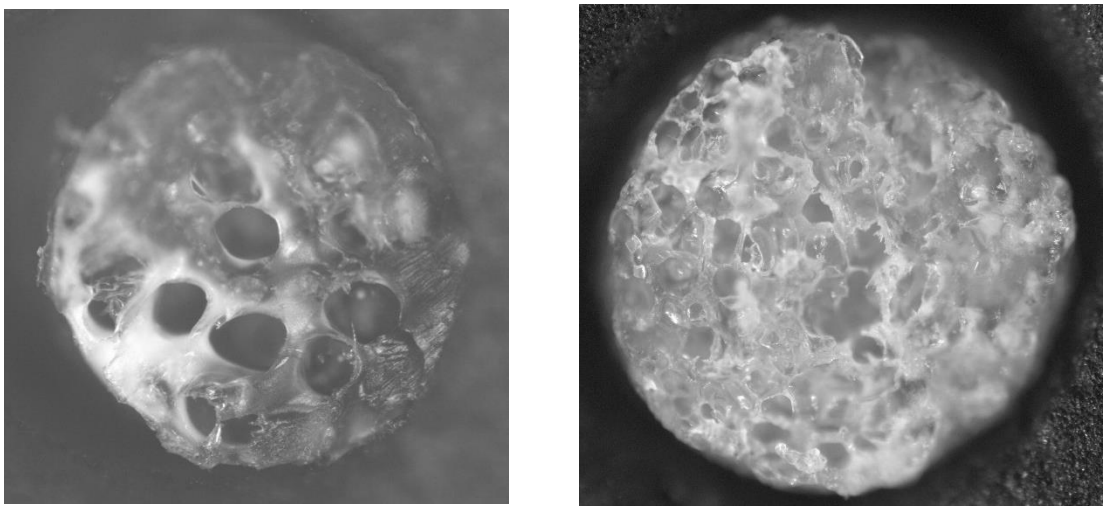

Figure 3.20 Effect of additive on the cell nucleation (left) without talc (Right) with 5% talc

3.11.4 Effect of additive content on cell nucleation

A series of experiments with different talc content from 2 wt% to 7 wt% have been performed to investigate the effect of additive content on the cell nucleation. The same conditions were applied to the polymer processed at 190° C and with die pressure of 50 atm and gas content of 3.5 wt%. Visual observation showed that increasing talc content could promote cell density in those experiments. Figure 3.21and 3.22 are the view of the cross section of these experiments. However, addition of talc content above 4 wt% could not significantly increase bubble nucleation. One reason could be agglomeration of talc particles, which indeed decrease their efficiency in playing role of nucleating sites. The scale of the equipment, operating temperature, mixing performance, blowing agent concentration or polymer type, influences this threshold. The other reason is the limitation of gas content in the polymer. Addition of talc particles increases the nucleation of bubbles which leads to a higher gas consumption in the process. Once the majority of the gas supply has been consumed, increasing the content of talc particles cannot enhance bubble nucleation dramatically.

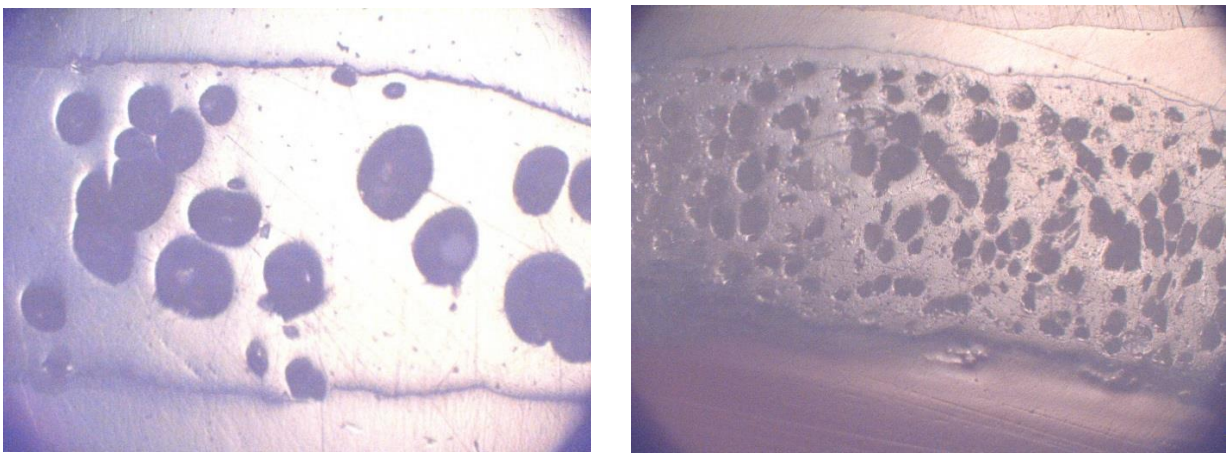

Figure 3.21 Effect of additive content on cell nucleation (left) without additive and (right) with 2% talc

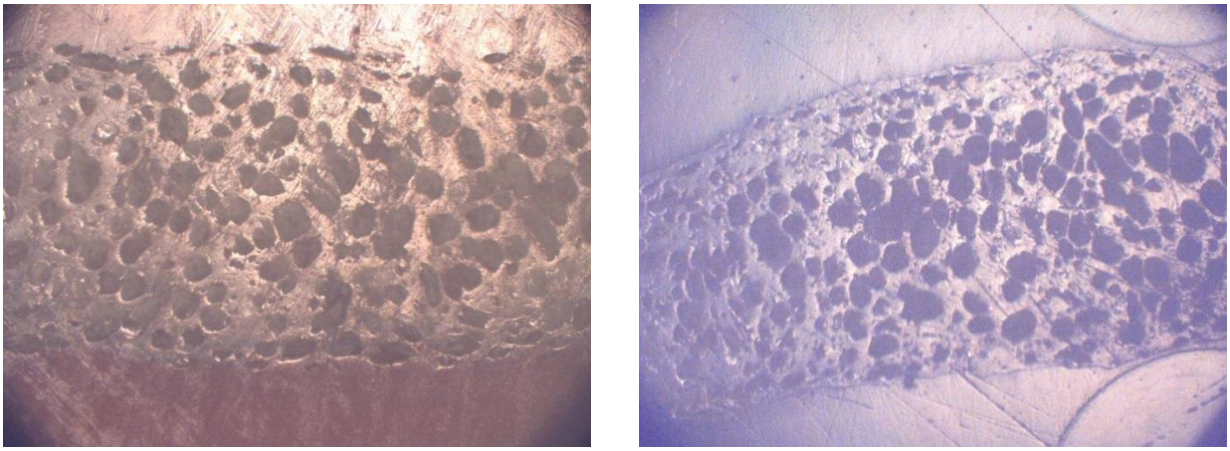

Figure 3.22 Effect of additive content on cell nucleation (left) with 4% talc and (right) with 7% talc

Chapter 4: Modeling and Simulation

4.1 Introduction

This chapter discusses the bubble growth in polypropylene foaming through experimental tests and finite element analysis. In order to have more precise predictions about the foam morphology, a finite element analysis based on the Galerkin method is used to solve the governing equations of the bubble growth process in two dimensions. At first, the governing equations and the underlying physics behind the process are explained, and non-dimensional forms of equations are presented. Then by adopting Galerkin method, those equations are discretized on the domain of our problem, the weak forms of the governing equations have been derived and then are entered to a computer program written in FreeFem++ software [110]. In order to test the validity of the program, the geometry and the conditions of driven cavity problem have been applied to the code and the simulation results have been compared with the experimental data from the literature. Subsequently, the validated program is used to simulate the growth of a single bubble with the assumptions of the well-known cell model. The sensitivity of the simulation results to the operating parameters are studied, and the results have been compared with the available experimental data. In the next section, the ability of the computer program for predicting the shape of bubbles at different operating conditions have been tested and compared with the experimental results. Finally, the ability of the cell model and two-dimensional model in the simultaneous simulation of bubble nucleation and bubble growth at different die pressures are tested. The results of cell density and cell size predictions compared with each other and with experimental data and the possible reasons for discrepancies have been explained.

4.2 Theoretical Background

4.2.1 Governing Equations

The expansion of a bubble or a group of bubbles in the solution of melted polymer and gas is an isothermal process. This expansion is integrated with the mass and momentum transfer between the bubbles and the solution around it. As a nucleated bubble tends to stabilize itself by establishing a balance between the high pressure inside and the atmospheric pressure outside through the expansion, the diffusion of gas from the polymer-gas solution to the bubble causes the bubble to gain

mass. The polymer that is used in our experiments is high melt strength polypropylene (section 3.10.1), which behaves as a viscoelastic fluid in the molten state, and thus a proper model needs to be employed to account for the rheological characteristics of the polymer. Consequently, in order to understand the underlying physics that govern the bubble growth process, momentum equation, continuity equation, constitutive equation, and the diffusion equation have to be solved together with the application of proper boundary conditions.

The governing equations that describe the flow of the polymer melt are conservation of momentum namely Navier Stokes equation:

$$\rho\left(\frac{\partial \mathbf{u}}{\partial t} + \mathbf{u}.\nabla\mathbf{u}\right) = -\nabla p + \nabla.\boldsymbol{\sigma} + \rho\mathbf{g}, \qquad \textit{Equation 4.1}$$

And conservation of mass or continuity equation:

$$\nabla.\mathbf{u} = 0 \qquad \textit{Equation 4.2}$$

Where ρ is the melt density in (Kg.m^{-3}), $\mathbf{u}$ is the velocity of the melt in (m.s^{-1}), t is time in (second), p is the melt pressure in (Pa), σ is the melt stress in (Pa), and $\mathbf{g}$ represents the body forces in (Newton). Due to the high viscosity of the polypropylene and relatively small expansion rate of bubbles, the Reynolds number, which is the ratio of inertia forces to the viscous forces, is small. For a sphere of diameter D moving at a velocity V through a fluid with viscosity μ and density ρ, the Reynolds number is defined as [144]:

$$\mathrm{Re} = \frac{\rho V D}{\mu} \qquad \textit{Equation 4.3}$$

Considering the dynamic of a bubble during the growth, it has the highest expansion velocity at the first moments of its growth and does not exceed $150\mu m/s$. The highest diameter that a bubble could reach in our experiments was 600 µm and the melt density and viscosity of our polypropylene are 750 Kg.m^{-3} and 22500 Pa.s respectively. By plugging these parameters into Equation 4.3, the Reynolds number will be obtained as:

$$\mathrm{Re} = \frac{\rho VD}{\mu} = \frac{750 \times 150 \times 10^{-6} \times 600 \times 10^{-6}}{22500} = 3000 \times 10^{-12} \qquad \textit{Equation 4.4}$$

In this case, the maximum Reynolds number can barely reach 3000×10^{-12} and is much less than 2300, which is the limit of the laminar flow. The fluid motion is smooth in this region and therefore, the inertia forces are very small compared to the viscose forces and the assumption of ignoring inertia term in the Navier Stokes equation is valid. By eliminating the inertia forces in Equation 4.1 and considering the isothermal condition and incompressibility of the viscoelastic melt, it will be simplified as below:

$$\nabla . \pi = 0 \qquad \textit{Equation 4.5}$$

Which $\pi = -pI + \sigma$ and is called Cauchy stress tensor. This tensor is a combination of isotropic pressure tensor ($-pI$) and extra stress tensors (σ) which the later one to be determined by a proper fluid model. The viscoelastic rheology is described by the Oldroyd-B model. This model is easy to implement numerically and does capture the essential rheological features of our interest. In addition, the similar studies in literature mainly used the Oldroyd-B model which able us to have a closer comparison between our results and their studies. The extra stress tensor in this model is a combination of Newtonian viscous stress (σ_s) with solvent viscosity μ and viscoelastic stress σ_p (polymer stress) with elastic modulus G and relaxation time of λ.

$$\sigma = \sigma_s + \sigma_p \qquad \textit{Equation 4.6}$$

The σ_s is the Newtonian stress tensor and is given by:

$$\sigma_s = 2\eta_s \mathbf{E} \qquad \textit{Equation 4.7}$$

Where η_s is the solvent viscosity and $\mathbf{E}$ is the rate of deformation tensor and can be determined as:

$$\mathbf{E} = \frac{1}{2}(\nabla \mathbf{u} + \nabla \mathbf{u}^{\mathrm{T}}) \qquad \textit{Equation 4.8}$$

Based on Oldroyd-B model, the polymer stress tensor σ_p can be obtained by the following equation:

$$\sigma_p + \lambda\left(\frac{\partial \sigma_p}{\partial t} + \sigma_p^{\nabla}\right) = 2\eta_p \mathbf{E} \qquad \textit{Equation 4.9}$$

where $\eta_p = G\,\lambda$ is the polymer viscosity, λ is the polymer relaxation time and σ_p^{∇} is upper-convected derivative of polymer stress and can be calculated by the following equation:

$$\sigma_p^{\nabla} = \mathbf{u}.\nabla\sigma_p - \left(\sigma_p.\nabla\mathbf{u} + \left(\nabla\mathbf{u}\right)^T.\,\sigma_p\right) \qquad \textit{Equation 4.10}$$

After inserting the above equation to the Equation 4.9, Equation 4.11 is obtained:

$$\sigma_p + \lambda\left(\frac{\partial \sigma_p}{\partial t} + \mathbf{u}.\nabla\sigma_p - \sigma_p.\nabla\mathbf{u} - \left(\nabla\mathbf{u}\right)^T.\,\sigma_p\right) = 2\eta_p \mathbf{E} \qquad \textit{Equation 4.11}$$

The total viscosity of the polymer melt is given by:

$$\eta = \eta_s + \eta_p = \mu + G\lambda$$

The diffusion of gas in from the solution (polymer-gas) to the bubble is described by a convection-diffusion equation:

$$\frac{\partial c}{\partial t} + \mathbf{u}.\nabla c = \nabla.(D\nabla c) \qquad \textit{Equation 4.12}$$

Where c and D are defined as gas concentration (in $mol.m^{-3}$) and diffusivity constant (in $m^2.s^{-1}$) in the polymer melt respectively. The rate at which a bubble gains mass is equal to the mass flux of dissolved gas diffusing into the bubble. The conservation of mass for the bubble results the following equation:

$$\frac{dm_b}{dt} = -\oint_{bubble\ surface} D\nabla c\,.\,\mathbf{n}\,ds \qquad \textit{Equation 4.13}$$

where m_b is the mass of the gas inside the bubble, D is the diffusion coefficient and **n** is the unit vector which is normal to the bubble surface and is pointing into the bubble. The gas in the bubble obeys the ideal gas law:

$$P_b V_b = m_b R_g T \qquad \textit{Equation 4.14}$$

where P_b is the pressure of gas inside the bubble, V_b is the bubble volume, R_g is the universal gas constant and T is the absolute temperature (in Kelvin). According to our assumptions, we only consider the isothermal expansion for bubbles where T remains constant. Using the ideal gas law, Equation 4.13 can be rewritten as:

$$\frac{d}{dt}\left(\frac{p_g V_b}{R_g T}\right) = -D\oint_{bubble\ surface} \nabla c \,.\, \mathbf{n}\, ds \qquad \textit{Equation 4.15}$$

4.2.2 Boundary Conditions

On the bubble surface, there is no shear stress and the normal stress obeys the Young-Laplace equation:

$$\mathbf{n}.\left(-pI+\sigma\right) = \left(-p_g + K\tau\right)\mathbf{n} \qquad \textit{Equation 4.16}$$

Where K is the surface curvature and τ is the surface tension. Gas concentration at the bubble surface obeys Henry's law:

$$c = H\,.\,p_g \qquad \textit{Equation 4.17}$$

Where H is the Henry's law constant ($mol.N^{-1}m^{-1}$).

When the growth of a single bubble based on the assumptions of the cell model is being studied, zero flux condition is considered on the outer boundary of the influence volume for the gas concentration (c). In the case of studying the growth of a group of bubbles, this assumption is applied to the outermost edges the polymer:

$$\mathbf{n}\,.\,\nabla c = 0 \qquad \textit{Equation 4.18}$$

A zero velocity field is assumed inside the polymer at the initial time.

4.2.3 Dimensionless form of equations

The length is scaled with the initial bubble radius (R_0), time with the polymer relaxation time (λ), pressure difference ($p - p_{atm}$) with the ($p_{g_0} - p_{atm}$) where p_{g_0} is the initial gas pressure in the bubble and is equal to saturation pressure or pressure at the die of the extruder. The gas concentration is scaled with $\frac{p_{g_0}}{R_g T}$ and the polymer stress with $\frac{\mu + G\tau}{\tau}$. The non-dimensional forms of equations 4.1, 4.2, 4.11, 4.12, 4.15 become:

$$\nabla . u = 0 \qquad \textit{Equation 4.19}$$

$$-De \nabla P + 2\beta \nabla . E + \nabla . \sigma_p = 0 \qquad \textit{Equation 4.20}$$

$$\frac{\partial \sigma_p}{\partial t} + u . \nabla \sigma_p + \sigma_p = 2\alpha E + \sigma_p . \nabla u + \left(\nabla u\right)^T . \sigma_p \qquad \textit{Equation 4.21}$$

$$\frac{\partial c}{\partial t} + u . \nabla c = N \nabla^2 c \qquad \textit{Equation 4.22}$$

$$\left(p_a + \left(p_{g_0} - p_a\right) P_g\right) V_b = p_{g_0} \left(V_{b_0} + N \int_t \oint_{bubble\ surface} \nabla c . \mathbf{n}\, ds\right) \qquad \textit{Equation 4.23}$$

Where parameters u, σ, E, t, V_b and c in the above equations are dimensionless form of velocity, polymer stress, rate of deformation, time, bubble volume and gas concentration respectively. Parameter P in the Equation 4.20 is equal to $P = \frac{p - p_a}{p_{g_0} - p_a}$. By applying the same rule to the boundary conditions, the following equations are obtained:

$$\mathbf{n} . \left(-pI + \sigma\right) = \left(-De\left(P_b + \frac{p_a}{\lambda}\right) + KR_0 \tau\right) \mathbf{n} \qquad \textit{Equation 4.24}$$

$$c = \frac{\Phi\left(p_{g0} + \left(p_{g0} - p_a\right) P\right)}{p_{g0}} \qquad \textit{Equation 4.25}$$

$$\mathbf{n} . \nabla c = 0 \qquad \textit{Equation 4.26}$$

In the equations Equation 4.19 to 4.26, the parameters De, P, β, α, N and Φ are as follow:

$$De = \frac{\tau\left(p_{g0} - p_a\right)}{\mu + G\tau},\ P = \frac{p - p_a}{p_{g0} - p_a},\ \beta = \frac{\eta_s}{\mu + G\tau},\ \alpha = \frac{\eta_p}{\mu + G\tau},\ N = \frac{D\tau}{R_0^2},\ \Phi = RTK_h$$

4.3 Finite element formulation

Finite element method is the most powerful numerical technique for computational fluid dynamics, is readily applicable to domains of complex geometries, and provides great freedom in the choice of numerical approximations. It reduces a system of partial differential equations to a system of algebraic equations that can be solved using traditional linear algebra techniques. In the finite element method, the domain of interest is subdivided into small subdomains called element. Over each element, the unknown variables are approximated by a linear combination of specific functions called shape functions, which are associated with the nodes of the element. The piecewise approximations for elements are assembled to obtain a global system of equations for the whole domain. One of the significant advantages of the finite element method is that a general purpose computer program can be developed easily to analyze various kinds of problems. FreeFem++ [110] is one of the open source FEM software that can be used for the finite element analysis. It is a free software based on the Finite Element Method and is an integrated product with its high-level programming language. The governing equations of problems are described in this software by their variational form, and it is possible to solve multi-equations, multi-variables, two or three-dimensional statics and time-dependent, linear or nonlinear coupled problems with this software. Introduction of geometry and description of boundary conditions are relatively easy in this software, and the automatic mesh generator based on Delaunay-Voronoi algorithm help users to focus on the primary goals of the simulation rather than tackling with time-consuming numerical details [145].

4.3.1 Derivation of weak forms

In order to discretize the governing equations of 4.19 to 4.23, the standard Galerkin method is used. A smooth domain $\Omega \in \mathbb{R}^2$ is the domain of our interest. We are looking for the weak solutions $\left(u, P, \sigma_p\right) \in U \times \mathrm{P} \times \Sigma$ and $c \in \mathrm{C}$ such that the solution spaces satisfyU $\in \mathrm{H}^1(\Omega)^2$, $\mathrm{P} \in L^2(\Omega), \Sigma \in \mathrm{L}^2(\Omega)^3, \mathrm{C} \in H^1(\Omega)$. By multiplying the partial differential equations of 4.19 to 4.23

by the smooth test functions $(\tilde{p},\ v,\ \tilde{\sigma}) \in \mathrm{U} \times \mathrm{P} \times \Sigma$ and $\tilde{c} \in \mathrm{C}$ respectively and integrating those equations over the domain (Ω), the following weak forms of 4.27 to 4.30 are obtained.

It is worth to mention that before multiplying the test function $\tilde{p}$ to the continuity equation of 4.19, we have to solve the singularity problem that will appear during the numerical iteration due to the lack of the pressure term in that equation. In order to address that issue, we shall use the pseudo-compressible approximation [146] by adding the term εP to the mass conservation equation where $\varepsilon = 10^{-10}$. Therefore, the equation of mass conservation will be transformed to Equation 4.27.

$$\int_{\Omega} \left\{ \left(\nabla . u + \varepsilon P \right) \tilde{p} \right\} d\Omega = 0$$

Equation 4.27

$$\int_{\Omega} \left\{ \left(De\, PI - 2\beta E - \sigma_p \right) : \nabla v \right\} d\Omega + \oint_{\Gamma} \left\{ \mathbf{n} . \left(-De\, PI + 2\beta E + \sigma_p \right) . v \right\} d\Gamma = 0$$

Equation 4.28

$$\int_{\Omega} \left[\frac{\partial \sigma_p}{\partial t} + u . \nabla \sigma_p + \sigma_p - 2\alpha\, E - \sigma_p . \nabla u - \left(\nabla u \right)^T . \sigma_p \right] : \tilde{\sigma}\ d\Omega = 0$$

Equation 4.29

$$\int_{\Omega} \left\{ \left[\frac{\partial c}{\partial t} + u . \nabla c \right] \tilde{c} + N\ \nabla c : \nabla \tilde{c} \right\} d\Omega = 0$$

Equation 4.30

4.4 Validation:

In order to test the validity of formulations and numerical approach adopted in this thesis and, the driven cavity problem has been selected for this purpose. The driven cavity problem has been a standard test case for a long time and was used by many researchers to test the reliability and validity of their numerical approach in fluid dynamics. This problem is about resolving a two-dimensional steady-state flow in a square domain and have some features that made it a suitable

problem for testing and comparison purpose. First, it has simple geometry that composed of a unit square with three walls at rest (vertical sides and bottom) and the lid (top wall) moves with a uniform velocity (U) tangent to the top side. Second, it has a simple boundary conditions and initial conditions, which are no-slip on the walls and with fluid initially at rest respectively, made it compatible with most numerical methods. Third and more important is the presence of tons of data in the literature which are the results of solving this problem both experimentally and numerically in different fluid regimes with different assumptions.

shows the geometry and boundary conditions for this problem.

$$\frac{\partial V}{\partial t}+(V.\nabla)V+\nabla p-\frac{1}{\mathrm{Re}}\nabla^2 V=0 \qquad \textit{Equation 4.31}$$

$$\nabla.V=0 \qquad \textit{Equation 4.32}$$

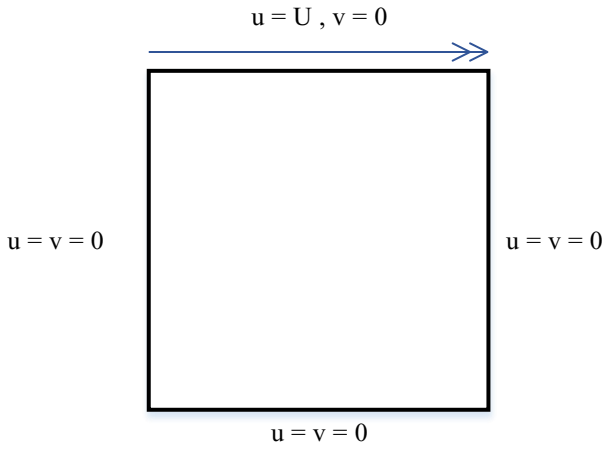

Figure 4.1 Geometry and boundary conditions of driven-cavity problem

For the purpose of comparison, the simulation results of the Ghia et al. [147] have been used which has tabular data for different Reynold numbers. The conditions of driven cavity problem have been applied to the code developed in this thesis, geometric domain is used and Dirichlet boundary conditions is imposed on every wall of the square. The results of the simulation have been considered as the steady state results when the maximum difference between the values of velocity components in two consecutive time step becomes less than 0.001 m/s. It is assumed that the viscoelasticity of

the polymer is negligible and only the Newtonian part of the fluid stress is dominant, therefore, the fluid acts as a Newtonian one. For deriving the non-dimensional forms of the equations, the scaling factors of ($\frac{x}{L}$) for lengths ($\frac{u}{U}$) for velocities are used. As a result, the non-dimensional forms of incompressible Navier-Stokes equation and continuity

equation have been obtained as follow:

$$\frac{\partial V}{\partial t}+(V.\nabla)V+\nabla p-\frac{1}{\mathrm{Re}}\nabla^2 V=0 \qquad \textit{Equation 4.31}$$

$$\nabla.V=0 \qquad \textit{Equation 4.32}$$

Where **V** is velocity vector of the fluid, **P** is the pressure and **Re** is the Reynold number which can be obtained by the following formula.

$$\mathrm{Re}=\frac{\rho UL}{\mu}$$

Where ρ, U, μ are the density, velocity, and viscosity of the fluid and L is the length of the cavity. As explained earlier, the fluid that was used in the extrusion foaming process is melted Polypropylene which operates in the range of 180 °C to 225°C. The polymer is highly viscose in that temperature range and the maximum Reynolds number this fluid is 3×10^{-9} (section 4.2.1). This number is far less than the Reynolds number at the boundary of the laminar flow (Re = 2300), and therefore, the behavior of flow in the extrusion process is categorized under the laminar regime. Due to these conditions, the data for Reynolds numbers that are less than 2300, was selected from Ghia's work [147] namely, Re = 100 and 400.

In order to discretize the domain of our problem, a 20×20 grid comprised of unstructured triangular elements was used in all three simulations. As can be seen in Figure 4.4 and 4.5, the results of Ghia et al. [147] simulations for streamline contours are compared with our simulations, and the velocity of the fluid in the vector form is depicted alongside the contours of streamlines. For the Reynolds number of 100, Figure 4.2 and 4.3 show the simulation results of velocity components (in x and y

directions) along the horizontal and vertical lines pass through the geometric center of the cavity and compared with the Ghia values.

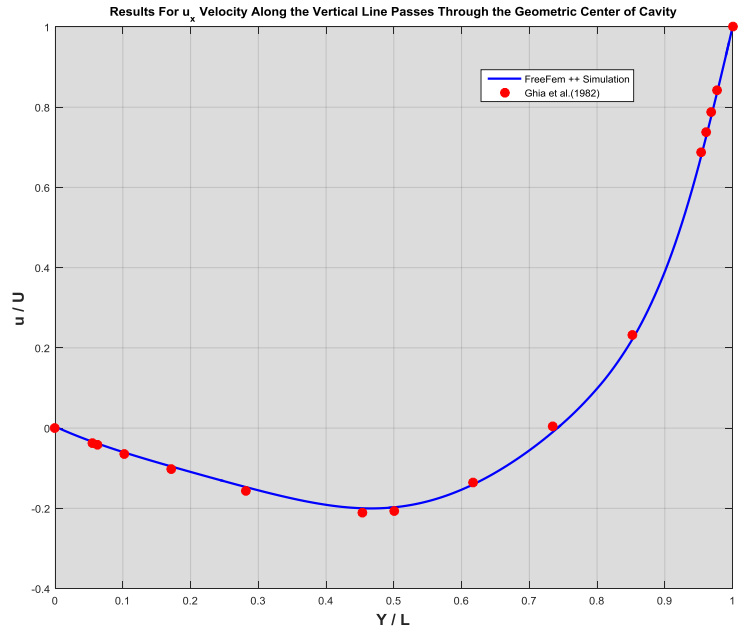

Figure 4.2 Simulation results of velocity components in x directions along the vertical line pass through the geometric center of cavity

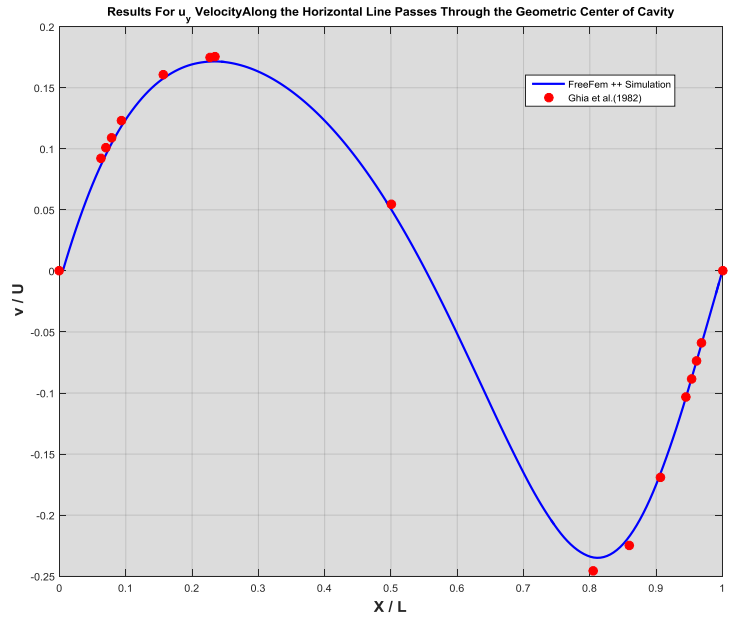

Figure 4.3 Simulation results of velocity components in y directions along the horizontal line pass through the geometric center of cavity

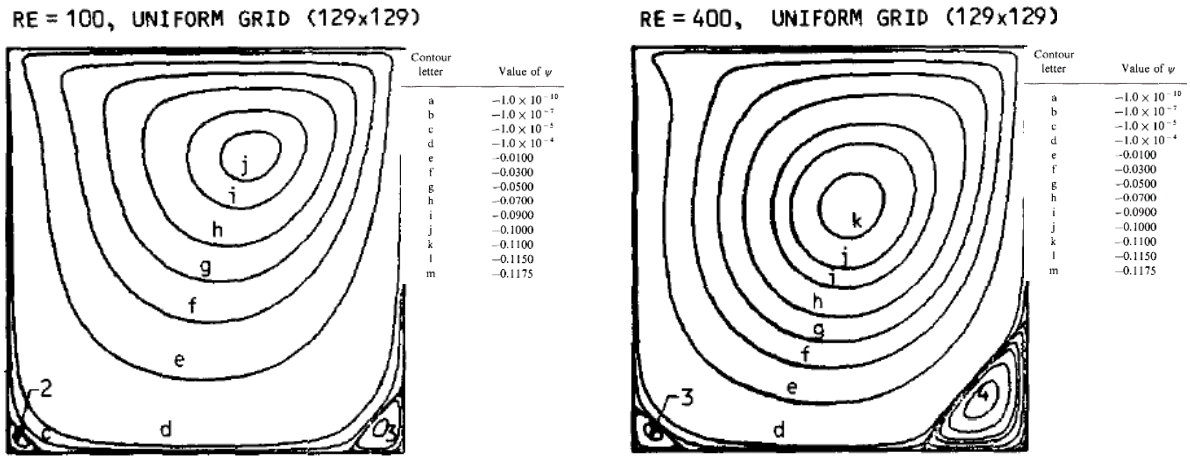

Figure 4.4 Streamline contour for the Reynolds number of 100 (left) and 400 (Right) from Ghia et al simulation [147]

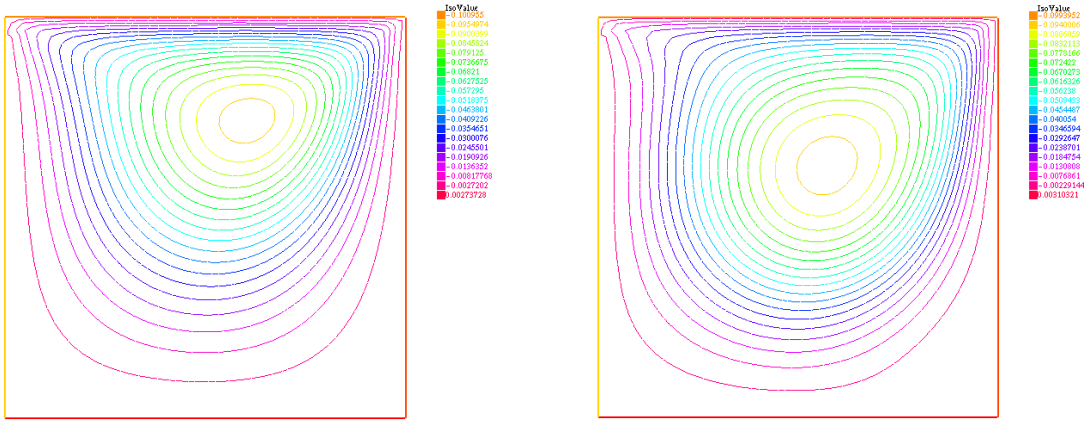

Figure 4.5 Streamline contour for the Reynolds number of 100 (left) and 400 (Right) (current study simulations)

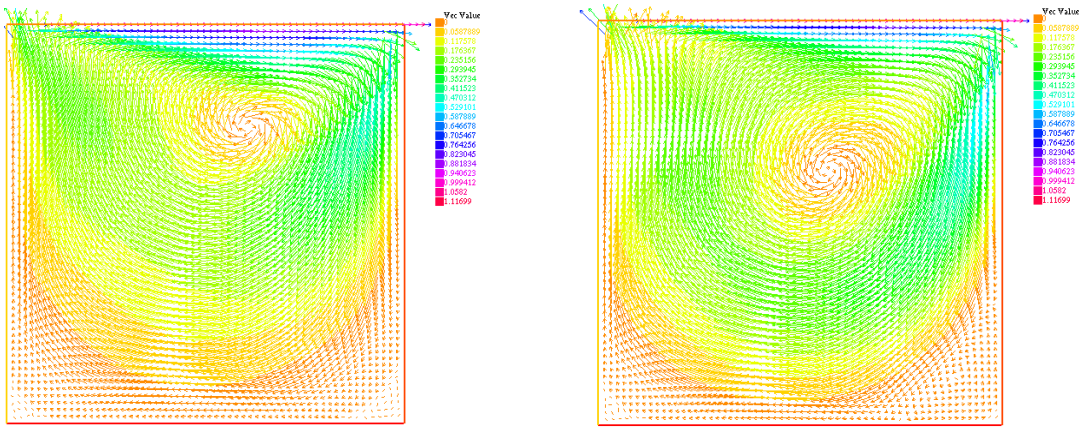

Figure 4.6 Velocity contour for the Reynolds number of 100 (left) and 400 (Right) (current study simulations)

4.5 Simulation Overview

The Finite element formulations namely the variational forms of the governing equations and corresponding boundary conditions, explained in section 4.3.1, are programmed in the Freefem++ software [110]. Considering the purposes of this thesis and the physics underlying the foaming phenomenon in the extrusion process, the simulation is decomposed into three different steps. At the first step, the growth of a single bubble based on the assumptions of the cell model is considered. Although the real extrusion process involves the simultaneous growth of bubbles that are clustered together and have mutual interactions, studying the evolution of an isolated bubble is a primary effort since a single bubble is the building block of the foam morphology. Moreover, it gives many useful insights about the nature of the foaming process that will be used in the more advance analysis. Therefore, in the first section, the growth dynamic of an abandoned bubble is considered and the effects of physical parameters on the growth rate and final bubble size are studied.

Considering the interaction of bubbles during the foaming process, the next section addresses the growth of a group of the bubbles that are nucleated and growing close to each other. Two approaches were used to consider the effects of neighboring bubbles during the growth phenomenon. The first one is Influence Volume Approach (IVA) which is a well-known method for predicting the final foam morphology and is based on the "cell model" and the "conservation of gas content" in the polymer. The second approach is a two-dimensional model based on the finite element method that is developed in this study. Unlike the IVA, the two dimensional model is capable of considering the nonuniform deformation of bubble boundary; therefore, it is used in section 4.11 to predict the geometries of bubbles that are growing in clusters. These two approach are then used to predict the final foam morphology of a series of experiments. These experiments were performed to study the effect of die pressure on the, number of bubbles, average bubble size, and final foam density. Predictions of the models are then compared with each other as well as experimental data and the possible reasons of discrepancies have been speculated.

4.6 Single bubble growth simulation

The importance of studying the growth of a single bubble that has not been affected by the adjacent cells cannot be ignored. In order to consider this issue, the growth of a bubble that has been nucleated in the polymer and is enclosed in a shell of the polymer has been studied. The bubble has the initial radius of 3µm and an initial pressure of 5MPa and is enclosed inside a polymer shell of 200µm. The polymer properties are the same as mentioned in Table 2. The result of the evolution of bubble during time is depicted in the following figures.

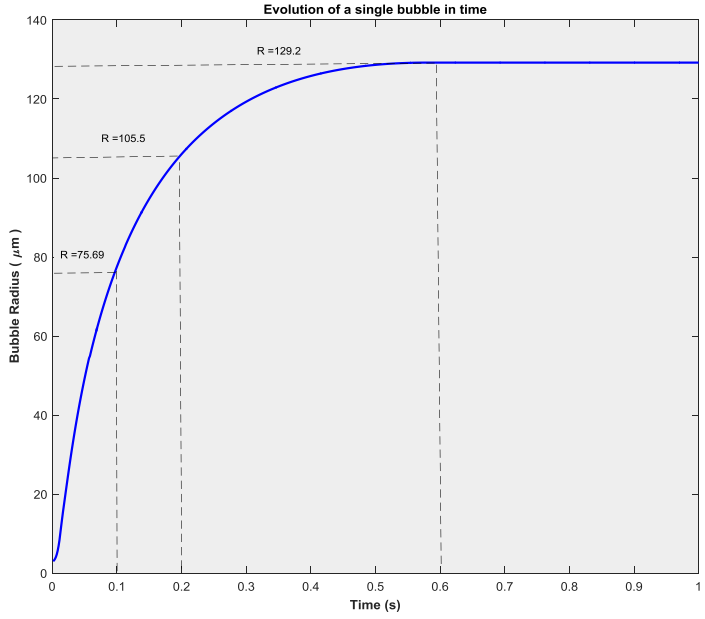

Figure 4.7 Bubble growth profile of a single bubble

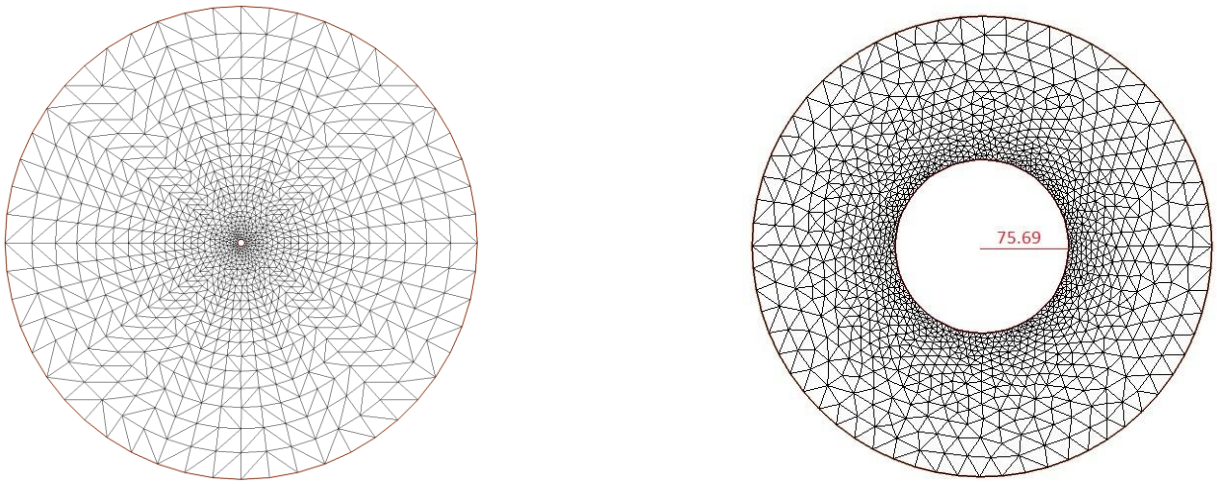

Figure 4.8 The bubble inside the polymer shell (left) before the beginning of the growth process (Right) at t=0.1 second

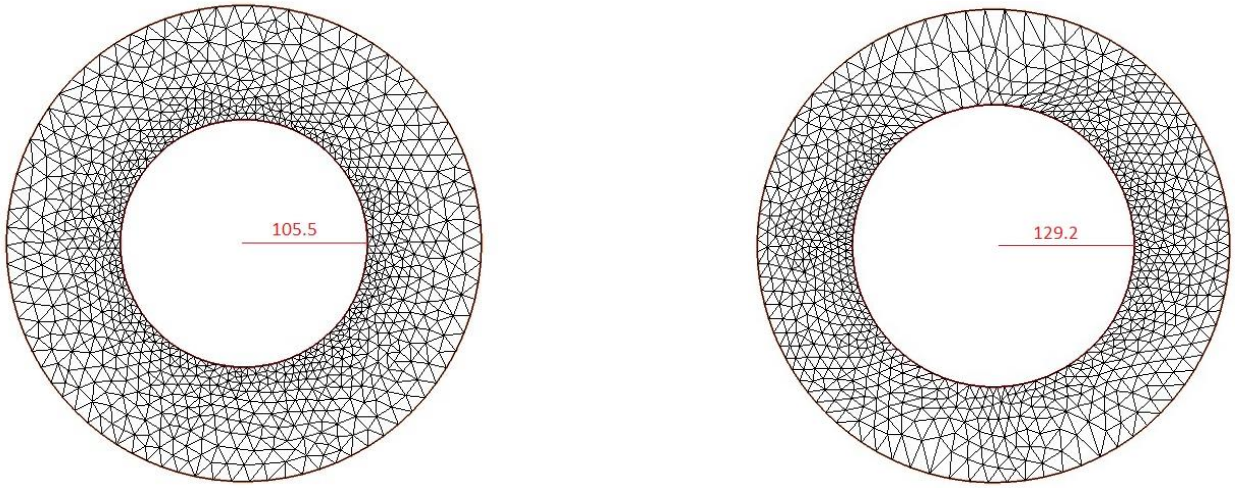

Figure 4.9The bubble enclosed inside the polymer shell at t=0.2(left) and t=0.6(Right)

4.6.1 Effect of initial bubble radius

Figure 4.10 shows the length of bubbles radii at each time during their growth for the bubbles started at the different initial radii (R_0). The results show that by varying R_0 from 0.2 µm to 20µm, the simulation predicts a larger equilibrium for the bubble with a bigger initial radius. However, it is clear that the initial growth rate of the bubble with smaller R_0 is higher. In addition, the effect of R_0 in the final radius is indiscernible for the bubbles with R_0 smaller than 3µm. Therefore, the assumption of choosing R_0=1 µm seems to be the same as the prediction of classical nucleation theory for R_0 to be less than one micrometer.

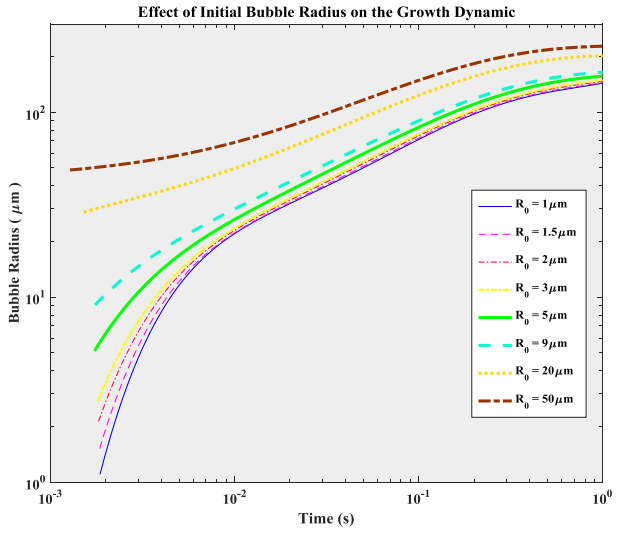

Figure 4.10 The effect of initial bubble radius on the growth profile

4.6.2 Effect of shell radius

The effect of shell radius on the bubble growth with the same initial radius is depicted in Figure 4.11. Almost all curves have a similar growth pattern at the early stage of their evolution. However, the difference becomes more clear at the later stage of their growth. A larger R_{shell} results in a larger volume of the solution that surrounds an individual bubble and therefore provides an increased available gas content in the polymer shell. As a result, a more gas content is available to diffuse into the bubble leading to a larger final radius. This effect is more pronounced at the later stages of the growth where the growth is more diffusion dominant. This effect can be seen by considering that the cells with smaller R_{shell} experience the lack of gas content at the later stages.

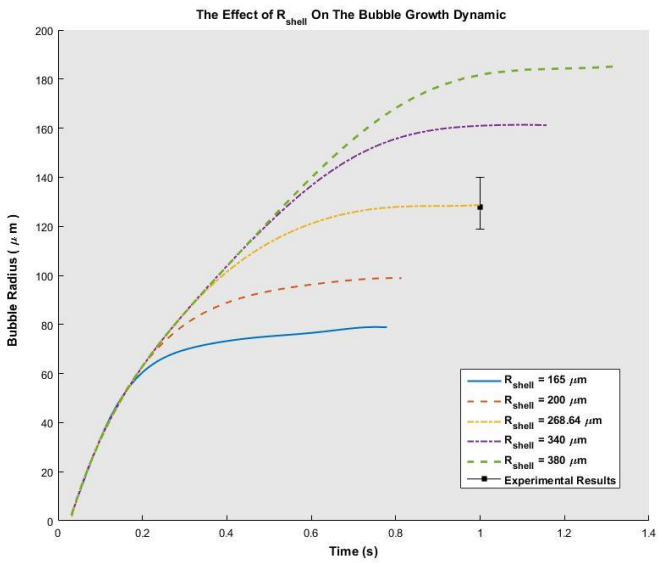

Figure 4.11 The effect of the shell radius on the bubble growth profile

4.6.3 Effect of Surface Tension (γ_{lg})

The nature of surface tension is a force that tries to minimize the surface area thus it has a retarding effect on the bubble growth. This force has a greater impact on the bubble growth when the surface curvatures is larger (smaller radius) and its effects diminish in low curvature (large radius), therefore, the effect of varying surface tension is only considerable at the early stages of the bubble evolution and has a negligible effect at the later steps. Eventually, it has no considerable effect on the overall growth profile and final bubble radius. One of the reasons for this insensitivity is the considerable nature of viscoelasticity of the polymer. At the viscoelastic materials, the effect of surface tension becomes less significant. As you can see in Figure 4.12 and 4.13, the difference in the bubble radius is more pronounced at the initial stages of growth and become negligible at the final stages.

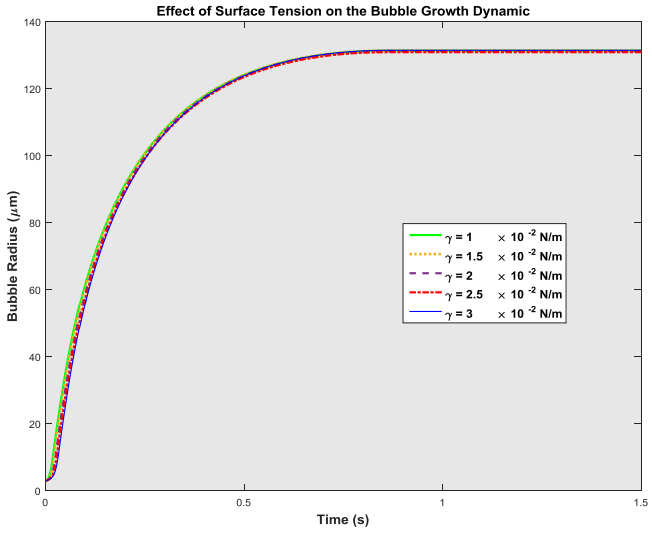

Figure 4.12 The effect of surface tension on the bubble growth profile(1)

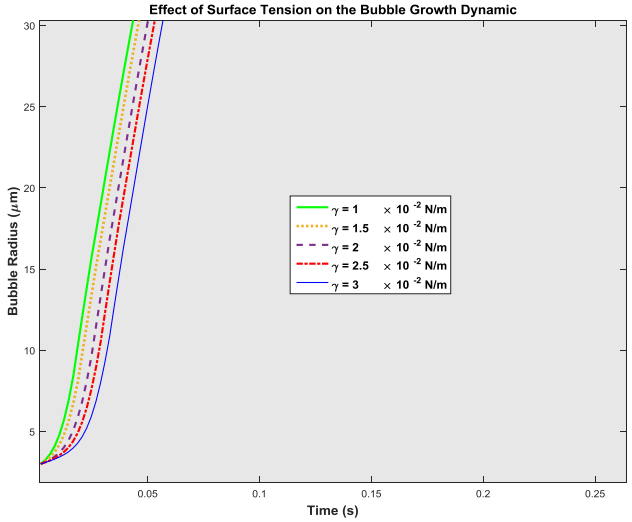

Figure 4.13 The effect of surface tension on the bubble growth profile (2)

4.6.4 Effect of diffusivity

Diffusivity coefficient is a measure for the magnitude of molar flux of the gas through the bubble surface per unit concentration gradient. Figure 4.14 shows the effect of changing diffusivity coefficient on the bubble growth profile by varying D from 5×10^{-10} to 1×10^{-8}. The results show a higher growth rate in the higher diffusivity coefficient as a result of faster gas transport into the

bubble. It should be mentioned that the effect of diffusivity coefficient is not the same for the entire time of growth. It primarily influences foaming dynamic but has a less pronounced effect at the end of the growth stages when the bubbles are stabilizing.

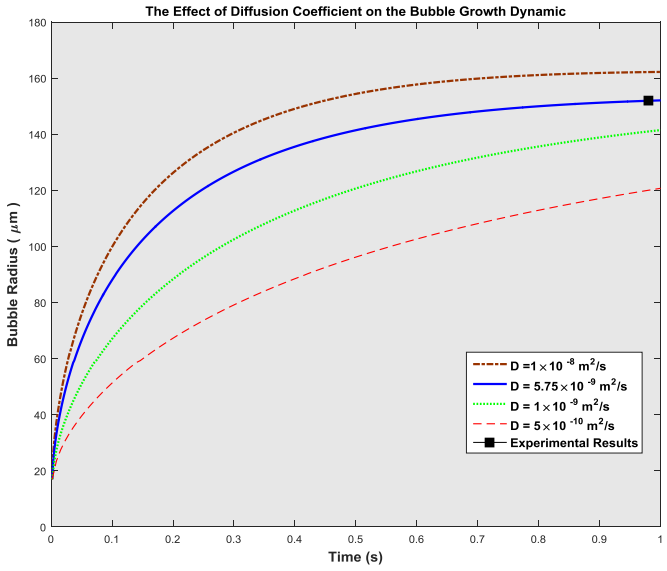

Figure 4.14 The effect of diffusivity on the bubble growth profile

4.6.5 Effect of Relaxation Time (λ)

Stress relaxation is a characteristic parameter of the viscoelastic fluids. It is a measurement for the time of stress accumulation or stress relaxation after initiation of a flow or cessation of a flow respectively. Longer Relaxation time is due to the dominance of elastic behavior over the viscous behavior in the polymer which results in slower stress relaxation and accumulation around the evolving bubble. Shorter relaxation time corresponds to faster stress accumulation and slower bubble growth, however, as can be seen in Figure 4.15 and 4.16 this variation in the growth rate is not huge and does not affect the final bubble radius to a considerable extent.

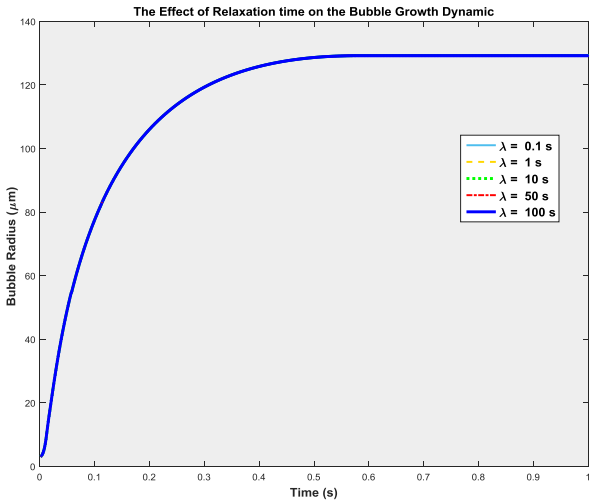

Figure 4.15 The effect of relaxation time on the bubble growth profile 1

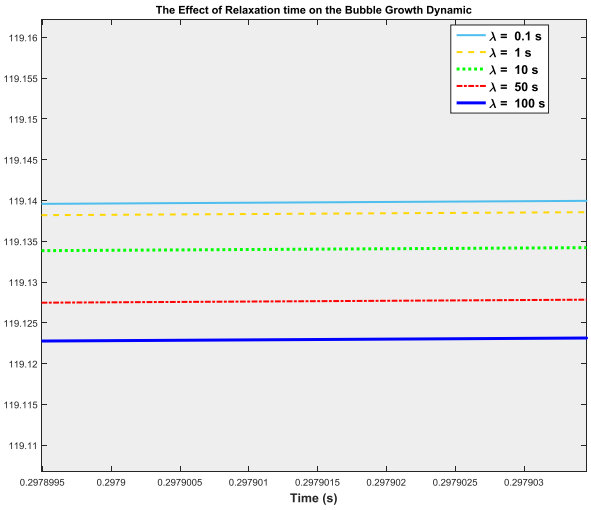

Figure 4.16 The effect of relaxation time on the bubble growth profile 2

4.6.6 The effect of initial polymer pressure

The pressure difference between the bubble and the surrounding environment is the primary driving force in the bubble growth process. As can be seen from Figure 4.17, the final bubble radius is increased by increasing the initial pressure. The Pressure difference is the most important factor that instigates the growth process by helping the trapped gas molecules to overcome the energy barrier for an irreversible growth. It can be assumed as the initial potential of the growth process. Besides

this fact, by an increase in the initial gas pressure, the solubility of the polymer increases which results in more gas content in the polymer and higher diffusion of gas through the bubble surface.

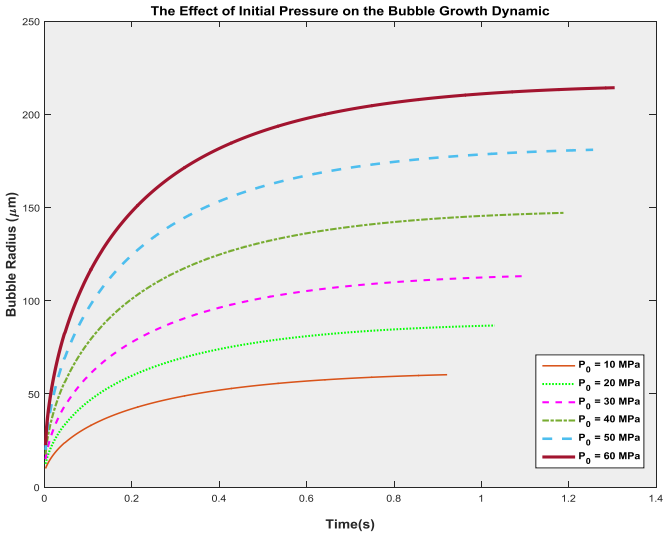

Figure 4.17 The effect of Initial bubble pressure on the its growth profile

4.6.7 Effect of solubility (Henry Constant)

Henry's constant is a measure for the solubility of the gas inside the polymer and is defined as the ratio of the dissolved gas concentration to the corresponding saturation pressure. A larger K_h means polymer has a higher capacity to dissolve gas at a certain pressure. Figure 4.18 shows the effect of varying the Henry's law constant between 1×10^{-6} and 1×10^{-4}. It is clear that for a polymer with a constant saturation pressure, a larger K_h leads to a higher gas concentration inside the polymer shell around the bubble, resulting in an increased rate of growth for the bubble.

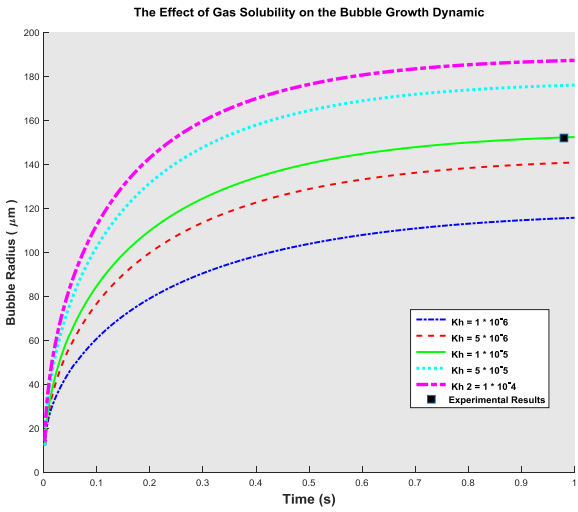

Figure 4.18 The effect of Henry's law constant on the bubble growth profile

4.7 Simultaneous nucleation and growth (Influence Volume Approach):

During the foaming process, both bubble nucleation and bubble growth processes are happening simultaneously, and they have a competition over the limited supply of the gas that is dissolved inside the polymer. Since the bubble nucleation and bubble growth are two subsequent events, simultaneous consideration of both of them is important for predicting foam dynamics accurately. In order to address this need, Shafi. et al [95] proposed a remarkable model that is called "Influence Volume Approach (IVA)". They used this model to study the effect of processing parameters on the final cells sizes and cells distribution. The idea behind this approach is describing basic models of bubble nucleation and bubble growth together with a total mass balance equation for all bubbles that play a role of jointing nucleation models with the bubble growth model. As a bubble expands, due to the gas diffusion into the bubble, a concentration gradient is generated inside the polymer around the bubble as is depicted in Figure 4.19. The parameter "S" denotes the radial position which the dissolved gas concentration is equal to the 95% of the concentration at the time of nucleation (C_s= 0.95 C_0). The volume of the polymer between the bubble and the S is called the influence volume (V_s). As the bubble expands, the concentration gradient also expands radially which means that the influence volume also grows. It was assumed that within the V_s, the nucleation is zero and no new bubble appears there. The volume outside the influence volume is called the non- influenced volume (V_L). The residual volume is the radial position where the gas concentration is equal to the

concertation at the time of nucleation C_0. This parameter is a free parameter and has to be approximated by trial and error method. In order to find the radius of the influence volume, the concentration gradient profile as a function of radius around the bubble is needed. For the case of simplicity, the integral method is commonly used in the literature to approximate the concentration profile around the bubble as a polynomial function [97].

The concept of IVA has been used in this thesis for the simultaneous analysis of the nucleation process and growth process. The assumptions of Shafi et al. [95] have been modified by considering that the (C_s=C_0), and therefore, the radius of influence volume is equal to the radius of residual volume (S=R_{cb}). Due to the proximity of the concepts of influence volume and the Cell Model, by considering the shell radius (explained in section 4.6.2) as the radius of the residual volume, we can have an easier calculation without sacrificing the accuracy. The concentration profile inside the influence volume is approximated by a 4th order polynomial function as:

$$\frac{C(r,\tau)-C(R,\tau)}{C_0-C(R,\tau)}=1-\left(1-x\right)^4$$

where

$$x=\frac{r^3-R^3}{R_{cb}-R^3}$$

And $\tau=t-t'$ where t is the time from the beginning of the process and t' is the time when the bubble is born. The gas concentration at the surface of the bubble obeys the Henry's law and is calculated by the following equation:

$$C(R,t-t')=P\left(t\right)\times K_h$$

Where K_h is the Henry's law constant and $P\left(t\right)$ is the system pressure at time t of the process.

Since every bubble has its own influence volume, the area of the non-influence volume at any time where the new bubbles can nucleate is calculated by subtracting the total influence volume of every bubble by at time t by the initial polymer volume [97]:

$$V_L(t) = V_p - \int_0^t V_L(t') J_{total}(t')\, V_s(t-t')\, dt' \qquad \textit{Equation 4.33}$$

Where V_p is the initial polymer volume.

When a new bubble is nucleated and an influence volume is assumed around that, the gas concentration in the non-influence volume drops. The average dissolved gas concentration in the non-influence volume is an important parameter since the nucleation rate (J) is directly affected by. The average gas concentration in non-influence volume is calculated by [97]:

$$\bar{C}(t)V_L(t) = C_0 V_L(0) - \int_0^t V_L(t') J_{total}(t') \frac{4\pi}{3} \frac{P_D(t-t')R(t-t')^3}{R_g T} dt' - \int_0^t V_L(t') J_{total}(t') \left\{ \int_{R(t-t')}^{Rres(t-t')} \{C_0 - C(r,t)\} 4\pi r^2 dr \right\} dt' \qquad \textit{Equation 4.34}$$

The first term on the righ-hand side of the above equation is the total gas content initially solved in the polymer before the start of nucleation. The second term is the total amount of gas exists inside the already nucleated bubbles, and the third term is the amount of the gas that exists in the influence volume of all bubbles. The following equation calculates the radius of the influence volume at any time during the process [97]:

$$R_{cb}(t-t') = S(t-t') = \left[\frac{4\pi}{3} R(t-t')^3 + V_s(t-t') \frac{3}{4\pi} \right]^{\frac{1}{3}} \qquad \textit{Equation 4.35}$$

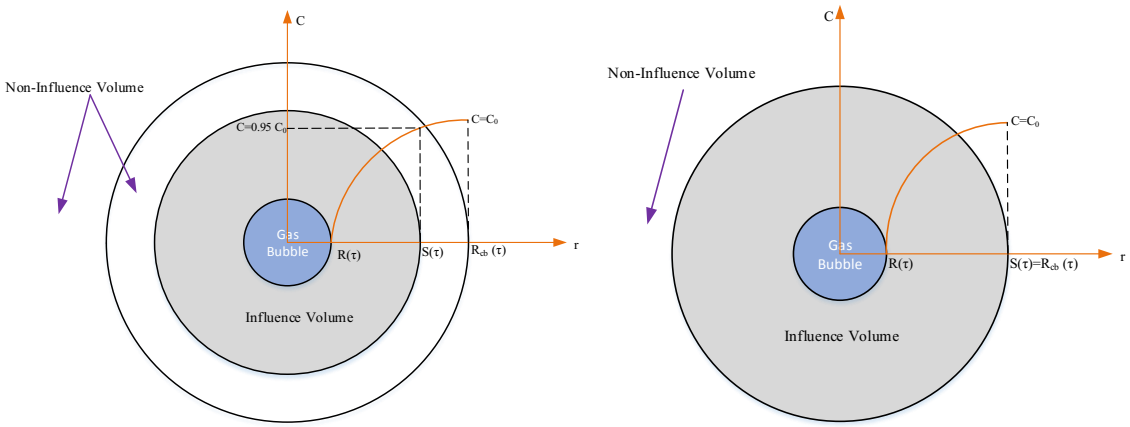

Figure 4.19 (Left) the Influence Volume Approach adopted by Shafi et al. [95] (Right) the modified Influence Volume Approach adopted in this study adopted [97]

4.8 Numerical Simulation Algorithm

The simulation approach of simultaneous bubble nucleation and bubble growth is performed in the following manner. At each time (t), the system pressure is calculated using the pressure drop profile in the die and the degree of supersaturation is calculated by deducting the system pressure from the pressure at the end of the latest nucleation. Using this parameter and the average gas concentration obtained from Henry's law, the equation for the rate of the bubble nucleation (Equation 3.16) is calculated and the result is compared with the nucleation threshold (J_{th}). In order to have nucleated bubbles, the calculated nucleation rate has to be greater than the nucleation threshold. For each bubble born at time t, the bubble growth is calculated through equations 4.19 to 4.23. Once the new bubble sizes have been obtained, the new average gas concentration in the polymer for the time $(t + \Delta t)$ has to be recalculated. Due to the continuous consumption of gas content and reduction of the free nucleating sites in the polymer, the gas concentration and the available volume of the polymer has to be updated at each time step. This can be achieved by considering the mass balance of gas and deducting the amount of gas that has been consumed for the bubble nucleation and bubble growth from the amount of the gas at time (t). The average gas concentration in the polymer for the time $(t + \Delta t)$ is obtained using the Equation 4.34 when the Influence Volume Approach is used and by directly dividing the total gas content by the available area of the polymer when the two-dimensional FEM is used. At the next time step, by retaining the information of the bubbles that

already exists, calculations of bubble nucleation and bubble growth is carried out in the similar manner to the previous time step. A summary of the numerical approach algorithm is depicted in Figure 4.20. In addition, a schematic of the evolution of bubbles during the growth process from the beginning to the end of the die is illustrated in Equation 4.10.

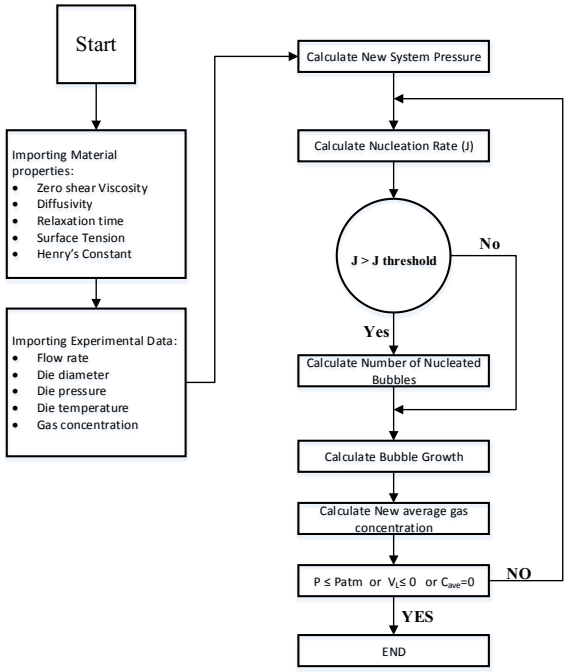

Figure 4.20 The flowchart illustrating the numerical algorithm followed in this study

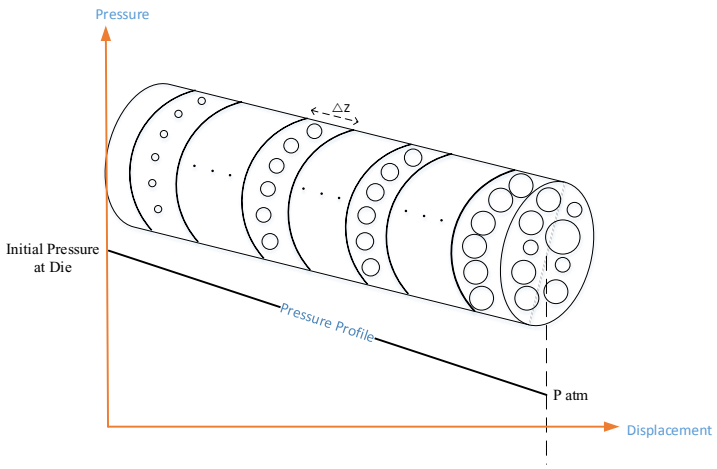

Figure 4.21 A Schematic of the evolution of bubbles during the growth process [97]

4.9 Multi-Bubble Growth

In the previous section, the growth of a single bubble has been considered, and the effect of parameters on its growth have been studied. However, in a real foaming process, the chance of having an abandoned single bubble which grows far from the other bubbles are not high especially when the concentration of dissolved gas and the die pressure are high. In the foaming process, bubbles are usually growing in groups and clusters, and the conditions of single bubble growth do not exist. Therefore, it is essential to study the growth of a group of bubbles since it is more likely to happen in the foaming process.

In the following sections, the importance of studying the dynamics of the group bubble growth is explained by comparing the simulation results of the two-dimensional model and the cell model on predicting the growth of a group of three bubbles growing in proximity to each other. It is followed by predicting the deformation of the boundary of bubbles with the 2D model in some actual experimental cases. In the last section, a series of experiments on studying the effects of die pressure on the cell size and cell density of PP foams are presented and compared with the simulation results of cell model and 2D model.

4.10 The Importance of Bubble-Bubble Interactions

As mentioned earlier, one of the assumptions of the cell model is that the neighboring bubbles do not have any interaction with each other. One of the consequences of this assumption is that bubbles remain spherical throughout the process. This assumption is not realistic and will not hold true in many cases. The growth of each individual bubble creates a stress field in the surrounding polymer which exerts a retarding force against the growth of the nearby bubbles. Furthermore, the movement of the boundary of a cell, due to the increase in the bubble radius, creates a velocity field in the polymer (Figure 4.22). Therefore, the velocity of any differential volume in the polymer melt is the resultant of the velocity profile of all bubbles. In addition, according to Equation 4.12, the velocity profile directly influences the gas concentration profile in the polymer. Figure 4.23 shows the difference of the concentration profile simulation between the cell model and the two dimensional model for a group of three bubbles growing near each other. As a matter of fact, not only the bubble nucleation creates a competition over the limited gas supply, but also the growth of the nearby

bubbles intensify this competition. However, it is not fair to discard the cell model for these weaknesses. The cell model can predict the growth of a bubble if that bubble grows in isolation far from other bubbles. This situation can happen in the foaming process both in high and low-density foams. However, the possibility of spotting such a bubble is higher when the cell density is low, and bubbles are more likely to nucleate far from the others. Besides low cell density foams, there are some possibilities of detecting this kind of bubbles in the medium and high cell density foams. The initial position for the bubble nucleation in the polymer is entirely random and by chance, some isolated bubbles can be found in these foams.

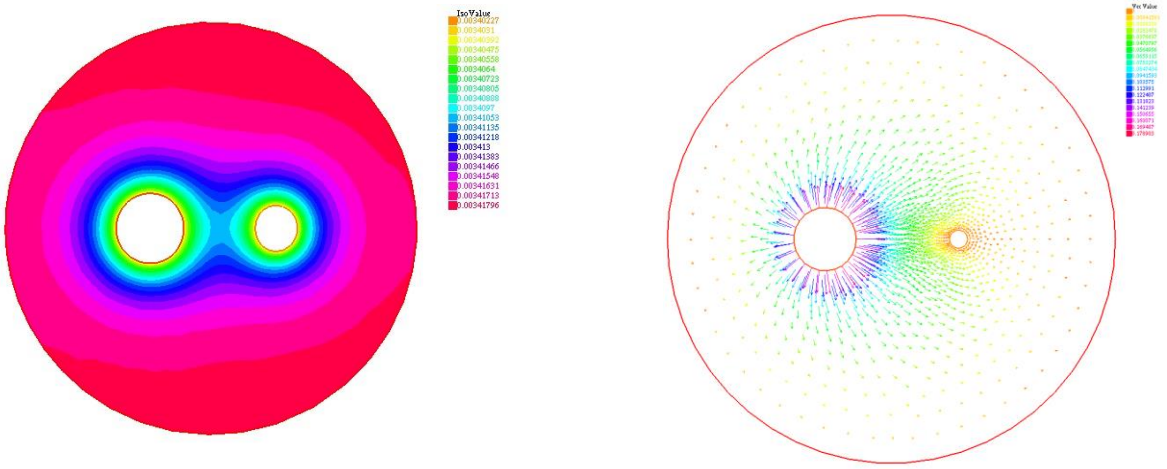

Figure 4.22 The contraction profile and velocity contour for the two bubbles by considering the mutual influences

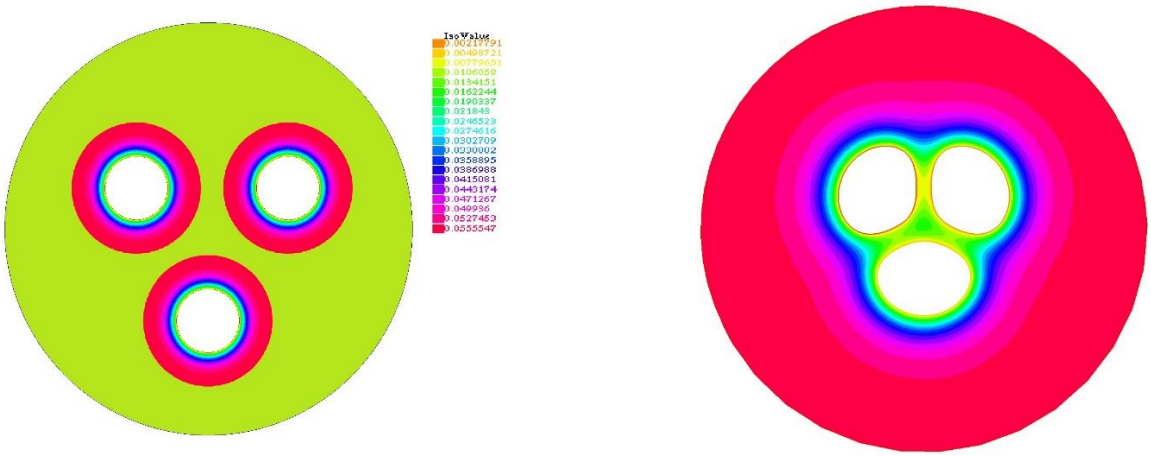

Figure 4.23 The difference between the concentration profile predicted by the dell model(left) and two-dimensional mode(right)

4.11 Prediction of the shape of bubbles by the two-dimensional model.

Two-dimensional model developed in this thesis is able to consider the interaction of bubbles during the actual foaming situation since it is working with the complete forms of Equation 4.19 to 4.23. These interactions deform bubbles in a way that they will not hold the perfect spherical shape they had at the first few moments of their birth. Depending on the initial nucleation positions of bubbles and the time differences between their births, they can be deformed in different ways. Sometimes a pair of two bubbles nucleate near each other and in other times, three or more bubbles are interacting with each other. These situations can be captured under the microscope when examining the samples that have been extruded at certain pressure and temperature. Once the experimental conditions are recorded, the simulation can be performed based on them. The age difference between the bubbles can be predicted by the semi-experimental nucleation model adopted in this thesis that was explained on section 3.9. Since the nucleation time of bubbles is determined, their initial pressure can be calculated easily using the die pressure and the pressure drop rate at the nozzle of extruder. Before using our numerical program to simulate the experimental tests, the conditions of group bubble growth in the Yue et al. [108] article have been imported to our program to test the validity and functionality of the FEM code. In that article, a cluster of 19 bubbles with the initial pressure of 8 bar, arranged in a hexagonal pattern inside the solution of CO_2 and a Newtonian fluid started to grow and press each other. The initial position of the bubble and the simulation results have been illustrated and compared in Figure 4.24. These results show a good agreement with the simulation of Yue et al. [108] at final equilibrium condition.

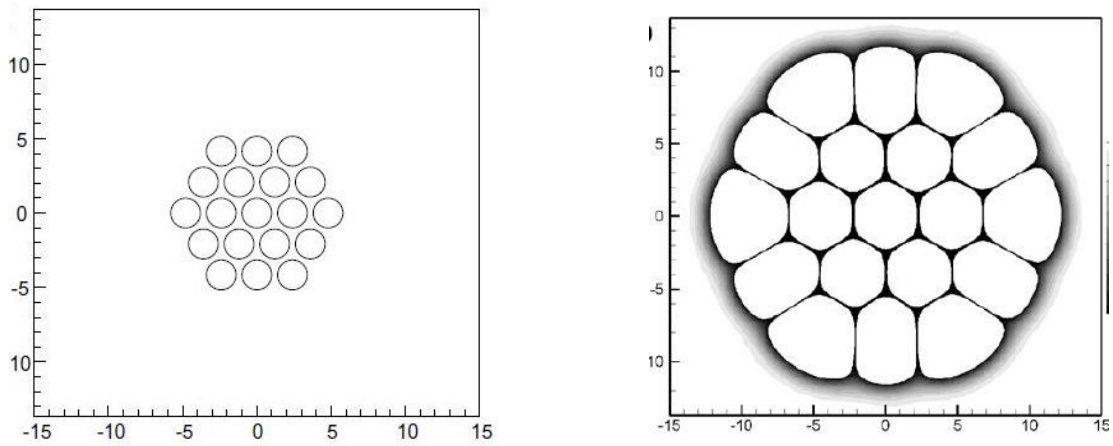

Figure 4.24 Simulation results of the group bubble growth from Yue et al. work [108].

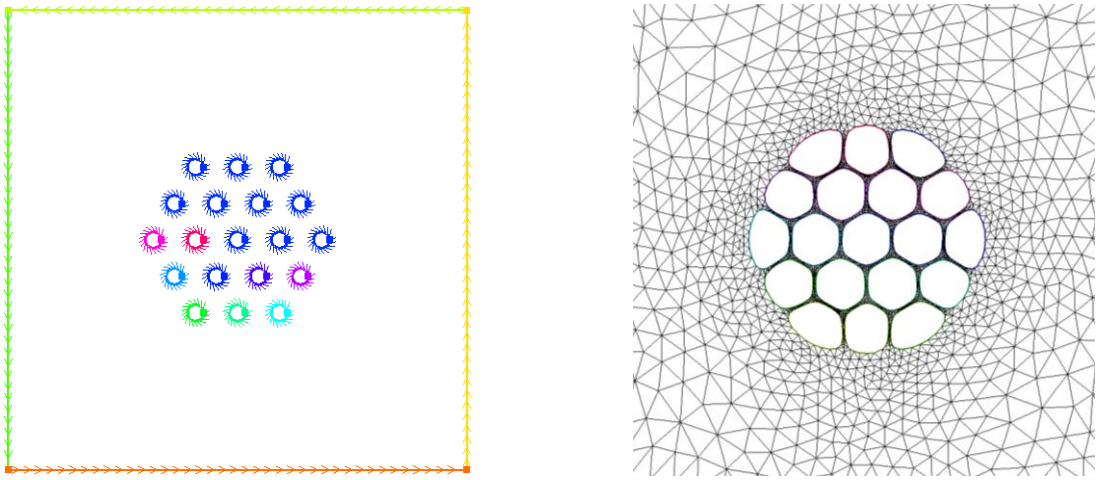

Figure 4.25 Simulation results of current study of the growth of a group of 19 bubbles with the conditions adopted by Yue et al. [108]

Four different cases have been selected for the purpose of simulation, a bubble pair (Figure 4.26), two cases for a group of three bubbles arranged in different ways (Figure 4.27and 4.28), and one case for a cluster of seven bubbles (Figure 4.29). The nucleated bubbles are placed in the same position as of the experimental case and the simulation run for the presumed operating conditions. The experimental conditions of the cases 1, 3 and 4 (Figure 4.26, 4.28 and 4.29) were the same, namely The initial pressure of 1.5 Mpa dissolved with 1.5 % CO2 at 190 °C. For the case #2, the initial pressure was 2Mpa, and dissolved with 2 % CO2 at 190 °C and was extruded from the 1 mm diameter die. The results are quite promising comparing to the cell model and are within 10 percent

error range. One of the most important reasons for discrepancies between the simulation results and the experimental observation is the shear flow produced by the flow of the polymer inside the extruder. The unavoidable shear stresses that exist in the polymer clearly affects the bubble boundary deformation and can rotate and stretch bubbles in the direction of flow. This effect is more pronounced in Figure 4.29. In order to include the shear stress generated by friction between the moving polymer and the parts that are in contacts with it such as screws and the interior wall of the extruder, a proper rheological model in addition to a precise inspection of the surface conditions of those parts has to be considered.

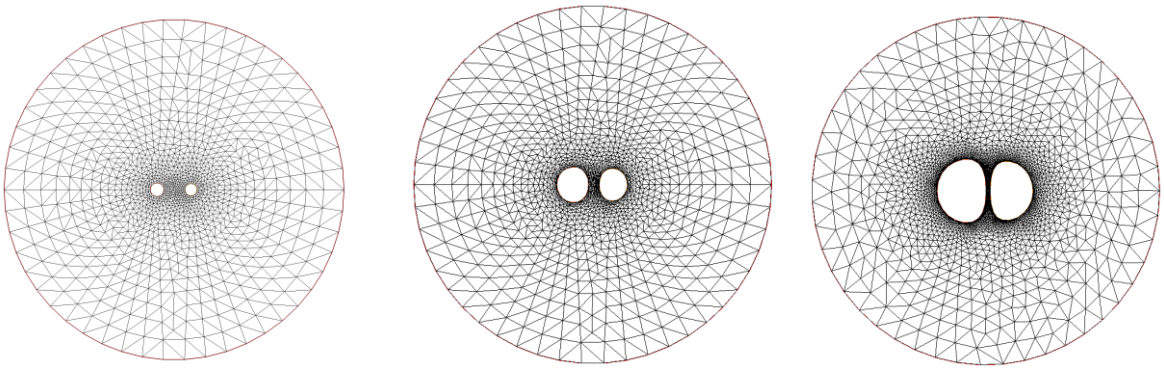

Equation 4.36 Time laps of the growth of a pair of bubbles with 0.1 difference in birth

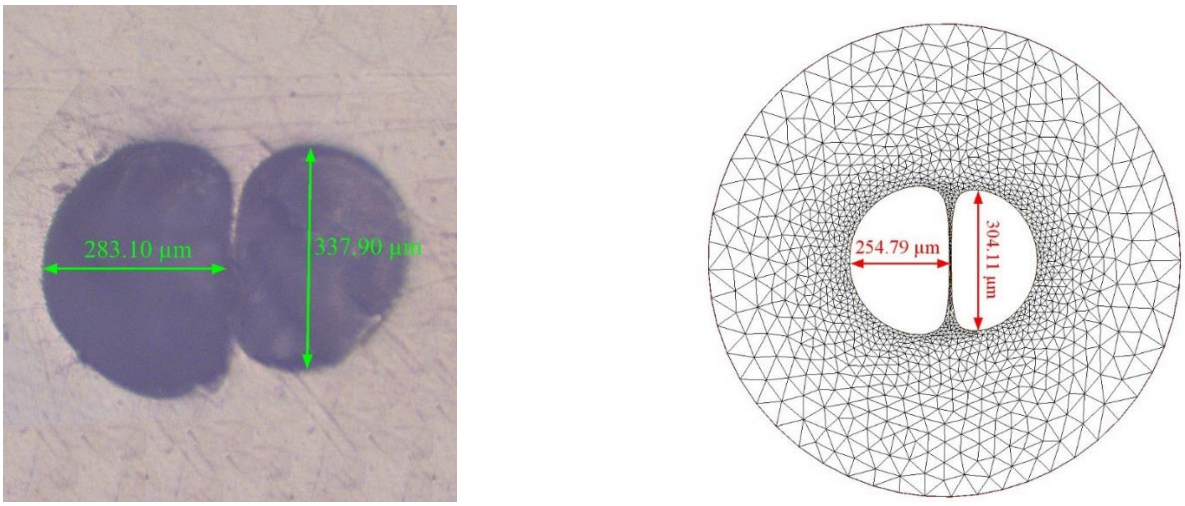

Figure 4.26 Simulation results for a pair of bubble nucleated near each other with 0.1 s difference in birth time

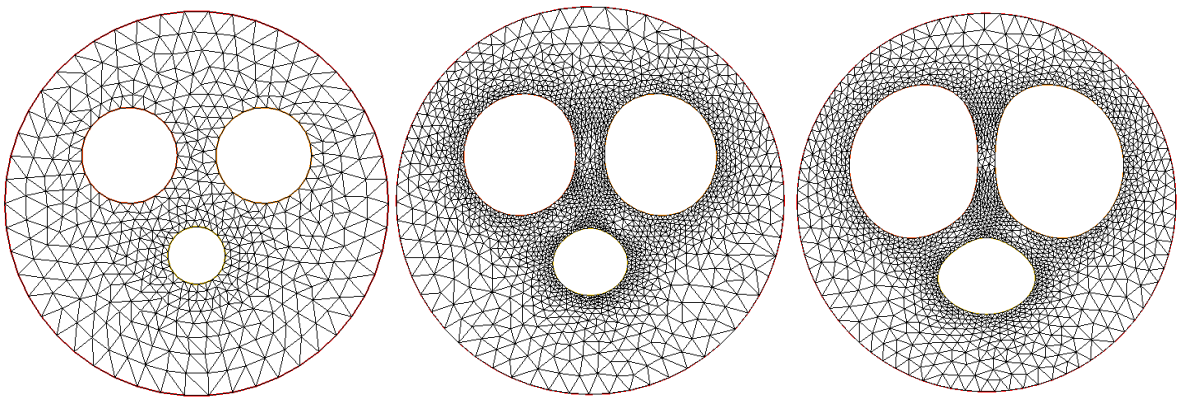

Equation 4.37 Time laps of the growth of a group of bubbles with 0.4 s difference in birth

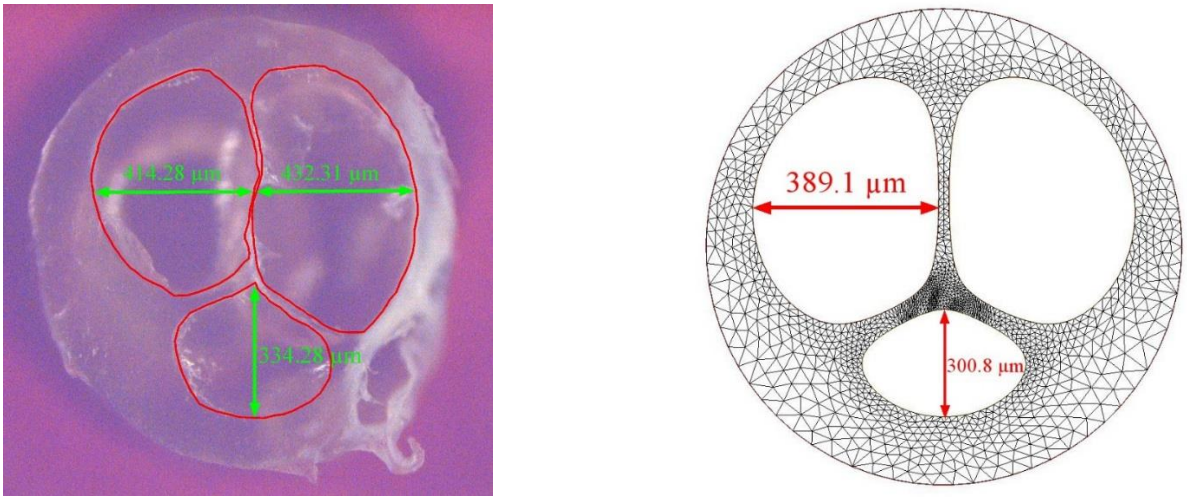

Figure 4.27 Simulation results for a group of bubbles nucleated near each other with 0.4 s difference in birth time

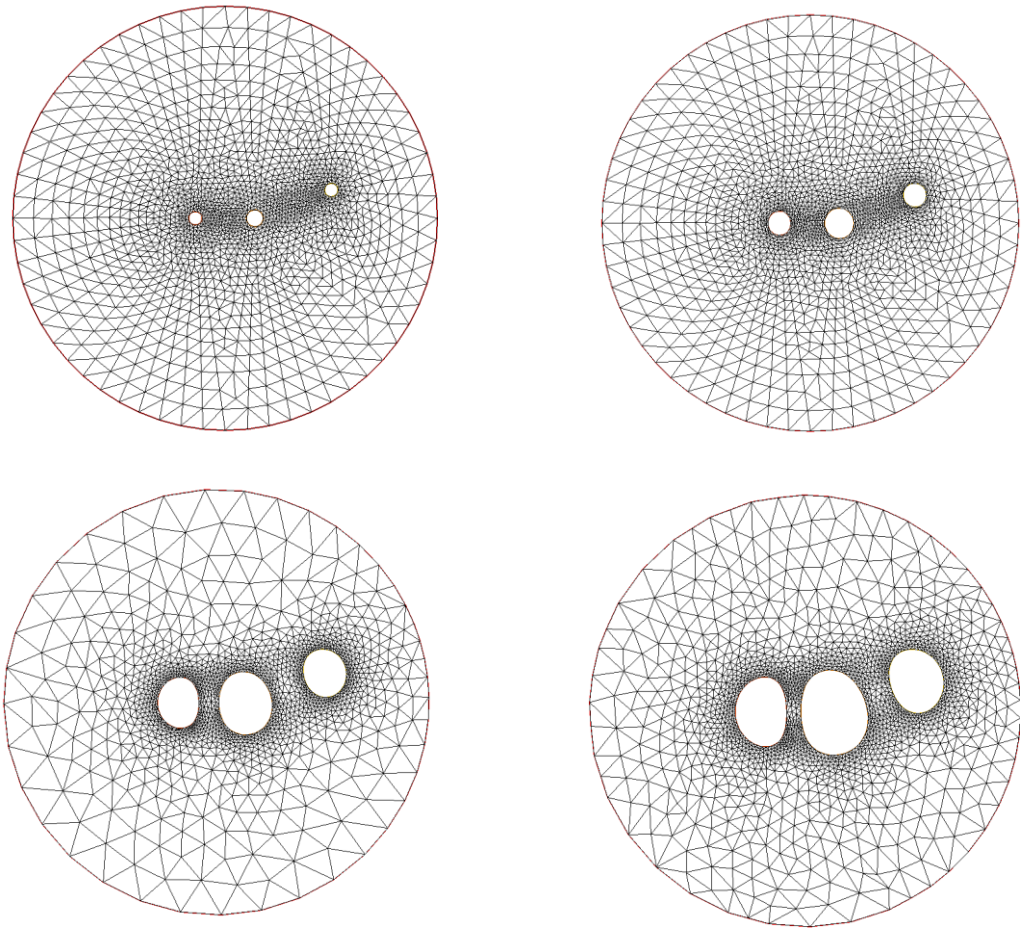

Equation 4.38 Time laps of the growth of a group of bubbles with 0.2 s difference in birth

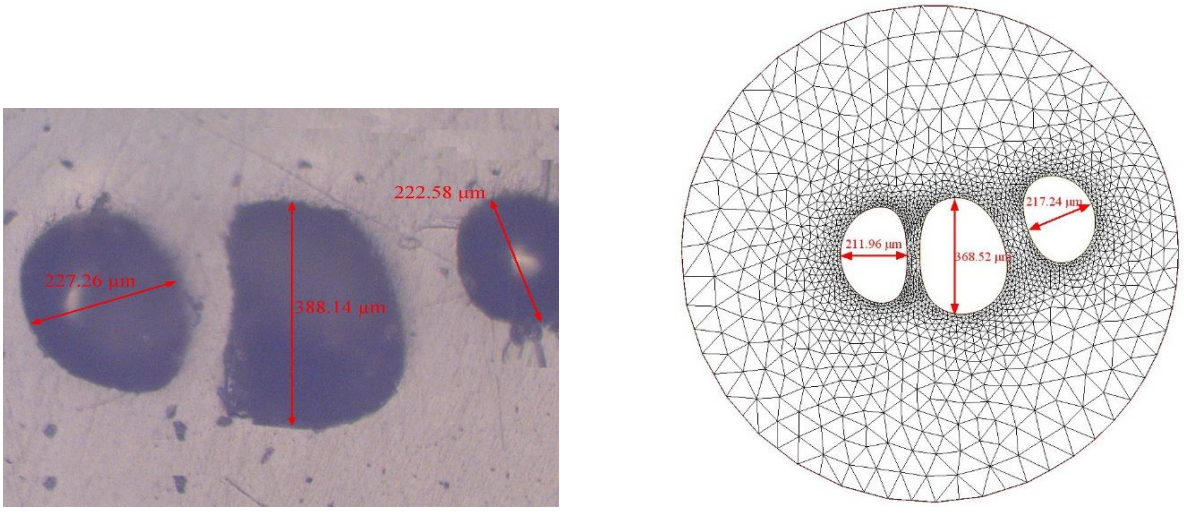

Figure 4.28 Simulation results for a group of bubbles nucleated near each other with 0.2 s difference in birth time

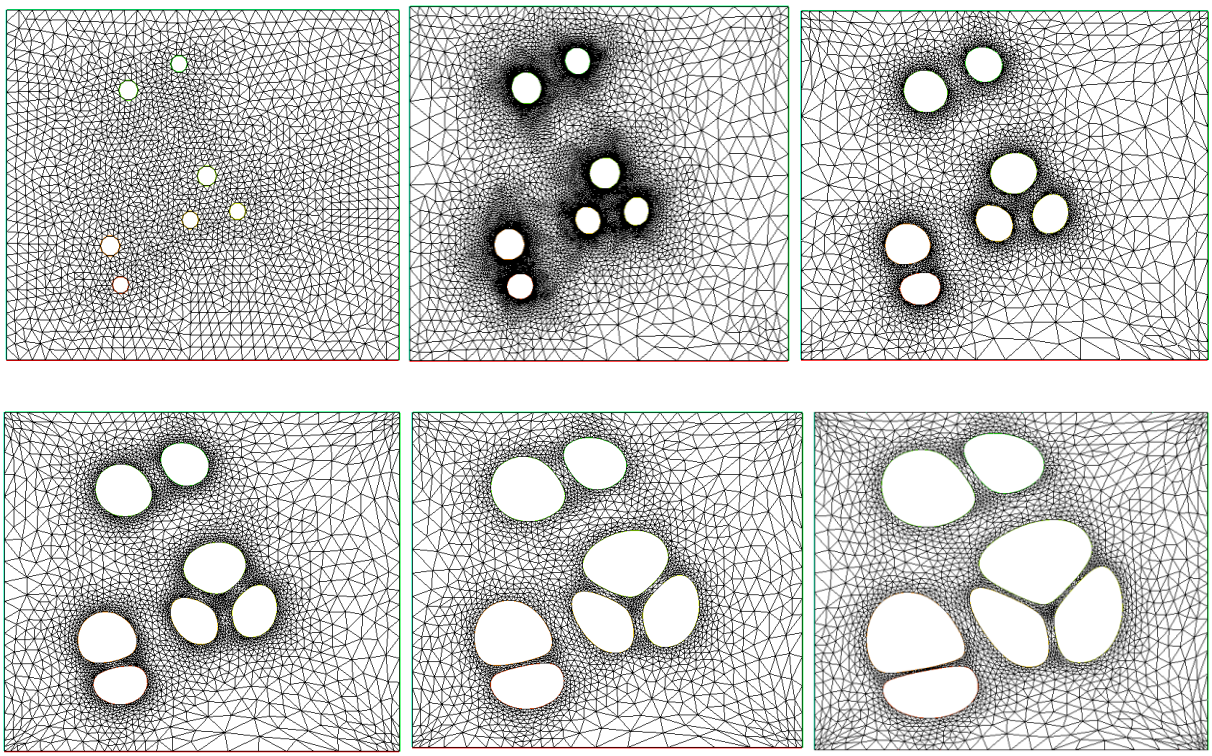

Equation 4.39 Time laps of the growth of a group of seven bubbles

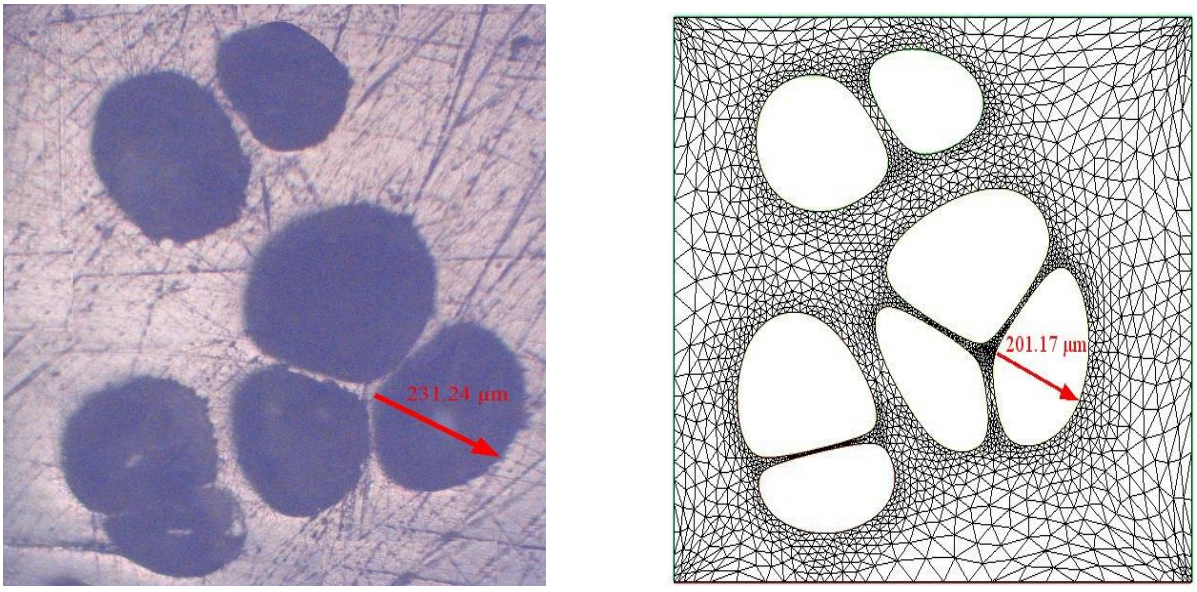

Figure 4.29 Simulation results for a group of bubbles nucleated near each other

4.12 Comparison of the cell model and two-dimensional model over the extruded foam density at different die pressures

Figure 4.30 shows the results of the simulated foam density by the cell model and two-dimensional model and compare it with the experimental results. The density of the extruded foams are obtained by using the image processing technique. The "ImageJ [148]" software has been used for this purpose. At each cross section, since the boundaries of bubbles are clear at each image, using the software tools, we can fill the interior area of the bubbles and then measure the total area of the bubbles at the cross section (Figure 4.31 and 4.32). Having the area of the whole cross section and the sum of the areas of bubbles, we can plug them into the following formula to obtain the ratio of the raw polymer density to extruded foam density.

$$\frac{\rho_{Polymer}}{\rho_{foam}} = \frac{1}{1-\frac{2A_g}{3A_T}} \qquad \textit{Equation 4.40}$$

Where the A_g is the sum of the area of the gas bubbles at each cross section and A_T is the total area of the cross section.

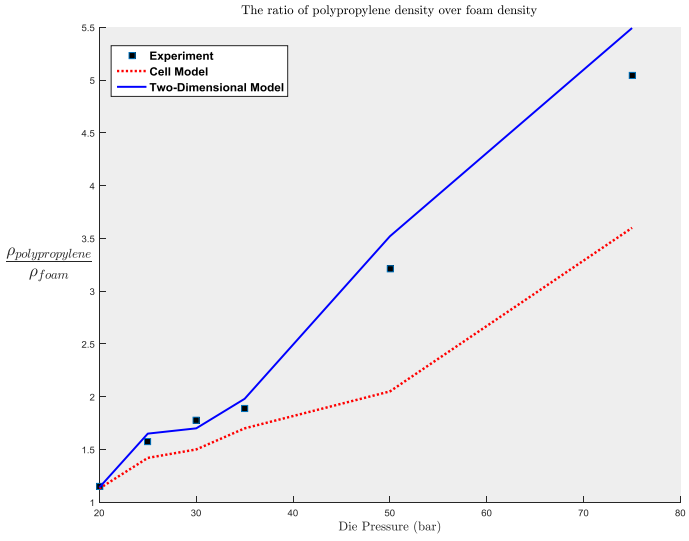

Figure 4.30 Simulation results of cell model and two-dimensional model for the foam density ratio

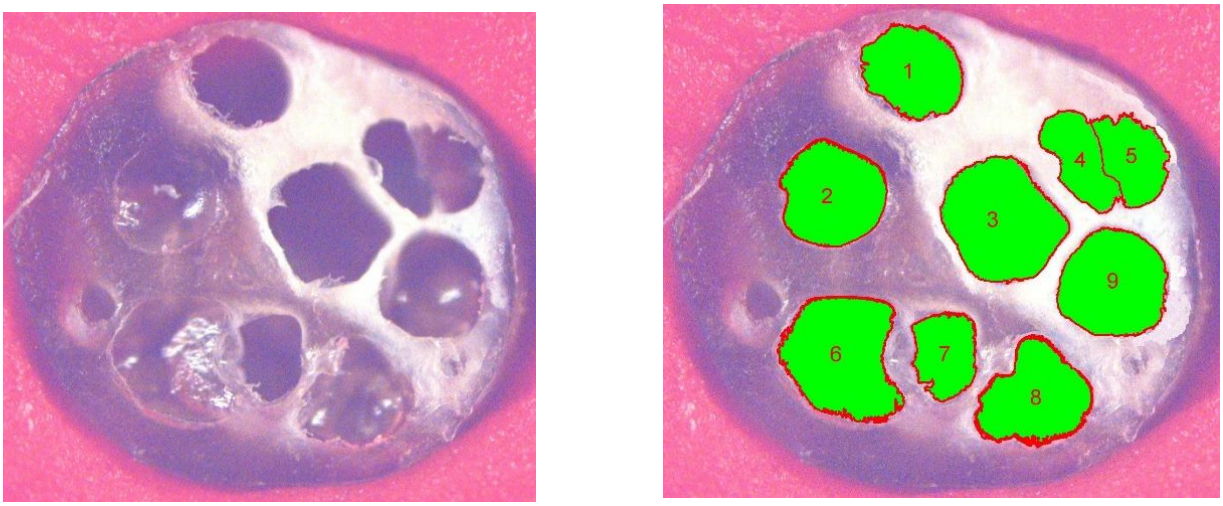

Figure 4.31 Image processing on the extruded foam

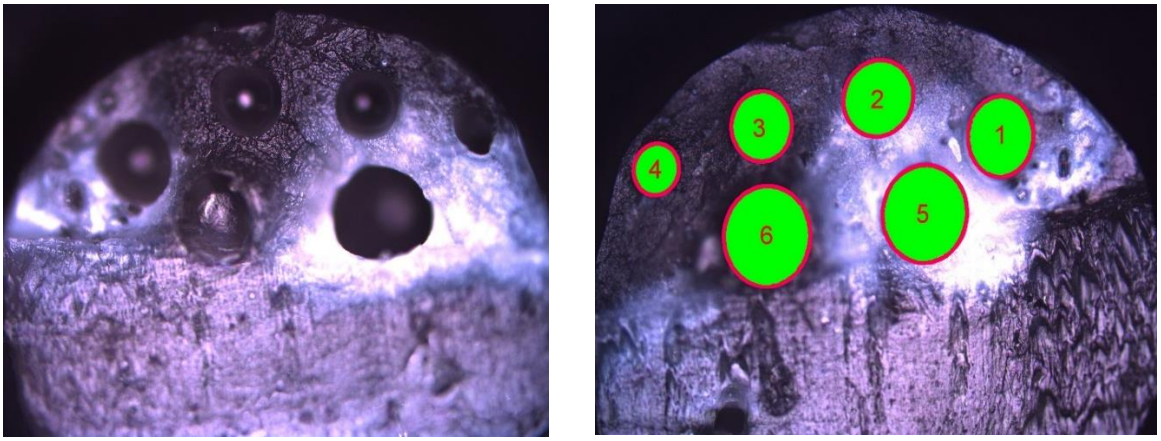

Figure 4.32 Image processing on the extruded foam

In order to examine the effect of die pressure on the growth of bubbles, a series of experiments with the same temperature profile (190℃ at the die) and operating conditions are conducted at six different pressures from 20 atm to 75 atm and in all cases the polymer was dissolved by 3 wt% of CO_2. The results of these experiments are presented in Figure 4.33 to 4.35. According to these figures, as the pressure goes up, the number of bubbles increases (higher final cell densities) and the average bubble size decreases.

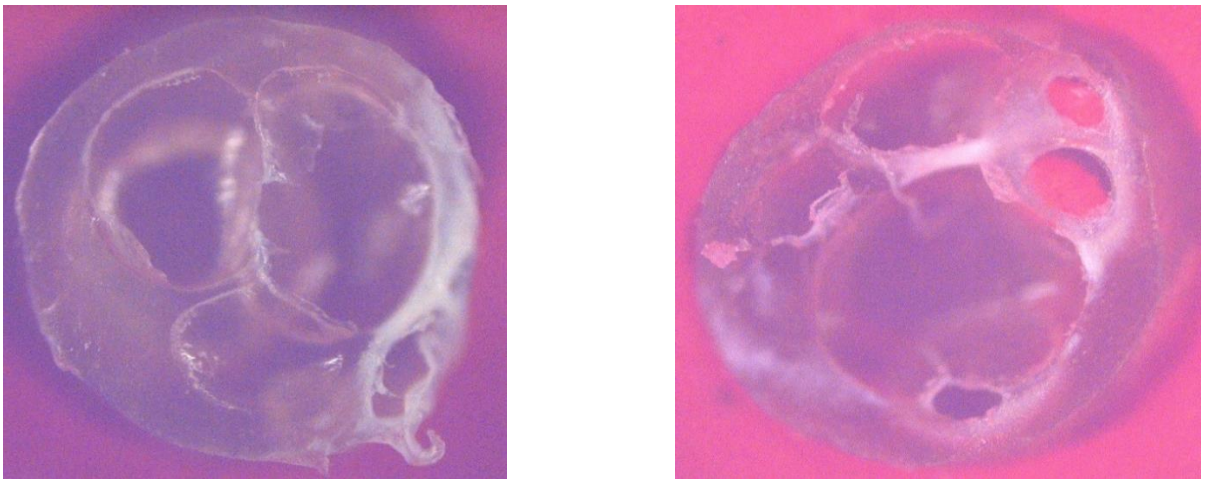

Figure 4.33 Experimental results for the extrusion of polypropylene at 20atm (Left) and 25atm (Right)

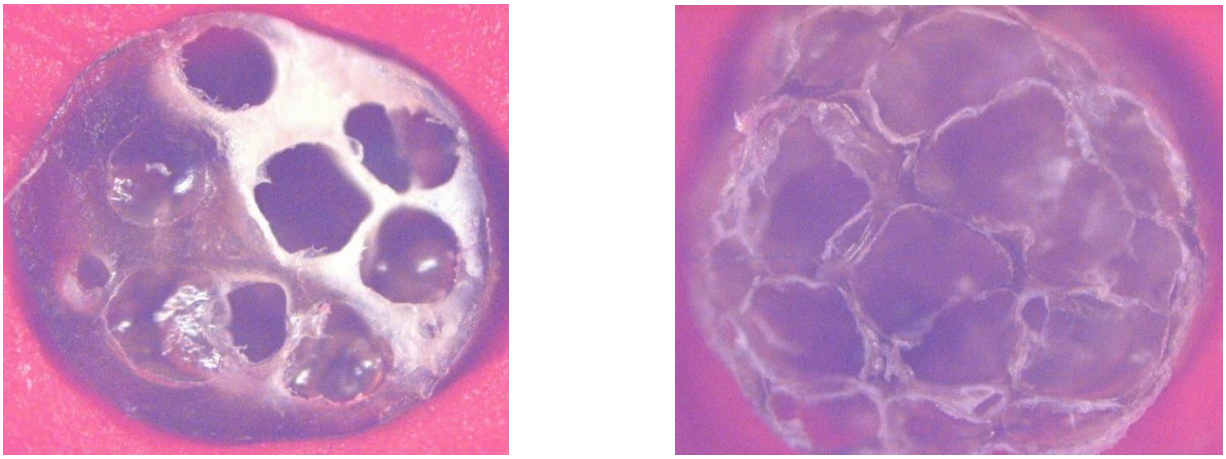

Figure 4.34 Experimental results for the extrusion of polypropylene at 30atm (Left) and 35atm (Right)

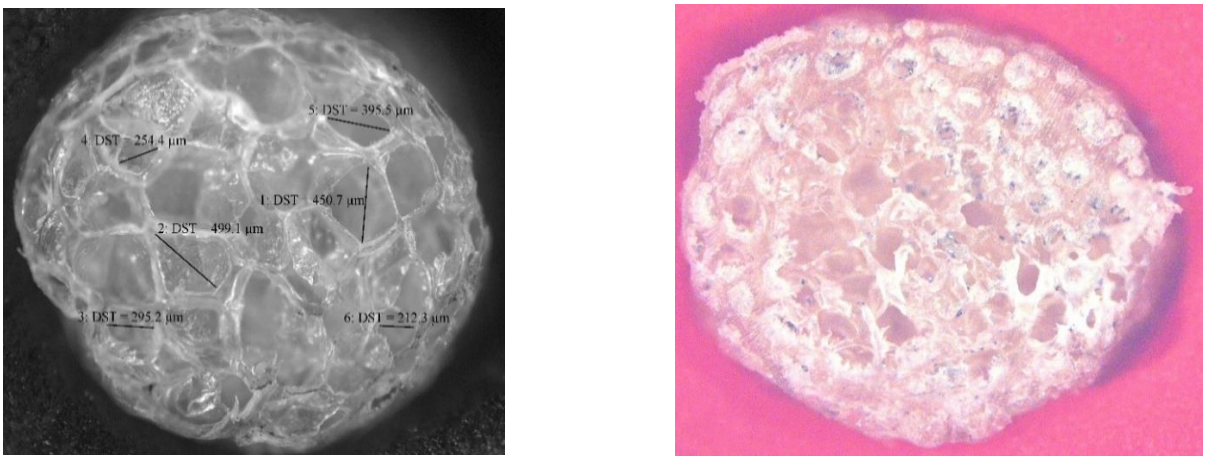

Figure 4.35 Experimental results for the extrusion of polypropylene at 50atm (Left) and 75atm (Right)

In the foaming process, the pressure difference ΔP (pressure at the die) is the main driving force for the bubble growth and bubble nucleation in the extrusion process. It is assumed that the pressure drops to the atmospheric pressure with a linear profile. Since the distance between the beginnings of the die, where polymer is at its highest pressure, to end of the die, where the polymer exits extruder and has the atmospheric pressure, is constant, by increasing the die pressure, the pressure drop rate $-\frac{dP}{dt}$ also increases. When the pressure of the polymer starts to drop, ΔP becomes higher. Once the ΔP become high enough to initiate the nucleation process (as explained in section 4.8), the gas content in the polymer starts to drop progressively due to the continuous consumption of gas molecules by both the nucleation of the new bubbles and their subsequent growth in addition to the growth of the previously nucleated bubbles. When the pressure at the die is lower, the pressure drop rate $-\frac{dP}{dt}$ is also smaller due to smaller. A lower$-\frac{dP}{dt}$ leads to a slower increase in ΔP and therefore, it takes a longer time for the polymer-gas solution to achieve a sufficient amount of ΔP to start the nucleation process. On the other hand, a higher die pressure (P_{Die}) causes a larger pressure drop rate ($-\frac{dP}{dt}$) and higher ΔP at the same time and thus a faster increase in the nucleation rate. As a result, more bubbles are nucleated in a shorter amount of time. When the number of bubbles at a nucleation step increases, it means a larger amount of gas should be consumed to nucleate new bubbles rather than increasing the size of previously nucleated bubbles. Therefore, the limited gas supply will be used for a larger number of bubbles and therefore, a smaller bubble sizes will be resulted. In addition, as the die pressure and pressure drop rate($-\frac{dP}{dt}$) increases, the entire nucleation process happens in a shorter period of time and since the difference in the bubble sizes is due to the difference in the nucleation times, as the entire process is shorten, bubble size would be more uniform.

Another important observation from Figure 4.33 to 4.35 is that the shape of bubbles deviates from a perfect sphere when the number of bubbles increases. Due to the increased bubble-bubble interactions, the boundary of a bubble experience a non-uniform stress field around itself, which is caused by the growth of neighboring bubbles. The inhomogeneity of the stress field around a bubble increases the expansion of the bubble in some directions and suppress it in some other directions. This effect causes bubbles to appear in different shapes rather a perfect sphere.

The experimental situations of Figure 4.33 to 4.35 have been numerically examined by simulations simultaneous of bubble nucleation and bubble growth in the corresponding operating conditions. The simulations performed by both the cell model and two-dimensional model and the results of cell density, average cell size and foam density ratio were compared with the experimental results. The nucleation model that was explained in section 3.9 was adopted for the prediction of cell numbers for both models.

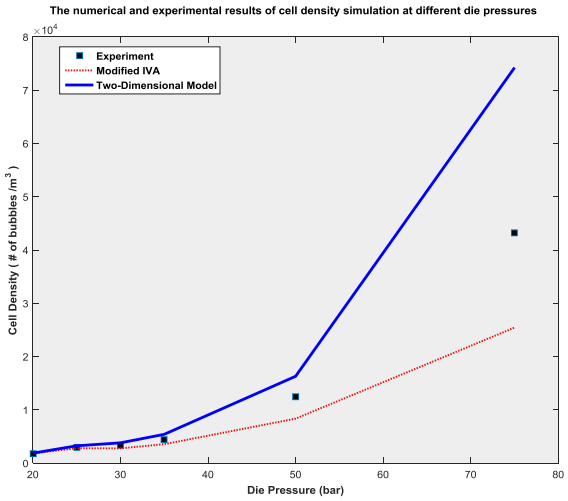

Figure 4.36 Simulation results of the cell model and two-dimensional model on the cell density of the foams

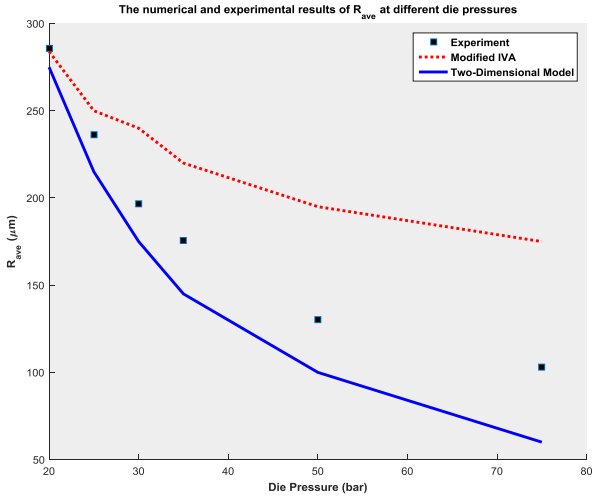

Figure 4.37 Simulation results of cell model and two-dimensional model for the average bubble size

Figure 4.36 shows the results of cell density predictions by both models. This figure reveals that the prediction of cell model is acceptable at the lower die pressures under 3.5Mpa; however, the

precision decreases and the simulation results drop below the experimental data at higher die pressure. According to section 4.7, the radius of the influence volume was one of the parameters that can be selected by trial and error. At the low die pressure, the radius of the influence volume can be chosen in a way that fit well with the final bubble radius at that pressure. The results of the experiment at low pressures have been chosen for determining that radius since chance of spotting an abandoned bubble is higher at low cell density foams and is more compatible with the assumptions of cell model. Once the radius of the influence volume is selected, the radius will remain the same for the rest of the simulations at different die pressures. However, predicting this parameter from the results of low initial pressure results in a larger value than if it was chosen from the experiments at high initial pressure. Therefore, the volume of influencing area is higher in this situation and more gas would be devoted to each individual bubble. Since the nucleation rate is a function of average gas concentration in the non-influenced regions, larger volume of the influence regions results in a smaller average gas concentration at the non-influence volume, which itself results in a slower nucleation rate and lower cell densities. Therefore, the cell density is underestimated in the cell model.

On the other hand, when the number of bubbles is lower and the influence volume is larger, bubbles have access to more gas content for growth and therefore more gas will be used to grow the existing bubbles. That is one of the reasons that the prediction of cell model for the average bubble size in overestimate the experimental results (Figure 4.37). Another reason is the increased interaction of bubbles at the higher initial pressures. Bubbles in the populated area restrict and suppress the growth of each other. These results proves that the validity of the cell model is restricted to the low cell density foams and the precision decays as the bubble-bubble interaction increases.

Despite the IVA method, the two-dimensional model overestimates the cell number because the nature of the adopted nucleation model is based on an exponential function. Although the constants of the Equation 3.16 can be selected at any initial pressure and the model can be used for the prediction of cell nucleation at any other initial pressure, but, the accuracy of the model decreases when the range of initial pressure increases. Therefore, the adopted nucleation model overestimates the number of cells at the high initial pressure and this overestimation results in an underestimation in the cell size since more gas has been used for the bubble nucleation rather than increasing the size of nucleated bubbles. Figure 4.37and Figure 3.7show these facts.

Chapter 5: Conclusion and Future Works

5.1 Summary and conclusion

The cell nucleation and growth mechanisms in the foaming of polypropylene were investigated through a series of theoretical studies, computer simulations, and experimental investigations in this thesis. First, the influence of changing processing conditions on the foam morphology such as cell size and cell density have been investigated qualitatively through experimental tests. These tests were conducted to illustrate the mechanisms under which the dissolved gas contents, the pressure drop rates, and the presence of additives affect polymeric foaming behaviors. The results showed that increasing pressure and pressure drop rate improve the morphology of the foam by increasing the number of cells and reducing the cell size. The influence of additives such as talc and glass fibers on the cell nucleation have been examined. The results showed that introducing additives such as talc even in a small content (0.5 %wt.) dramatically increase the number of cells. However, this improvement is not linearly proportional to the additive content. For the case of increasing talc content in the polymer, the addition of talc above 4 %wt. could not significantly increase the bubble nucleation. Computer simulations of the bubble growth phenomena during plastic foaming were conducted using finite element method and Freefem++ software [110]. The evolution of a single bubble, as the building block of the foam structure, has been performed based on the assumption of the cell model that has been widely used in the literature. The results showed that the first moments of the growth process (in the case we examined less than 0.3) involve the rapid increase in the bubble radius up to 80% of the final radius.

Furthermore, the sensitivity of growth dynamics on the processing parameters and common assumptions of the cell model such as initial bubble radius, shell radius, initial bubble pressure, and gas concentration have been investigated. Among them, the initial bubble pressure and gas concentration, diffusivity and shell radius were the most critical parameters in determining the final bubble size. These studies revealed that estimating the initial bubble radius as any number less than 5μm is reasonable since the actual R0 is assumed to be in the order of nanometers and final bubble size did not change considerably. The shell radius is a free parameter that has to be chosen based on the individual conditions in the experiment. The results showed that the effect of the size of the shell

radius is noteworthy in the later stages of the growth and the initial stages coincide with each other. Based on our experimental data, this quantity has been estimated 268.64μm.

The effect of gas concentration and any parameter that can have influences on it such as Henry constant is huge on the bubble growth rate and final bubble size. Increasing gas concentration promotes bubble growth rate and final bubble size and elongates the time of the process. Also; these simulations showed that the effect of surface tension and relaxation time is not considerable in the growth profile of the bubble.

For the case of choosing a proper nucleation model, by compromising between the accuracy of the results and complexity of the models, a modified nucleation model based on refining the heterogamous nucleation mechanism has been adopted. This model modifies the discrepancies between the prediction of the model and experimental analysis by introducing the energy reduction factor and pre-exponential factor to the conventional model. The results showed that these two factors are functions of operating temperature and additive content.

The numerical analysis extended to the actual foaming process where the bubbles are growing close to each other and have important mutual interactions. A two-dimensional model based on the finite element method, which has been developed in this thesis, is used to study the interaction of bubbles during the foaming process and to investigate simultaneous bubble nucleation and bubble growth phenomenon in the foaming process. The ability of the two-dimensional model for predicting non-uniform deformation of bubble boundaries has been tested by simulating the deformation of groups of three, four and seven bubbles at the different initial positions in the melt. These analyses have been compared with the experimental results of the extrusion foaming process. The comparisons showed that unlike the previous models, the two-dimensional model is capable of considering the non-homogenous stress field and gas concentration in the polymer the simulation results are in the good agreement with the experimental results.

In the foaming process, the nucleation and growth processes take place simultaneously, and the dynamics of one process affect the other process. In addition to our two-dimensional model, the well-known simulation approach for simultaneous bubble nucleation and growth, namely Influence Volume Approach (IVA), has been modified and adapted for analysis and comparisons. A series of six experiments with the same temperature profile (190 ℃ at die) and gas content (3.1%) were

conducted at different die pressures. The result of the simulations of the IVA and 2D model have been compared in the average bubble radius, cell density and the density of the final foam. These results revealed that due to neglecting bubble-bubble interactions, consideration of enclosing a polymer shell around each bubble, and oversimplifying the assumptions, IVA overestimate the cell size and underestimate the cell density at the high pressures where mutual bubbles influences cannot be disregarded. On the other hand, the two-dimensional model could predict the final bubble size and bubble density with acceptable precision. However, the accuracy of the 2D model decays at high pressures. This increased error is the result of the incapability of nucleation models and not the finite element model. The reason is that the accuracy of the modified nucleation approach decreases in a wide pressure range.

5.2 Contribution

- A novel two-dimensional model based on the finite element method and Lagrangian approach that is capable of considering the mutual interactions of bubbles and is capable of predicting the non-uniform boundary deformation of bubbles in the extrusion process.
- A combined experimental and numerical analysis of the extrusion foaming process in two dimensions.

5.3 Recommendations and future works

Although a huge effort has been done in developing the numerical analysis of the extrusion process, more investigations are still needed to turn these models into more comprehensive and more accurate ones that can be used in all types of the processes where nucleation happens. Thus, further work should be carried out to:

- Developing a model capable of considering the shear flow in the extrusion process.
- Addressing the vital needs for a proper nucleation model that can be used in the extrusion foaming process with enough accuracy.

Developing a practical method for taking advantage of chemical nucleating agents with customized properties.

Bibliography

[1] M. Altan, "Thermoplastic foams: Processing, manufacturing, and characterization," *In Recent Research in Polymerization. IntechOpen,* 2017.

[2] D Tammaro et al., "Validated modeling of bubble growth, impingement and retraction to predict cell-opening in thermoplastic foaming," *Chemical Engineering Journal,* vol. 287, pp. 492-502, 2016.

[3] Hani E Naguib et al., "Fundamental foaming mechanisms governing the volume expansion of extruded polypropylene foams," *Journal of applied polymer science,* vol. 91, no. 4, pp. 2661-2668, 2004.

[4] "Commodity plastics," [Online]. Available: https://en.wikipedia.org/wiki/Commodity_plastics. [Accessed 10 04 2019].

[5] S. N. S. Leung, *MECHANISMS OF CELL NUCLEATION, GROWTH, AND COARSENING IN PLASTIC FOAMING: THEORY, SIMULATION, AND EXPERIMENT,* University of Toronto, 2009.

[6] "CARBON FIBER SANDWICH PANEL," Rock West Composites, [Online]. Available: https://www.rockwestcomposites.com/cftfs-mm-dl-group.

[7] Okolieocha et al., "Microcellular to nanocellular polymer foams: Progress (2004–2015) and future directions–A review," *European Polymer Journal,* vol. 73, pp. 500-519., 2015.

[8] Shau Tarng Lee et al., Polymeric Foams, Science and Technology, New York: CRC Press, 2007.

[9] "Products of AS Composite Inc.," [Online]. Available: https://www.ascomposite.com/en/product.

[10] W. Wang et al., "Effects of High-pressure CO2 on the Glass Transition Temperature and Mechanical Properties of Polystyrene," *Journal of Polymer Science Polymer Physics Edition,* vol. 20, no. 8, pp. 1371-1384, 1982.

[11] D. Koros et al., "Sorption and Transport of CO2 Above and Below the Glass Transition of Poly(Ethylene Terephthalate)," *Polymer Engineering and Science,* vol. 20, no. 1, pp. 14-19, 1980.

[12] N. Kumar et al., "A Process for Making Microcellular Thermoplastic Parts," *Polymer Engineering and Science,* vol. 1329, no. 30, p. 1323, 1990.

[13] J. Kumar et al., "Microcellular PVC," *Journal of Vinyl Technology,* vol. 14, no. 4, pp. 191-197, 1992.

[14] V. Kumar, "Microcellular Polymers: Novel Materials for the 21st Century," *Progress in Rubber and Plastics Technology,* vol. 9, no. 1, pp. 54-70, 1993.

[15] J. Kumar et al., "A Process to Produce Microcellular PVC," *International. Polymer Processing,* vol. 3, no. 1, pp. 191-197, 1993.

[16] J. Kumar et al., "Production of Microcellular Polycarbonate Using Carbon Dioxide for Bubble Nucleation," *Journal of Engineering for Industry,* vol. 116, no. 4, pp. 413-420, 1994.

[17] V. Schirmer et al., "Novel Reduced-density Materials by Solid-state Extrusion: Proof-of-Concept Experiments," *Cellular Polymers,* vol. 23, no. 6, pp. 369-385, 2003.

[18] N. Baldwin et al., "Microcellular Plastics Processing Technology (1)," *Journal of Japan Society of Polymer Processing (SEIKEIKAKOU),* vol. 6, no. 3, pp. 187-194, 1994.

[19] L. Park et al., "A Study of Cell Nucleation in the Extrusion of Polypropylene Foams," *Polymer Engineering and Science,* vol. 37, no. 1, pp. 1-10, 1997.

[20] N. Park et al., "Filamentary Extrusion of Microcellular Polymers Using a Rapid Decompressive Element," *Polymer Engineering and Science,* vol. 36, no. 1, pp. 34-48, 1996.

[21] N. Park et al., "Effect of the Pressure Drop Rate on Cell Nucleation in Continuous Processing of Microcellular Polymers," *Polymer Engineering and Science,* vol. 35, no. 5, pp. 432-440, 1995.

[22] A. Volmer et al., "Nucleus Formation in Supersaturated Systems," *Zeitschrift für Physikalische Chemie,,* vol. 119, no. 3-4, pp. 227-301, 1926.

[23] L. Farkas, "The Velocity of Nucleus Formation in Supersaturated Vapors," *Zeitschrift für Physikalische Chemie,* vol. 125, p. 236, 1927.

[24] B. Zeldovich, "On the Theory of New Phase Formation: Cavities," *Acta Physicochim URSS,* vol. 18, no. 1, pp. 1-22, 1943.

[25] J. Gibbs, The Scientific Papers of J. Willard Gibbs, vol. 1, New York, 1961.

[26] K. J. Blander et al., "Bubble nucleation in liquids," *AIChE Journal,* vol. 21, pp. 833-848, 1975.

[27] A. Ward et al., "On the thermodynamics of nucleation in weak liquid–gas solutions," *Journal of Basic Engineering transactions of the ASME,* vol. 92, no. 4, pp. 695-704, 1970.

[28] W. Forest et al., "Effect of a dissolved gas on the homogeneous nucleation pressure of a liquid," *Journal of Chemical Physics,* vol. 66, pp. 2322-2330, 1976.

[29] W. Forest et al., "Homogeneous nucleation of bubbles in solutions at pressures above the vapor pressure of the pure liquid," *Journal of Chemical Physics,* vol. 69, pp. 2221-2230, 1978.

[30] S. Tucker et al., "Critical state of bubbles in liquid-gas solutions," *Journal of Applied Physics,* vol. 46, pp. 4801-4808, 1975.

[31] M. Katz et al., "Condensation and Boiling: Corrections to Homogeneous Nucleation Theory for Nonideal Gases," *Journal of Colloid and Interface Science,* vol. 42, no. 3, pp. 496-502,, 1973..

[32] E. Ward et al., "Conditions for Stability of Bubble Nuclei in Solid Surfaces Contacting a Liquid-gas Solution," *Journal of Applied Physics,* vol. 56, no. 2, pp. 491-500, 1984.

[33] A. Ward et al., "Heterogeneous bubble nucleation and conditions for growth in a liquid-gas system of constant mass and volume," *Journal of Applied Physics,* vol. 54, pp. 1833-1843, 1983.

[34] R. Cole, "Boiling nucleation," *Advances in Heat Transfer,* vol. 10, pp. 85-166, 1974.

[35] P. Wilt, "Nucleation rates and bubble stability in water-carbon dioxide solutions," *Journal of Colloid and Interface Science,* vol. 112, pp. 530-538, 1986.

[36] J. Fisher, "The fracture of liquids," *Journal of Applied Physics,* vol. 19, pp. 1062-1067, 1948.

[37] N. Fletcher, "Size effect in heterogeneous nucleation," *Journal of Chemical Physics,* vol. 29, pp. 572-576, 1958.

[38] .J. Jarvis et al., "Bubble nucleation mechanisms of liquid droplets superheated in other liquids," *Journal of Colloid and Interface Science,* vol. 50, pp. 359-368, 1975.

[39] R. Apfel, "Vapor nucleation at a liquid–liquid interface," *Journal of Chemical Physics,* vol. 54, pp. 62-63, 1971.

[40] M. Blander, "Bubble Nucleation in Liquids," *Advances in Colloid and Interface Science,* vol. 10, no. 1, pp. 1-32, 1979.

[41] G. Moore, "Vaporization of Superheated Drops in Liquids," *AIChE Journal,* vol. 5, no. 4, pp. 458-466, 1959.

[42] M. Volmer et al., "A nuclei formation in supersaturated states," *Zeitschrift fur Physikalische Chemie,* vol. 119, pp. 227-301, 1926.

[43] Shau-Tarng Lee et al., Foam Extrusion Principles and Practice, Second Edition ed., C. B. P. S.T. Lee, Ed., 2014: CRC Press Taylor & Francis Group.

[44] J. Frenkel, Kinetic Theory of Liquids, Oxford: Clarendon Press, 1946.

[45] A. Harvey et al., "On Cavity Formation in Water,," *Journal of Applied Physics,* vol. 18, no. 2, pp. 162-172, 1947.

[46] Harvey et al., "Removal of Gas Nuclei from Liquids and Surface," *Journal of the American Chemical Society,* vol. 67, no. 1, pp. 156-157, 1945.

[47] Harvey et al., "Bubble Formation in Animals – II. Gas Nuclei and their Distribution in Blood and Tissues," *Journal of Cellular Physiology,* Vols. 23-34, no. 1, p. 24, 1944.

[48] Harvey et al., "Bubble Formation in Animals – I. Physical factors," *Journal of Cellular Physiology,* vol. 24, no. 1, pp. 1-22, 1944.

[49] Jones et al., "Bubble Nucleation from Gas Cavities – A Review," *Advances in Colloid and Interface Science,* vol. 80, no. 1, pp. 27-50, 1999.

[50] Han et al., "Bubble Nucleation in Polymeric Liquids. II. Theoretical Considerations," Polymer Sciences, Part B," *Polymer Physics,* vol. 28, no. 5, pp. 743-761, 1990.

[51] S. Lee, "Shear Effects on Thermoplastic Foam Nucleation," *Polymer Engineering and Science,* vol. 33, no. 7, pp. 418-422, 1993.

[52] Leung et al., "Numerical Simulation of Polymeric Foaming Processes Using a Modified Nucleation Theory," *Plastics, Rubber and Composites: Macromolecular Engineering,* vol. 35, pp. 93-100, 2006.

[53] Leung et al., "Effects of Nucleating Agents' Shapes and Interfacial Properties on Cell Nucleation," *Journal of Cellular Plastics,* 2009.

[54] K. Taki, "Experimental and Numerical Studies on the Effects of Pressure Release Rate on Number Density of Bubbles and Bubble Growth in a Polymeric Foaming Process," *Chemical Engineering Science,* vol. 63, pp. 3643-3653, 2008.

[55] R. Ward et al., "Stability of Bubbles in a Closed Volume of Liquid-Gas Solution," *Journal of Applied Physics,* vol. 53, no. 9, pp. 6076-6084, 1982.

[56] Kamiya et al., "CO2 Sorption and Dilation of Poly(Methyl Methacrylate)," *Macromolecules,* vol. 31, no. 2, pp. 472-478, 1998.

[57] Han et al., "Bubble nucleation in polymeric liquids. I. Bubble nucleation in concentrated polymer solutions," *Journal of Polymer Science Part B: Polymer Physics,* vol. 28, no. 5, pp. 711-741, 1990.

[58] N.S. Ramesh et al., "The heterogeneous nucleation of microcellular foams assisted by the survival of microvoids in polymers containing low glass transition particles. Part I: Mathematical modeling and numerical simulation," *Polymer Engineering & Science,* vol. 34, no. 22, pp. 1685-1697, 1994.

[59] N.S.Ramesh et al., "The heterogeneous nucleation of microcellular foams assisted by the survival of microvoids in polymers containing low glass

transition particles. Part II: Mathematical modeling and numerical simulation," *Polymer Engineering & Science,* vol. 34, no. 22, pp. 1685-1697, 1994.

[60] J. kweeder et al., "Nucleation of microcellular polystyrene foam," *SPE ANTEC Tech,* p. 1398, 1991.

[61] B. Feng et al., ""Prediction of bubble growth and size distribution in polymer foaming based on a new heterogeneous nucleation model," *Journal of Rheology ,* vol. 48, no. 2, pp. 439-462, 2004.

[62] B. Venerus et al., "Analysis of Diffusion-Induced Bubble Growth in Viscoelastic Liquids," *Journal of Non-Newtonian Fluid Mechanics,* vol. 75, no. 1, pp. 55-75, 1998.

[63] S. Lee, Foam Extrusion, Principles and Practice, Lancaster, PA: Technomic, 2000, p. 111–112.

[64] Niyogi et al., "Modeling of bubble-size distribution in free rise polyurethane foams," *AIChE Journal,* vol. 38, no. 8, pp. 1170-1184, 1992.

[65] Youn et al., "Bubble growth in reaction injection molded parts foamed by ultrasonic excitation," *Polymer Engineering & Science,* vol. 39, no. 3, pp. 457-468, 1999.

[66] Newman et al., "Modeling the ultraviolet photodegradation of rigid polyurethane foams," *Industrial & engineering chemistry research,* vol. 40, no. 15, pp. 3346-3352, 2001.

[67] Lee et al., Polymeric Foams: Mechanisms and Materials, CRC PRESS, 2004.

[68] Geier et al., "Macro and micro-scale modeling of polyurethane foaming processes," in *AIP Conference Proceedings*, 2014.

[69] Y. Zhao, *Modeling and experimental study of polyurethane foaming reactions,* Columbia: University of Missouri, 2015.

[70] Rao et al., "The kinetics of polyurethane structural foam formation: Foaming and polymerization," *AIChE Journal,* vol. 63, no. 7, pp. 2945-2957, 2017.

[71] L. Rayleigh, "On the Pressure Developed in a Liquid During the Collapse of a Spherical," *Philosophical Magazine,* vol. 34, pp. 94-98, 1917.

[72] M. Epstein et al., "The Stability of Gas Bubbles in Liquid-Gas Solutions," *The Journal of Chemical Physics,* vol. 18, no. 9, p. 1305, 1950.

[73] L. Scriven, "On the Dynamics of Phase Growth," *Chemical Engineering Science,* vol. 10, no. 1, pp. 1-13, 1959.

[74] Barlow et al., "Diffusion of Gas from a Liquid into an Expanding Bubble," *IBM Journal of Research of Development,* vol. 6, pp. 329-337, 1962.

[75] R. Darby, "The dynamics of vapour bubbles in nucleate boiling," *Chemical Engineering Science,* vol. 19, pp. 39-49, 1964.

[76] Gent et al., "Nucleation and growth of gas bubbles in elastomers," *Journal of applied physics,* vol. 40, no. 6, pp. 2520-2525, 1969.

[77] Street et al., "“Dynamics of Phase Growth in Viscous, Non-Newtonian Liquids. Initial Stages of Growth," *Industrial and Engineering Chemistry Fundamentals,* vol. 10, no. 1, pp. 54-64, , 1971.

[78] Rosner et al., "Effects of Interface Kinetics, Capillarity and Solute Diffusion on Bubble Growth Rates in Highly Supersaturated Liquids,," *Chemical Engineering Science,* vol. 27, no. 1, pp. 69-88, 1972.

[79] L. Zana E. and Leal, "Dissolution of a Stationary Gas Bubble in a Quiescent Viscoelastic Liquid," *Industrial and Engineering Chemistry Fundamentals,* vol. 14, no. 3, pp. 175-182 , 1975.

[80] Villamizar et al., "Studies on structural foam processing II. Bubble dynamics in foam injection molding," *Polymer Engineering & Science,* vol. 18, no. 9, pp. 699-710, 1978.

[81] R. D. Patel, "Bubble growth in a viscous Newtonian liquid," *Chemical Engineering Science ,* vol. 35, no. 11, pp. 2352-2356, 1980.

[82] Han et al., "Studies on structural foam processing. IV. Bubble growth during mold filling," *Polymer Engineering and Science,* vol. 21, no. 9, pp. 518--533, 1981.

[83] Papanastasiou et al., "Bubble growth and collapse in viscoelastic liquids analyzed," *Journal of Non-Newtonian Fluid Mechanics,* vol. 16, no. 1-2, pp. 53-75, 1984.

[84] R. K. Upadhyay, "Study of bubble growth in foam injection molding." Advances in Polymer Technology," *Journal of the Polymer Processing Institute,* vol. 5, no. 1, pp. 55-64, 1985.

[85] H. S.Y, "Bubble Growth in Thermoplastic Structural Foams," *Polymer Engineering and Science,* vol. 16, no. 4, pp. 270-275, 1976.

[86] H. Han et al., "Oscillatory Behavior of a Gas Bubble Growing (or Collapsing) in Viscoelastic Liquids," *AIChE Journal,* vol. 28, no. 6, pp. 1002-1009, 1982.

[87] J. Street, "The Rheology of Phase Growth in Elastic Liquid," *Journal of Rheology,* vol. 12, no. 1, pp. 103-131, 1968.

[88] Amon et al., "A study of the dynamics of foam growth analysis of the growth of closely spaced spherical bubbles," *Polym. Engg. Sci,* vol. 24, no. 13, pp. 1026-1034, 1984.

[89] Arefmanesh et al., "Diffusion-induced growth of a gas bubble in a viscoelastic fluid," *Rheologica Acta,* vol. 30, no. 3, pp. 274-283, 1991.

[90] N.S. Ramesh et al., "Numerical and experimental studies of bubble growth during the microcellular foaming process," *Polymer Engineering & Science,* vol. 31, no. 23, pp. 1657-1664, 1991.

[91] Amon et al., "A Study of the Dynamics of Foam Growth: Simplified Analysis and Experimental Results for Bulk Density in Structural Foam Molding," *Polymer Engineering and Science,* vol. 26, no. 3, pp. 255-267, 1986.

[92] Lee et al., "Study of thermoplastic foam sheet formation," *Polymer Engineering & Science,* vol. 36, no. 19, pp. 2477-2482, 1996.

[93] Lee et al., "Study of Foam Sheet Formation; Effect of Foam Thickness and Cell Density," in *ASME annual Conference*, Atlanta, 1996.

[94] P. Payvar, "Mass transfer-controlled bubble growth during rapid decompression of a liquid," *International journal of heat and mass transfer,* vol. 30, no. 4, pp. 699-706, 1987.

[95] Shafi et al., "Bubble Size Distributions in Freely Expanded Polymer Foams," *Chemical Engineering Science,* vol. 52, no. 4, pp. 635-644, 1992.

[96] Joshi et al., "Prediction of Cellular Structure in Free Expansion of Viscoelastic Media," *Journal of Applied Polymer Science,* vol. 67, no. 9, pp. 1353-1368, 1998.

[97] Shimoda et al., "Polymeric Foaming Simulation for Extrusion Processes," *Journal of Cellular Plastics,* vol. 37, no. 6, pp. 517-536, 2001.

[98] R. G. Larson, Constitutive Equations for Polymer Melts and Solutions, 1 ed., H. Brenner, Ed., Butterworth-Heinemann, 1988, p. 20.

[99] Taki et al., "Visual observations of batch and continuous foaming processes," *Journal of Cellular Plastics,* vol. 39, no. 2, pp. 155-169, 2003.

[100] Taki et al., "Visual observation of CO2 foaming of polypropylene-clay nanocomposites," *Polymer Engineering & Science,* vol. 44, no. 6, pp. 1004-1011, 2004.

[101] Popinet et al., "Bubble collapse near a solid boundary: a numerical study of the influence of viscosity," *Journal of Fluid Mechanics,* vol. 464, pp. 137-163, 2002.

[102] Caboussat et al., "Numerical simulation of free surface incompressible liquid flows surrounded by compressible gas," *J. Comput. Phys,* vol. 203, pp. 626-649, 2005.

[103] A. Caboussat, "A numerical method for the simulation of free surface flows with surface tension," *Comput. Fluids,* vol. 35, pp. 1205-1216, 2006.

[104] Beechem et al., "Bubble growth mechanism in carbon foams," *Carbon,* vol. 43, pp. 1055-1064, 2005.

[105] Everitt et al., "Bubble growth in a two-dimensional viscoelastic foam," *J. Non-Newtonian Fluid Mech,* vol. 137, pp. 46-59, 2006.

[106] Everitt et al., "Competition and interaction of polydisperse bubbles in polymer foams," *J. Non-Newtonian Fluid Mech,* vol. 137, pp. 60-71, 2006.

[107] Bruchon et al., "Direct 2D simulation of small gas bubble clusters: From the expansion step to the equilibrium state," *International Journal for Numerical Methods in Fluids,* vol. 54, no. 1, pp. 73-101, 2007.

[108] Yue et al., "An arbitrary Lagrangian–Eulerian method for simulating bubble growth in polymer foaming," *Journal of Computational Physics,* vol. 226, no. 2, pp. 2229-2249, 2007.

[109] Leung et al., "Evaluation of Classical Nucleation Theory Using Visualization Data," *SPE, ANTEC, Technical Papers,* vol. 2, pp. 2592-2596, 2005.

[110] Open Source, [Online]. Available: https://freefem.org/.

[111] S. N. S. Leung, "Mechanism of Cell Nuncleation, Growth and Coarsening In Plastin Foaming: Theory, Simulation, and Experiment," University of Toronto, Toronto, 2009.

[112] "The perfect combination of chemistry and physics," Lehmann&Voss&Co, [Online]. Available: https://www.luvobatch.de/en/product-groups/blowing-agents/.

[113] "Foamazol Chemical Foaming Agents," Bergen International Inc., [Online]. Available: http://www.bergeninternational.com/chemical-foaming-agents-product-finder.html.

[114] Polychem Dispersion Inc., [Online]. Available: http://www.dispersions.com/.

[115] "Process 11 Parallel Twin-Screw Extruder," ThermoFisher Scientific, [Online]. Available: https://www.thermofisher.com/order/catalog/product/567-7600.

[116] M. Azad, *Manufacturing of Sandwich Panels Using Recycled Thermoplastic Composites in a Continuous Extrusion Line,* Montreal, Quebec: Concordia University, 2016.

[117] C. Rauwendaal, Polymer extrusion; revised 4th edition, Hanser, 2001.

[118] F. G. Martelli, Twin-screw extruders:a basic understanding, New York: Van Nostrand Reinhold, 1983.

[119] B. International, "CHEMICAL FOAM EXTRUSION PROCESSING GUIDE," 2008. [Online]. Available: http://www.bergeninternational.com/files/Extrusion-Processing-Guide.pdf.

[120] Sato et al., "Solubilities of carbon dioxide and nitrogen in polystyrene under high temperature and pressure," *Fluid Phase Equilibria,* vol. 125, no. 1-2, pp. 129-138, 1996.

[121] Sato et al., "Solubilities and diffusion coefficients of carbon dioxide and nitrogen in polypropylene, high-density polyethylene, and polystyrene under high pressures and temperaures," *Fluid phase equilibria,* vol. 162, no. 1-2, pp. 261-276, 1999.

[122] Wong et al., "High-precision gravimetric technique for determining the solubility and diffusivity of gases in polymers," *Journal of Polymer Science Part B: Polymer Physics,* vol. 36, no. 12, pp. 2025-2032, 1998.

[123] Andre Blasig et al., "Magnetic suspension balance study of carbon dioxide solubility in ammonium-based polymerized ionic liquids: Poly(p-vinylbenzyltrimethyl ammonium tetrafluoroborate) and poly([2-(methacryloyloxy)ethyl] trimethyl ammonium tetrafluoroborate)," *Fluid Phase Equilibria,* vol. 256, no. 1-2, pp. 75-80, 1 August 2007.

[124] Blasig et al., "Magnetic suspension balance study of carbon dioxide solubility in ammonium-based polymerized ionic liquids: poly (p-vinylbenzyltrimethyl ammonium tetrafluoroborate) and poly ([2-(methacryloyloxy) ethyl] trimethyl ammonium tetrafluoroborate)," *Fluid phase equilibria,* vol. 256, no. 1-2, pp. 75-80, 2007.

[125] Hasan et al., "Determination of solubilities of CO2 in linear and branched polypropylene using a magnetic suspension balance and a PVT apparatus," *Journal of Chemical & Engineering Data,* vol. 55, no. 11, pp. 4885-4895, 2010.

[126] Li et al., "Solubility measurements of N2 and CO2 in Polypropylene and ethene/ Octane Copolymer," *Applied Polymer Science,* vol. 103, pp. 2945-2953, 2007.

[127] Park et al., "Filamentary extrusion of microcellular polymers using a rapid decompressive element," *Polymer Engineering and Science,* vol. 36, no. 1, pp. 34-38, 1996.

[128] J. Gibbs, "The Scientific Papers of J. Willard Gibbs," Dover, New York, 1961.

[129] Park et al., Foam Extrusion, Principles and Practice, New York: CRC Press, Taylor & Francis Group, 2014.

[130] Tucker et al., "Critical state of bubbles in liquid-gas solutions," *Journal of Applied Physics,* vol. 46, pp. 4801-4808, 1975.

[131] M. a. K. J. Blander, "Bubble Nucleation in Liquids," *AIChE Journal,* vol. 21, no. 5, pp. 833-848, 1975.

[132] Leung et al., "Numerical Simulation of Polymeric Foaming Processes Using a Modified Nucleation Theory," *Plastics, Rubber and Composites Macromolecular Engineering,* vol. 35, pp. 93-100, 2006.

[133] R. Cole, "Boiling Nucleation," *Advances in Heat Transfer,* vol. 10, pp. 86-166, 1974.

[134] G. Moore, "“Vaporization of Superheated Drops in Liquids," *AIChE Journal,* no. 4, pp. 458-466, 1959.

[135] R. Apfel, "Vapor Nucleation at a Liquid-Liquid Interface," *The Journal of Chemical Physics,* vol. 54, no. 1, pp. 62-63, 1971.

[136] J. Jarvis et al., "Bubble Nucleation Mechanisms of Liquid Droplets Superheated in Other Liquids," *Journal of Colloid and Interface Science,* vol. 50, no. 2, pp. 359-368, 1975.

[137] B. A. Company, "FINALBROCH 501 GB 2016 02 BBDaploy high melt strength PPSCREEN," [Online]. Available: http://www.borouge.com/IndustrySolution/Images1/Daploy_BR/FINALBROCH%20501%20GB%202016%2002%20BBDaploy%20high%20melt%20strength%20PPSCREEN.pdf.

[138] Borealis AG Company, [Online]. Available: https://www.borealisgroup.com/company/about-borealis/overview.

[139] B. AG, "Daploy™ High-Melt-Strength PP Bro brochure," 2016. [Online]. Available: http://www.borouge.com/IndustrySolution/Images1/Daploy_BR/FINALBROCH%20501%20GB%202016%2002%20BBDaploy%20high%20melt%20strength%20PPSCREEN.pdf.

[140] Ahirwal et al., "Large amplitude oscillatory shear and uniaxial extensional rheology of blends from linear and long-chain branched polyethylene and polypropylene," *Journal of Rheology,* vol. 58, no. 3, pp. 635-658, 2014.

[141] Laguna-Gutierrez et al., "Understanding the foamability and mechanical properties of foamed polypropylene blends by using extensional rheology," *Journal of Applied Polymer Science,* vol. 132, no. 33, 2015.

[142] Marcelo Antunes et al., "Study of the Influence of the Pressure Drop Rate on the Foaming Behavior and Dynamic-Mechanical Properties of CO2 Dissolution Microcellular Polypropylene Foams," *Journal of Cellular Plastics,* vol. 46, no. 6, pp. 551 - 571, 2010.

[143] J. Zeldovich, "On the theory of new phase formation, cavitation," *Acta Physicochimica U.R.S.S,* vol. 18, pp. 1-22, 1943.

[144] R. S. Subramanian, *Reynolds Number.*

[145] Frederic Hecht et al., FreeFem++ manual, T. Edition, Ed., Laboratoire Jacques-Louis Lions, Universite Pierre et Marie Curie, Paris.

[146] W. JIAJAN, *SOLUTION TO INCOMPRESSIBLE NAVIER STOKES EQUATIONS BY USING FINITE ELEMENT METHOD,* 2010.

[147] GHIA et al., "High-Re Solutions for Incompressible Flow Using the Navier-Stokes Equations and a Multigrid Method," *JOURNAL OF COMPUTATIONAL PHYSICS,* vol. 48, pp. 387-411, 1982.

[148] https://imagej.nih.gov/ij/.

[149] Ward et al., "On the Thermodynamics of Nucleation in Weak Liquid-Gas Solutions," *Journal of Basic Engineering ASME,* vol. 92, no. 4, pp. 695-704, 1970.

[150] Katz et al., "Condensation and boiling: Corrections to homogeneous nucleation theory for nonideal gases," *Journal of Colloid and Interface Science,* vol. 42, pp. 496-502, 1973.